NTNU
Norwegian University of
Science and Technology

ROBUSTNESS ANALYSIS OF RADIATION TREATMENT PLANS FOR BREAST CANCER

A COMPARATIVE STUDY BETWEEN PROTONS AND PHOTONS

TFY4910

Andrea HØEG
Faculty of Natural Sciences (NV)

supervised by
Jomar FRENGEN and Anne Beate L. MARTHINSEN

January 10, 2019

Preface

The present report is my M.Sc. thesis in Biophysics and Medical Technology for the Norwegian University of Science and Technology. The presented work was carried out at the Department of Radiotherapy, Cancer Clinic at St. Olavs Hospital in Trondheim, during the fall of 2018.

I would like to thank my supervisors Jomar Frengen and Anne Beate Langeland Marthinsen, for their guidance and support during this project. A special thanks to both for being a great source of inspiration, and being available for discussions. Though we may not have agreed on all concepts, I think this has only spiked healthy discussions which is important in new research. I am grateful for this opportunity to learn firsthand from skilled personnel in radiotherapy planning. I would also like to thank Stina Svensson at the Research Department at RaySearch Laboratories in Sweden, for guidance regarding scripting in RayStation, which is the radiation treatment planning program used at St. Olavs. I would especially like to thank Sondre Vik Furuseth, for his continuous inspiration and support. I am grateful for my classmates, and for the motivating and enthusiastic environment we have created after we started our specialization in biophysics.

When I first learned about particle therapy, I asked myself: Why are we not doing this in Norway? When I tell my friends and family about the topic, and the fundamental differences between particulate and electromagnetic radiation, they are left with the same question. With the ongoing debate in Norway about national proton treatment facilities, I knew, when it was my time to chose project and master thesis, proton therapy was the subject I wanted to explore.

Andrea Høeg

Summary

Proton therapy does in theory propose improved dose distributions and thereby a possible more favorable treatment outcome for breast cancer patients than photon therapy. The technique has a great potential in sparing organs at risk, which for breast cancer patients are, among others, the heart and the lungs. The challenge with proton radiation compared to photon radiation is that the dose distribution is more sensitive to changes in patient anatomy during the treatment course. To compensate for this, the proton treatment plans may be made more robust during the treatment planning. The question investigated in this thesis is whether the potential benefit of proton therapy is sacrificed if the proton plans are made more robust. In this master thesis, various aspects of robustness of treatment plans for breast cancer radiation with both photons and protons have been studied. Changes in anatomy during the treatment session can be visualized by comparing the planning CT to cone-beam CTs taken at different treatment fractions. Such cone-beam CTs can be used to make deformed image registrations with the planning CT, to evaluate the actually delivered dose to the patient anatomy. This tool can also be used to evaluate the need for replanning during a treatment course. To investigate the sensitivity of isocenter deviations, a script has been made that incrementally changes the setup deviations of the treatment fields in different directions and recalculates the dose, to evaluate the plan robustness. The evaluation tools developed in this thesis have been used to compare the robustness of proton and photon plans for ten patients with right-sided breast cancer. This retrospective treatment planning project showed that the proton plans were as robust as the photon plans for isocenter perturbations up to $\pm$ 4.5 mm. It also showed that the proton plans were less robust than the photon plans in the deformed image registration analysis, in the sense that the target coverage and organ at risk sparing had a higher relative change. However, the protons plans still had adequate target coverage and reduced doses to the organs at risk, compared to the photon plans.

Sammendrag

Protonterapi gir teoretisk sett en forbedret dosefordeling og dermed et mulig gunstigere behandlingsresultat for brystkreftpatienter enn fotonterapi. Teknikken har et stort potensiale for å spare risikoorganer, som for brystkreft pasienter er bl.a. hjertet og lungene. Utfordringen med protonstråling sammenlignet med fotonstråling er at dosefordelingen er mer sensitiv for endringer i pasientens anatomi gjennom behandlingsløpet. For å kompensere for dette kan protonplanene lages mer robuste under doseplanleggingen. Spørsmålet som undersøkes i denne avhandlingen er om de potensielle gevinstene av protonterapi blir ofret om protonplanene blir laget mer robuste. I denne masteroppgaven blir ulike aspekter av robusthet av strålebehandlingsplaner for brystkreft undersøkt, for både proton- og fotonplaner. Endringer i anatomi gjennom behandlingsforløpet kan bli visualisert ved å sammenligne planleggings CTen med cone-beam CT-bilder tatt ved ulike behandlingsfraksjoner. Slike cone-beam CTer kan bli brukt til å lage derformerte bilderegistreringer med planleggings CTen, for å evaluere den faktisk leverte dosen til pasient anatomien. For å undersøke sensitiviteten til doseplanen for isocenterendringer, ble det utviklet et script som inkrementelt endret setup-avvikene for strålefeltene i ulike retninger og rekalkulerte dosen, for å evaluere robustheten av planene. Verktøyene utviklet i denne oppgaven ble brukt i robusthetsanalyse av foton- og protondoseplaner for ti pasienter med høyresidig brystkreft. Denne retrospektive doseplanleggingsstudien viste at protonplanene var like robuste som fotonplanene for isocenterforflytninger opp til $\pm$ 4.5 mm. Den viste også at protonplaner var mindre robuste enn fotonplaner i den deformerte bilderegistreringsanalysen, i den forstand at dosen til målvolum og friske organer hadde en større relativ endring. Protonplanene viste likevel tilstrekkelig dekning av målvolumene og reduserte doser til risikoorganer, sammenlignet med fotonplanene.

Table of Contents

Abbreviations

- **3D-CRT** 3-Dimensional Conformal Radiation Therapy
- **ADD** Accumulated Delivered Dose
- **ANACONDA** ANAtomically COnstrained Deformation Algorithm
- **BEV** Beam's Eye View
- **CBCT** Cone Beam Computed Tomography
- **CI** Conformity Index
- **CT** Computed Tomography
- **CTV** Clinical Target Volume
- **DIR** Deformed Image Registration
- **DNA** Deoxyribonucleic Acid
- **DVH** Dose Volume Histogram
- **GTV** Gross Tumor Volume
- **HI** Homogeneity Index
- **HU** Hounsfield Unit
- **ICRP** International Commission on Radiological Protection
- **ICRU** International Commission on Radiation Units and Measurements
- **IM** Internal Margin
- **IMPT** Intensity Modulated Proton Therapy
- **IMRT** Intensity Modulated Radiotherapy
- **ITV** Internal Target Volume
- **LET** Linear Energy Transfer

- **LINAC** Linear Accelerator
- **MR** Magnetic Resonance
- **NRPA** Norwegian Radiation Protection Authority
- **OAR** Organ At Risk
- **PAD** Planned Accumulated Dose
- **POI** Point Of Interest
- **PTV** Planning Target Volume
- **RBE** Relative Biological Effectiveness
- **ROI** Region Of Interest
- **SM** Setup Margin
- **SOBP** Spread-Out Bragg Peak
- **TM** Total Margin
- **VMAT** Volumetric Modulated Arc Therapy
- **pCT** planning CT

Chapter 1

Introduction

Proton therapy has since its introduction for medical use, generated a great deal of attention and discussion. Dr. Robert Wilson was the first to propose protons for radiation therapy in 1946. His suggestion was to utilize the finite range of protons, which could potentially spare surrounding healthy tissue. The first patient was treated at the Lawrence Berkeley Laboratory in 1954 [1]. The use of protons for radiotherapy caught the attention of radiation oncologists in Uppsala, Sweden. Based on the original idea of Dr. Wilson, the Gustav Werner Institute initiated a series of animal experiments, to study biological effects. The first patient was treated in 1957, and after a decade, 69 patients had received proton therapy at the Gustav Werner Institute [1]. It is especially interesting to note that the Revised State Budget in Norway for 2018 granted 3.1 billion NOK for establishment of two proton centers in Norway, Oslo and Bergen [2].

When any new medical technology is introduced, it must find acceptance. For radiation treatment, improved dose distributions and a more favorable treatment outcome should be demonstrated. This often means a more closely confined dose to the tumor volume, while also reducing the dose to normal structures. When proton therapy was introduced, it caught interest mainly because it showed a superior dose deposition compared to conventional photon radiation therapy available at that time. Today, the difference between photon and proton dose conformity to target volumes has decreased. This is mainly due to the development of intensity-modulated radiotherapy (IMRT) and volumetric modulated arc therapy (VMAT). Advanced photon therapy techniques can further improve target coverage, but compromises are inevitable, as the total energy deposited in the patient will not be reduced, only distributed differently. Proton therapy can achieve improvements using scanning-beam technology. Spot scanning, more commonly known as pencil-beam scanning, allows for adjustments of the width of the proton

beam and intensity-modulated proton therapy (IMPT), on a spot-by-spot basis [1]. The main physical advantage of proton therapy is its lower exit dose, which is afforded by the finite range of the primary proton beam. This translates to potentially fewer and less severe side- and late effects of the treatment, compared to photon therapy. The use of proton therapy has indicated a lower risk of secondary malignancies [3]. Pediatric and young patients with curative intentions can become long-term survivors, and will thus have a great benefit of proton therapy [4].

The Particle Therapy Co-Operative Group, report that as of January 2017, close to 150.000 patients have received proton therapy worldwide [5]. The facility that has delivered, by far, the most treatments is the Loma Linda University Medical Center (CA, US). Researchers at this center have published many articles discussing possible skin-sparing and immobilization techniques when using proton beams for breast cancer patients [6, 7]. Despite the early enthusiasm for proton therapy, it is still considered as an "exotic" treatment modality in many countries. Proton therapy treatment plans can be made more conform than photon plans. Hence, the accuracy and precision of the treatment planning and delivery of protons are highly influenced by random and systematic uncertainties. Such uncertainties arise from for instance organ delineation, tissue heterogeneities, organ and patient motion. Immobilization and reproducible patient positioning will play an increasingly important role as the radiation therapy techniques improve [1].

1.1 Robustness

The use of proton therapy for cancer treatment is increasing [5], primarily because of its power to limit the dose to normal tissues, which is associated with fewer treatment-related toxicities. Because of its sharply defined dose deposition, proton therapy is highly sensitive to range and setup uncertainties, and the effect of such uncertainties could be accentuated compared to photon therapy. When the conformity of a treatment plan is optimized, the question is if a robust target coverage sacrifice the sparing of organs at risk (OARs). Various studies have evaluated robust optimization techniques for proton therapy, with the goal of improved treatment plans [8, 9]. Proton plans have shown to maintain coverage of target volumes in worst-case scenarios, without sacrificing the sparing of normal tissues, for lung, base-of-skull and prostate cancer [8], but the indications are not as strong for all tumor types. In this thesis, breast cancer patients will be studied.

A common workflow for radiotherapy includes acquisition of an image sequence prior to the treatment, typically using computed tomography (CT). This image sequence is used to plan the treatment, based on the prescribed dose. The dose is typically delivered in fractions, over several days. Patient anatomy changes during the treatment, due to for instance tumor change in shape and size, weight loss or gain, organ motion, patient positioning and possible seromas. The term

robustness will in this thesis mean the ability of a treatment plan to maintain its original objectives throughout the course of treatment. As time passes, a treatment plan might end up being far from optimal, and studies show that target dose deviation tend to increase with the total dose delivered [10]. Almost all clinics use image-guided radiotherapy, which means that an image sequence is acquired, typically using cone beam CT (CBCT), when the patient is positioned at the treatment couch. This image is used to reposition the patient to ensure optimal delivery according to the plan. However, the CBCTs does not give sufficient data to decide whether the initial treatment plan should be modified.

Two robustness evaluation tools are developed in this thesis. Firstly, a program which simulates two-dimensional isocenter shifts of the treatment plans, which is used to evaluate in which direction the plans are sensitive. Secondly, by tracking the dose delivered to the patient in each fraction, one can assess the dose delivered to the tumor and the OARs, based on the geometry of the patient from the CBCTs. The CBCT values are not in Hounsfield units, and hence some density deformation is needed. This requires deformed image registrations between the planning CT (pCT) and the CBCTs. The actually delivered dose can then be evaluated on these image sets, and be compared to the planned dose on the pCT.

The purpose of this *in silico* thesis is to evaluate the dose distribution of both proton and photon plans, when the plans are subject to change. The question at hand is if the proton plans sacrifice their theoretical advantage of OAR sparing, if optimized to be as robust as possible in terms of target coverage.

1.2 Breast Cancer Patients

The main OARs when irradiating the breast are the lungs and the heart. The skin is also at risk, and one should strive to limit the dose to avoid skin toxicities from the radiation. To my knowledge, no comparative, *in silico* study between the robustness of the two treatment modalities have been made specifically for breast cancer patients. The novelty of this project lies in the direct comparison of parameters drawn from perturbed proton and photon dose distributions of the same patients, to evaluate the robustness of breast cancer treatment plans.

Chapter 2

Theory

2.1 Radiobiology

Radiobiology involves the study of the action and effect of ionizing radiation on living things [11]. For a comparative analysis between proton and photon therapy, it is important to understand their interaction mechanisms with human tissue. When radiation deposits energy in biological material, there is a distinction between excitations and ionizations. An excitation is the raising of an orbital electron to a higher energy level, without actual ejection of the electron. Ionization is the ejection of orbital electrons from an atom or molecule, and does in general require more energy than excitations.

2.1.1 Electromagnetic and Particulate Radiation

Ionizing radiation is usually classified as either electromagnetic or particulate. Electromagnetic ionizing radiation includes x- and γ-rays, which are waves carrying electromagnetic radiant energy. The quantum of the electromagnetic field is termed a photon, which has zero rest mass and is uncharged [11]. This terminology reflects the way the photons are produced, either extranuclearly, or intranuclearly. X-rays are produced extranuclearly, in practice often by an electrical device that accelerates charged particles towards a target, where part of the incoming kinetic energy is converted to x-rays. γ-rays are produced intranuclearly, which means they are emitted by radioactive isotopes. Electromagnetic radiation is indirectly ionizing. The x-rays or γ-rays do not produce chemical or biological damage themselves, but rather deposit some of their energy to secondary charged particles. These secondary particles can interact directly with the absorbing material and produce damage.

Particulate radiation includes electrons, protons, α-particles, neutrons, neg-

ative π-mesons, and heavy, charged ions [11]. Electrons, protons and heavy, charged particles are used in radiation therapy, the two latter only in specialized facilities. Electrons are accelerated in a linear accelerator (LINAC) or a betatron. They are accelerated to the desired energy, either for electron therapy directly, or to hit a target, usually tungsten, to produce photons. Protons and heavier particles have higher mass than electrons, and require more complex and expensive equipment to be accelerated to useful energies [11]. All charged particles are directly ionizing, meaning that they deliver energy to matter directly, through weak Coulomb-force interactions. Provided that they have sufficient kinetic energy, they can disrupt the atomic structure of the absorber directly, and produce chemical and biologic changes.

2.1.2 Biological Effects of Radiation

The overall goal of radiotherapy is to kill tumor cells, whilst sparing normal tissue. The critical target of the radiation is deoxyribonucleic acid (DNA) of tumor cells. The mechanism of cell killing is primarily by production of damage to the DNA by breakage of chemical bonds [11]. Many of the lesions produced by radiation in DNA are successfully repaired by the cell itself.

A break in one of the two strands in the DNA helix, shown in Figure 2.1, has little biologic effect as the cell can repair itself using the opposite strands as a template. Breakage in the two strands directly, or close to, opposite one another may lead to a lethal damage, as the double-strand break cleaves the DNA helix, with a smaller chance of repair.

One distinguish between direct and indirect action of radiation. Direct action of radiation is exhibited by secondary charged particles, liberated from incoming radiation. These are most often electrons, which can interact directly with the DNA to produce an effect, as shown in Figure 2.1. Indirect action of radiation occurs when the liberated charged particle interacts with other atoms or molecules in the cell (particularly water) to produce free radicals. Free radicals carry an unpaired orbital electron, which are highly chemically reactive, and can damage the DNA. See the schematic representation in Figure 2.1.

2.1.3 Linear Energy Transfer and Relative Biological Effectiveness

The International Commission on Radiation Units and Measurements (ICRU) [12], defines the linear energy transfer (LET), of a material, for a traversing charged particle as

$$\text{LET} = \frac{dE}{dl}, \tag{2.1}$$

where dE is the mean energy lost by the charged particles due to electronic interactions when traversing a distance dl. The LET is a measure of average ionization density, and is the energy transferred per unit length of the track, in units of J/m.

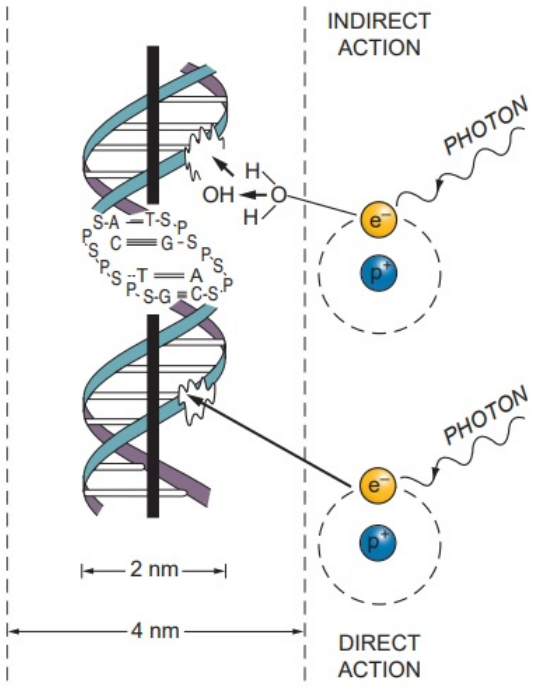

Figure 2.1: Direct and indirect actions of radiation, by ejected orbital electron or free radicals, respectively. The DNA helix, schematically shown to the right, consist of two strands of nucleotides (shown in blue and purple). A nucleotide is composed of a nitrogenous base, a sugar and a phospate group, and is joined to the next nucleotide by covalent bonds between a sugar and a phosphate group. The nitrogenous bases are bound together by hydrogen bonds, making the double-stranded DNA. A double-strand breakage will result in cleavage of the helix, and is believed to be the most important lesions produced by radiation. S, sugar; P, phosphorus; A, adenine; T, thymine; G, guanine; C, cytosine. Courtesy of [11].

The optimal LET, producing the largest effect, is 100 keV/μm, where the average separation between ionizing events coincides with the diameter of a DNA double helix (2 nm) [13].

The International Commission on Radiological Protection (ICRP) defines the relative biological effectiveness (RBE), as the ratio of a dose of a given LET, a reference radiation, to a dose of the radiation considered, that gives an identical biological effect [14]. RBE values depend on the dose, dose rate, and biological endpoint.

2.2 Interaction of Radiation with Matter

2.2.1 Photon Interactions with Matter

As explained in Section 2.1.1, γ-rays are high-energy photons with no mass nor electrical charge, which can not directly ionize matter. They cause damage by indirect ionizations, through three key interaction mechanisms with matter [11]. At high energies, in the proximity of a nucleus, the photon may disappear as a photon and reappear as a positive and negative electron pair (pair production). The photon may scatter and loose energy by collisions with atomic electrons (Compton effect), or completely disappear after interacting with the absorbing material (photoelectric effect).

- **Photoelectric effect:** By interaction with the material, the photoelectric effect leads to the emission of photoelectrons from an atom of the absorber. It occurs in the vicinity of an atom, where the photon's energy is converted into releasing an electron, usually from the inner atomic shell. Electrons are only emitted by the photoelectric effect if the incoming photon reaches or exceeds a threshold energy, equal to the binding energy of the particular electron of the material. The photoelectron ejected obtains the remaining energy of the photon, E_e

  $$E_e = h\nu - E_b, \tag{2.2}$$

  where $h\nu$ is the incident photon energy, and E_b is the binding energy of the photoelectron in its orbital shell.

- **Compton scattering:** The Compton effect, or Compton scattering, is the scattering of photons by atomic electrons, usually resulting in a decrease in energy of the incident photon. The photon thus have an increased wavelength after the interaction. Part of the energy of the photon is transferred to the recoiling electron, giving rise to a secondary electrons. The kinetic energy K, of the recoiling electron, will depend on the scattering angle of the photon. Energy conservation gives for the kinetic energy of the electron

  $$K = E_\gamma - E'_\gamma = E - mc^2, \tag{2.3}$$

  where E_γ and E'_γ is the incident and resultant energy of the photon, respectively, and E is the total energy of the recoil electron including its rest mass energy mc^2.

- **Photon pair production:** Photon pair production is the creation of an electron and a positron. For electron-positron pair production to occur, the incident photon must have an energy above the energy of the rest mass of two

electrons, equal to 1.02 MeV [11]. The situation must also allow for both energy and momentum to be conserved, requiring a presence of an electric field, usually from a nucleus. A photon pair production can hence not occur in free space. The entire photon energy is converted into the creation of an electron-positron pair with total kinetic energy given by

$$K_- + K_+ = E_\gamma - 2mc^2. \tag{2.4}$$

Here, K_- and K_+ represents the energy of the electron and positron, respectively, and E_γ is the energy of the incident photon, and $2mc^2$ is the rest mass energy of the two products.

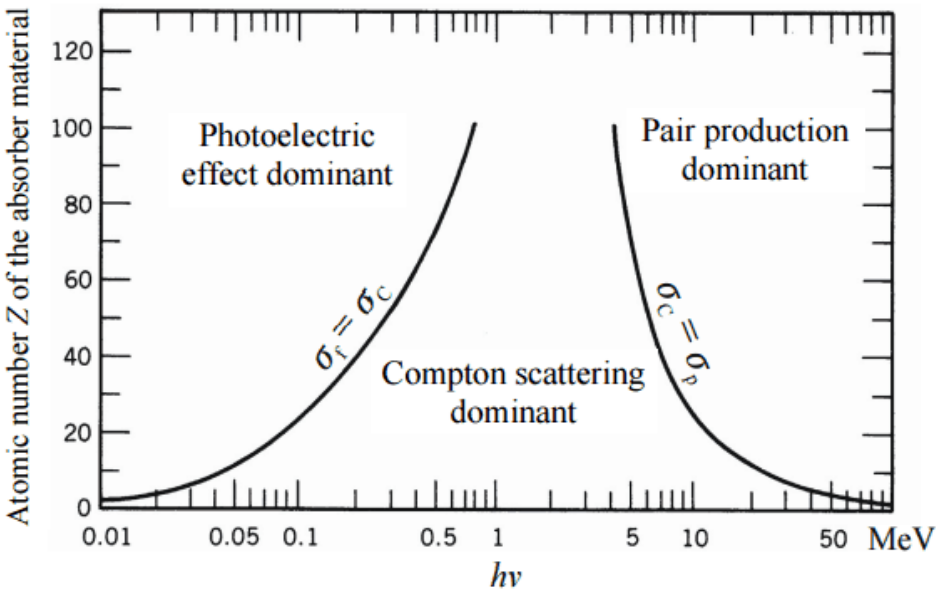

Figure 2.2: The relative importance of various processes of gamma radiation interaction with matter, depending on the absorbing material Z, and photon energy hv. σ_f, cross-section for photoelectric effect; σ_C, cross-section for Compton effect; σ_p, cross-section for pair production. Courtesy of [13].

The cross-section of an interaction between two particles is defined as the area transverse to their relative motion where they can meet and interact with each other [11]. It can be interpreted as a quantity expressing the likelihood of an interaction event between two particles. Figure 2.2 indicates which interaction mechanism is more likely for a certain energy and absorber. Medical LINACs operate with photon energies between 4 and 25 MeV [11], and the effective atomic number of various human tissue usually lies beneath 10 [15], which makes the Compton

process the dominant interaction mechanism for photons used in radiotherapy. The dose is delivered by atomic electrons set in motion, rather than from the primary photons themselves.

2.2.2 Proton Interactions with Matter

The outline of this chapter is partly based on a project thesis done prior to this master thesis [16]. Protons are charged particles, and the dominant interaction mechanism is inelastic collisions. They interact with matter in three distinct ways [1]. By collisions with atomic electrons, the protons slow down (stopping). If colliding with atomic nuclei, the protons can be deflected (scattered). If the collision with the atomic nuclei is head-on, the incoming proton can eject nucleons (nuclear interaction).

- **Stopping:** In this interaction mechanism, energy is transferred from the charged proton to atomic electrons due to Coulombic interactions. An important fact is that protons can stop in solid or liquid matter, and beyond the stopping point the dose is negligible. The range of penetration of protons is nearly proportional to the kinetic energy squared, meaning that for a monoenergetic proton beam, all protons will stop at approximately the same depth. The spread in the stopping point is called range straggling. The cross section, the probability of interaction, is highly dependent on the momentum of the proton [1]. Slower protons are longer in contact with the atomic electrons, and more momentum is transferred. The proton beam slows down through many of these small energy transitions, until it finally promptly stops, and deposits the rest of its energy in the so-called Bragg peak. Hence, the rate of energy loss highly depends on the proton energy and on the stopping material, i.e. the density of available atomic electrons.

- **Scattering:** Protons are commonly only deflected a very small angle after a single atomic nucleus interaction. The scattering angle will increase with increasing density of the absorbing material [11]. The resulting angular spread of a clinical proton beam is mainly due to the random combination of many such small deflections.

- **Nuclear Interactions:** This is the least understood interaction, but fortunately, nuclear interactions are relatively infrequent, and simple approximations take them into account well enough for the purpose of radiotherapy. If a primary proton simply scatters elastically off a nucleus, or leaves it mildly excited, the outgoing proton retains its characteristics. Inelastic collisions, where the proton enters the nucleus and knocks out one or more protons or neutrons, happens infrequently. These secondary nucleons can have much lower energies and much larger scattering angles than the primary protons.

Thus, some dose is deposited just after the reaction site. Approximately 20% of 160 MeV protons does this kind of reaction before stopping [1], and may contribute to the range straggling discussed above.

The Bragg Peak

The interaction mechanisms described above come together to determine the shape of the depth-dose curve for protons. A depth-dose curve shows the relative dose distribution as a function of depth in a material. It describes the penetration ability of a beam, which depends on the beam energy and quality, and the absorbing material. Manipulations of the Bragg peak, for instance using beams of various energies, are used to cover the target and spare healthy tissue in treatment planning [13]. Such a spread-out Bragg peak (SOBP), with uniform dose over an imagined tumor at 16-30 cm depth, is shown in Figure 2.3.

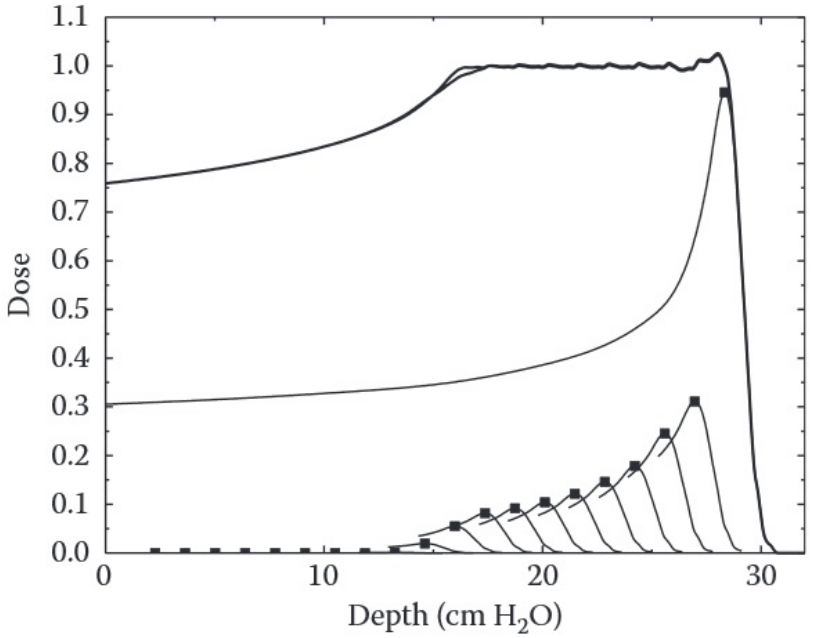

Figure 2.3: The SOBP is the sum of several individual Bragg peaks, obtained by delivery of proton beams at different energies. A uniform dose is given to the material lying at 16-30 cm depth. Courtesy of [1].

Energy

For proton radiotherapy energies, (50-300) MeV, the proton is an elementary particle with a rest energy $mc^2 = 938.27$ MeV, and a charge $e = +1.602 \cdot 10^{-19}$ C.

At such energies, the relativistic effects are non-negligible, with a speed in the order of the speed of light, $c = 3 \cdot 10^8$ m/s. Hence, calculating their speed v, and momentum $p = \gamma m v$, is done by the relevant special relativity equations. Here, γ is the Lorentz factor, and m is the mass. For a given kinetic energy K [1],

$$\beta = \frac{v}{c} = \frac{pc}{K + mc^2}, \tag{2.5}$$

$$(K + mc^2)^2 = (pc)^2 + (mc^2)^2. \tag{2.6}$$

It is important to realize that energy lost by a proton beam exceeds the energy deposited locally in a patient. Neutral secondaries, coming from Bremsstrahlung or nuclear interactions, may deposit their energy outside the patient volume.

Stopping

As previously mentioned, protons slow down in matter primarily due to myriad collisions with atomic electrons. The longer a proton interacts with an electron, the greater the loss of energy from the proton. In other words, the rate of energy loss increases as the protons slows down, giving rise to the peak of ionization near the end of the range of the protons. The beam has sharp edges, with little side-scatter. The possibility of precisely confining a high-dose region to a tumor volume, whilst minimizing the dose to the surrounding normal tissue, is obviously attractive in radiotherapy.

Bethe and Bloch derived the theoretical rate of energy loss for fast charged particles in matter around 1933. In SI units the Bethe-Bloch formula states that a particle with speed v, charge z, and energy E is [17]

$$-\left\langle \frac{dE}{dx} \right\rangle = \frac{4\pi}{m_e c^2} \frac{nz^2}{\beta^2} \left(\frac{e^2}{4\pi\epsilon_0} \right)^2 \left[\log\left(\frac{2m_e c^2 \beta^2}{I(1-\beta^2)} \right) - \beta^2 \right], \tag{2.7}$$

where

- x is the distance into a target of electron number density n,
- I is the mean excitation potential, which is dependent on the absorbing material,
- c is the speed of light,
- ϵ_0 is the vacuum permittivity,
- $\beta = v/c$,
- e is the electron charge,
- m_e is the electron rest mass.

What is important to realize in this equation, is that the energy loss of protons, Equation 2.7, is inversely proportional to the velocity squared. When charged particles interact with matter, the number of primary particles decrease slightly, but their energy decreases continuously. This causes the Bragg peak, as the entire beam stops at approximately the same depth. Charged particles have a higher energy transfer per unit length than uncharged particles, and the energy deposition increases with decreasing velocity, causing the large dose deposition just before they stop.

Accounted for protons in an elementary material of atomic number Z and relative atomic mass A, Equation (2.7), for the mass stopping power S/ρ, becomes

$$\frac{S}{\rho} = -\frac{1}{\rho}\frac{dE}{dx} = 0.3072\frac{Z}{A}\frac{1}{\beta^2}\left(ln\frac{2m_e c^2\beta^2}{I(1-\beta^2)} - \beta^2\right)\frac{\text{MeV}}{\text{g/cm}^2}, \tag{2.8}$$

where ρ is the density. Equation (2.8) represents the rate of energy loss for protons due to atomic electrons only. Protons will also lose some energy by elastic scattering on atomic nuclei, but this contribution is less than 0.1% for energies above 1 MeV [1]. Protons with energies in the range of 70 MeV to 250 MeV are typically used for proton therapy [11].

2.2.3 The Theoretical Advantage of Protons

The clinical gains of using protons instead of photons in radiotherapy can be summarized in three principles [11]. These are based on the dosimetric advantages of charged particles.

- For the same dose to the target volume, protons may deliver a lower absorbed dose to normal tissues than high-energy x-rays.
- There is no clinical advantage to be gained by irradiating normal tissues that do not harbor malignant cells.
- There is little difference in the radiobiologic properties of protons used for therapy and high-energy x-rays; this includes repair, oxygen enhancement ratio, and response through the cell cycle. The only relevant difference, is the dose distribution.

By comparing radiation qualities and types, it is evident that the energy deposition varies. The sharply defined Bragg peak for proton therapy, occurs at a depth in tissue that depends on the initial energy of the particles. A composite SOBP is shown in Figure 2.4, together with a photon beam. Photons have no charge, which is the reason why dose is not deposited in the superficial regions. As explained in Chapter 2.2.1, the dose is delivered by secondary atomic electrons, rather than from the primary photons themselves, and this cloud of secondary electrons takes

some distance to build up. This is called the build-up region, which is clinically useful as it spares the skin.

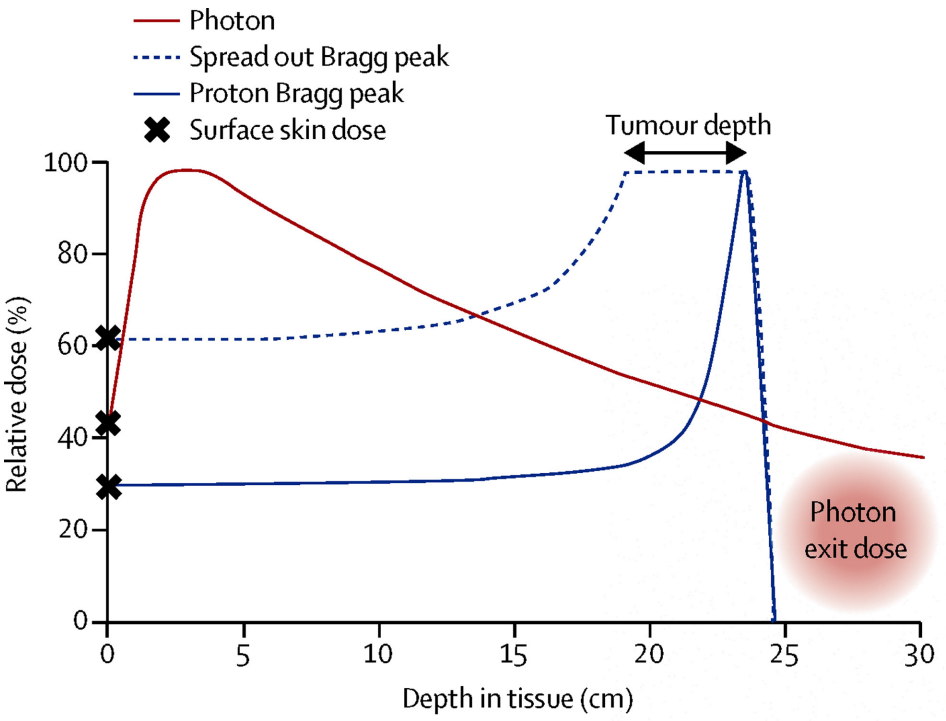

Figure 2.4: Depth-dose curves for photon and proton beams. The modulated proton beam results in a SOBP with loss of skin-sparing, but also a negligible dose behind the tumor. Courtesy of [18].

2.3 Evaluation Metrics

2.3.1 Volume Definitions

In radiotherapy, three-dimensional contours are defined from the planning CT (pCT) of the patient. The radiation report 2012:09 by the Norwegian Radiation Protection Authority (NRPA) [19] defines volumes for external beam radiation therapy. From the pCT, two types of volumes should be defined; the gross tumor volume (GTV), and the clinical target volume (CTV).

The GTV is the visualized tumor from the pCT, and thus what is called an anatomical volume. In many cases, the GTV can be removed by surgery. It can consist of the primary tumor, regional lymph nodes, distant metastases, and/or local residues. The CTV is a volume that contains the GTV and/or areas where one suspects subclinical malignant disease, relevant for treatment.

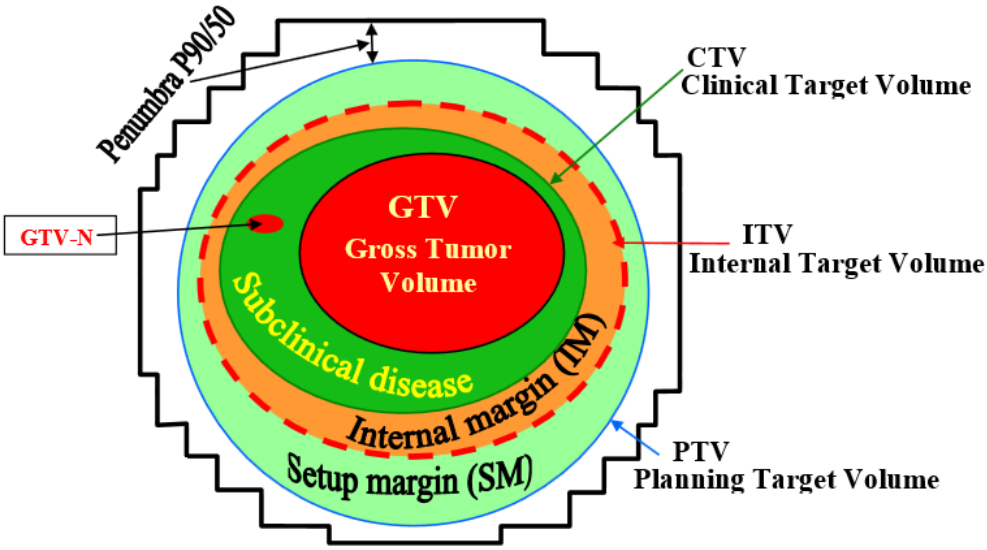

Figure 2.5: Graphical representation of various volume definitions. The penumbra is the distance between the 90% and 50% dose levels on a cross-section dose profile, perpendicular to the central axis at a certain depth. The GTV-N is a GTV for a lymph node outside the main GTV. Courtesy of the NRPA [19].

To ensure the requisitioned dose to the CTV, it is common to consider margins for different deviations and variations, in addition to tumor spread. The internal target volume (ITV), is the CTV and a margin for internal movement (the internal margin (IM)), for instance due to breathing and anatomical changes from the previous fraction. The ITV also accounts for inaccuracies in target delineation. The setup margin (SM), accounts for assumed patient movement and inaccuracies in patient alignment and beam fields between different fractions. Such deviations could be due to interfractional or intrafractional movement, planning of patient positioning, or poor adjustment of equipment. The total margin (TM), encloses all inaccuracies and variations in patients and equipment, and is hence a combination of IM and SM

$$TM = \sqrt{IM^2 + SM^2}. \tag{2.9}$$

The TM is normally added to the CTV to define the planning target volume (PTV). The PTV is a geometrical volume that aims to ensure that the requisitioned dose, with an acceptable likelihood, is delivered to the CTV, considering all geometrical uncertainties included in the TM. Thus, one can assume that the prescribed dose is delivered to the CTV, as long as the CTV moves only within the

boundaries of the PTV. A schematic of the different volumes and margins is shown in Figure 2.5.

2.3.2 Dose and Volume Parameters

The ICRU have defined various characteristic values for distributions relevant for radiotherapy [20]. The average absorbed dose D_{avg}, to a volume V, is defined as

$$D_{avg} = \frac{1}{V}\int_0^{D_{max}} D\frac{dV(D)}{dD}dD, \tag{2.10}$$

where D_{max} is the maximum dose to the volume V, and $dV(D)/dD$ is the increment of volume per absorbed dose at absorbed dose, D. D_{median}, or D_{50}, is the absorbed dose received by 50% of the volume. Similar nomenclature is used for other values of interest, giving the generalized equation for a specified region of interest (ROI)

$$D_x = \text{The dose received by x\% of the volume.} \tag{2.11}$$

For target volumes it is custom to report the near-minimum and near-maximum absorbed doses, which are the D_{98} and D_{02} respectively [20]. D_{min} is the minimum dose to a specified ROI.

The volume that received a specified dose, y, can be reported as

$$V_y = \text{The volume that received } y \text{ Gy to a specified ROI,} \tag{2.12}$$

where gray is the derived unit of ionizing radiation dose, Gy = J/kg [1]. The y in Equation 2.12 can also be expressed as a percentage of the prescribed dose ($V_{y\%}$) instead of absolute value of dose ($V_{y\text{Gy}}$). A dose-volume histogram (DVH) relates the radiation dose to tissue volume, typically visualized in a graph where the x-axis is the dose and the y-axis is the percentage of volume. An illustration of a selection of such parameters is shown in Figure 2.6.

2.3.3 Dose Homogeneity and Dose Conformity

To evaluate the quality of the total dose-field, and not just specific points from the DVH, one can report the homogeneity index (HI) and conformity index (CI). The dose homogeneity to a specified volume, characterizes the uniformity of the absorbed-dose distribution within that volume. It is usually reported for the target volume. Different definitions of the HI have been proposed, and the ICRU suggests the following [20]

$$\text{HI}_{\text{ICRU}} = \frac{D_2 - D_{98}}{D_{50}}, \tag{2.13}$$

meaning that a HI_{ICRU} of 0 indicates a dose that is homogeneously distributed throughout the volume. RayStation defines the HI differently [21],

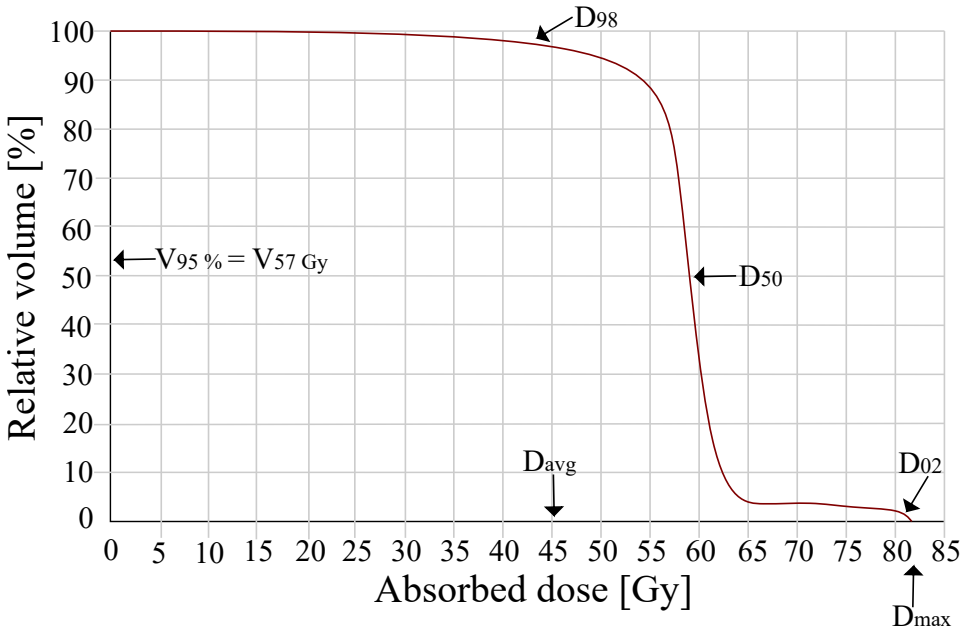

Figure 2.6: An illustration of some of the parameters often used in dose reporting. The figure shows a DVH of an imagined ROI, with a prescribed dose of 60 Gy.

$\text{HI}_{\text{RS}} = D_x/D_{(100-x)}$, which is the definition that will be used in this study. A HI_{RS} of 1 thus indicates a uniform dose distribution to the specified ROI.

The dose conformity characterizes the degree to which the high-dose region of the field conforms to the target volume. The ICRU and RayStation have equal definitions of the CI [20, 21]

$$\text{CI} = \frac{\text{ROI volume covered by a specified isodose}}{\text{total isodose volume}}, \tag{2.14}$$

making a CI of 1 a highly conformed dosage profile for the specified ROI. Isodose curves are lines that contour regions that receive an equal dose of radiation, [13].

2.3.4 ICRU Levels of Reporting

The ICRU have defined three levels of dose reporting [20]. These include, but are not limited to, the following

- **Level 1** describes the minimum standards for reporting of a dose prescription. It includes reporting of the absorbed dose to target volumes and OARs, and below these standards, radiotherapy should not be performed. This level of reporting is not adequate for complex treatment plans, such as IMRT, VMAT or proton therapy.

- **Level 2** is the standard level for dose reporting. All volumes of interest, both targets and OARs are delineated, and DVH for all volumes of interest are computed. Metrics included in level 2 reporting are D_{50}, D_{avg}, D_{98}, D_{02}, and V_x for ROIs.

- **Level 3** include recommendations for optional reporting of research and novel developments. Here, one should also include the HI and CI.

2.3.5 The Hounsfield Scale

CT numbers are given on a quantitative scale, the Hounsfield scale, which describes radiodensity. The Hounsfield unit (HU) scale is a linear transformation of the measured linear attenuation coefficient μ, given by

$$\text{HU} = \frac{\mu - \mu_{water}}{\mu_{water} - \mu_{air}} \times 1000, \tag{2.15}$$

where μ_{water} and μ_{air} are the linear attenuation coefficients of water and air, respectively. The equation transforms the measured linear attenuation coefficient into one which is defined as zero HU for water, and -1000 HU for air, at standard pressure and temperature [13]. The HU is commonly used in CT scanners to express density in a standardized and convenient form. The radiodensity, measured in HU, is inaccurate in CBCT scans because different areas in the scan appear with different greyscale values depending on their relative positions in the organ being scanned. This means that two separate positions of identical density, may not be given the same HU, because the image value of a voxel of an organ depends on the position in the image volume, as shown in Figure 2.7. HUs measured from identical anatomic areas with both CBCT and CT are not identical. This is explained by the difference in reconstruction of image sets for the two techniques [22].

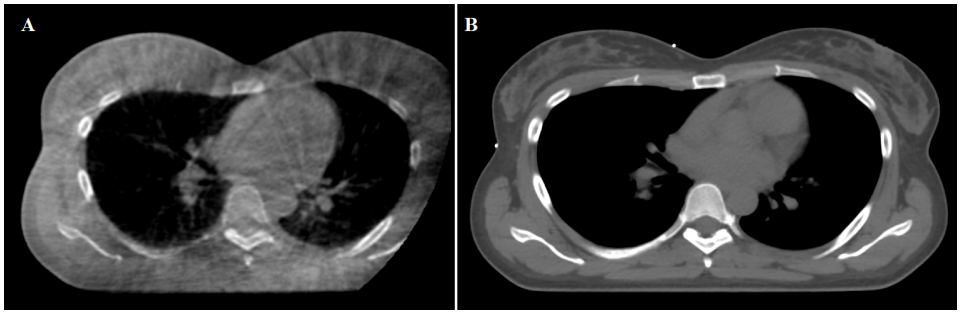

Figure 2.7: A) a CBCT and B) a pCT of the same slice of the same patient. The field of view is reduced in the CBCT to limit the dose to unnecessary parts of the patient.

2.4 Treatment Planning and Delivery

2.4.1 Treatment Planning System

A treatment planning system is mainly used for planning and evaluating treatment of cancer. It consists of a computer, software for dosage calculation for graphic and alphanumeric data [21]. Using image and dosimetric data, clinicians can plan the optimum treatment parameters to match treatment goals and constraints. The dose depositions are calculated based on the physics explained in Section 2.2 and models that accounts for the stochastic effects of radiation interactions. Examples of treatment planning systems are Elekta's Monaco, Philips' Pinnacle, Varian's Eclipse and RaySearch's RayStation.

2.4.2 Robust Optimization in RayStation

When proton therapy was introduced, the first implementations of robust planning in treatment planning systems were developed [9]. RayStation developed a minimax method that takes the uncertainties into account during the plan optimization for protons [23], which can now be clinically used for both protons and photons. The minimax optimization aims at minimizing the penalty of a worst-case scenario. As protons have a high stopping power dependency, and steep beam dose gradients, proton therapy is highly sensitive to errors, and conventional margins might be considered insufficient to ensure robustness of treatment plans. The two main error sources in proton therapy are range and setup uncertainties. Range uncertainties may arise from inaccuracies in the CT imaging. Patient positioning, organ contouring, and mechanical inaccuracies in the delivery unit cause setup uncertainties. A robust treatment plan accounts for such uncertainties. The conventional method is to plan with margins, as explained in Chapter 2.3.1.

RayStation treatment planning system has implemented a robust minimax optimization method to account for sharp dose deposition gradients, which are sensitive to anatomical changes [23]. For n functions $f_1, ..., f_n$, that are all required to be robust over the scenarios in a set S, and which have nonnegative importance weights $w_1, ..., w_n$, a minimax optimization problem can be formulated as

$$\min_{x \in X} \max_{s \in S} \sum_{i=1}^{n} w_i f_i(d(x; s)), \tag{2.16}$$

where X is the set of feasible variables, e.g. spot weights for IMPT, and $d(x; s)$ is the dose distribution as a function of the variables x, given the scenario s.

In RayStation one can generate optimized plans by adding user-defined treatment constraints with different weights of importance, which work according to the minimax method. The result for a proton pencil beam scanning plan is a spot position pattern with optimized spot weights [21].

2.4.3 Hybrid Based Deformable Registration in RayStation

A hybrid deformable registration uses image intensity and anatomical information to perform the deformation of a density grid. The anatomical information is given as either ROI(s), or point(s) of interest (POI), defined in both the target and the reference image. The result of a deformable registration algorithm is a displacement field from the reference image set to the target image set. The displacement field can be used to deform a dose defined on the target image set to the reference image set geometry, as well as mapping anatomical structures between the image sets. The anatomically constrained deformation algorithm (ANACONDA) is used for deformable image registrations in RayStation. The problem is formulated as a non-linear optimization problem where the objective function, f, is a combination of an image similarity term, grid regularization terms, a shape based regularization term, and anatomical penalty terms [21, 24].

The ANACONDA performs a rigid transformation, aligning the images (M: $\mathbf{R}^3 \rightarrow \mathbf{R}^3$). The deformation grid is a set of gridpoints arranged in voxels. The algorithm then computes a vector field defined on this grid, called the deformation vector field. A vector at gridpoint $x_i \in \mathbf{R}^3$ is denoted $v_i \in \mathbf{R}^3$. The nonlinear optimization problem with objective function f: $\mathbf{R}^n \rightarrow \mathbf{R}$, is formulated [24]

$$f(v) = \alpha C(v) + \zeta H(v) + \gamma S(v) + \delta D(v), \tag{2.17}$$

where $\alpha, \gamma, \delta \in \mathbf{R}$ are non-negative weights, n is the number of variables, which equals three times the number of gridpoints, and ζ: $\mathbf{R}^3 \rightarrow \mathbf{R}$ is a non-negative, real valued weight function. The terms $C(v), H(v), S(v)$, and $D(v)$ describes the objective function f [24]. The term $C(v)$ is the correlation coefficient of image similarity between target and reference image sets. $\zeta H(v) + \gamma S(v)$ describes the regularization of the deformation grid. $D(v)$ describes the controlling structures, ROIs and POIs, should there be any to guide the deformation algorithm.

2.4.4 Perturbed Doses in RayStation

Optimizing with robust criteria may partly overcome the challenge with conventional margins. However, it is still important to evaluate the robustness of the plan. In RayStation, doses can be computed including a perturbation of the dataset, to evaluate the robustness of the original plan. Perturbations can be specified as a scaling of mass density in patient material, and/or a shift of the isocenter in the sagittal, coronal and/or transverse plane [21].

2.4.5 Patient Coordinate System in RayStation

Data sets containing patient coordinates in files exported from RayStation, follow the Digital Imaging and Communications in Medicine, DICOM, standard. For the head first supine position, the coordinates are defined as shown in Figure 2.8. Note that the positive y-axis is in the posterior direction.

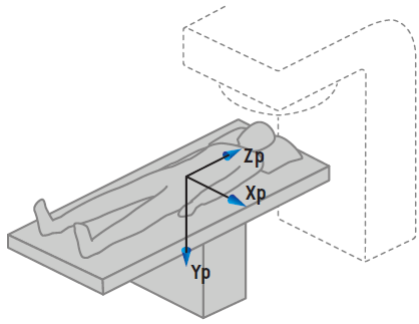

Figure 2.8: Patient coordinate system for the head first supine position. Courtesy of [25].

2.4.6 Delivery of Photons

Megavoltage electron accelerators are used for cancer treatment with photon and electrons. Such a LINAC is mounted on a drum structure (gantry) which can rotate 360 degrees. A beam limiting device is mounted on the gantry, containing components for beam shaping, such as scatter filters (for electrons), collimators, flattening filters and diaphragms.

A metal tube is fed with an electromagnetic field in the micro-frequency range, which propagates in the tube. Electrons are injected at the same side as the electromagnetic field. The electrons are accelerated when they have the right phase relative to the electromagnetic field. The electrons gain energy from the microwaves travelling down a waveguide. They are then deflected by a magnet before the radiation reaches the patient. Patients are treated either using electrons directly or by creating Bremsstrahlung photons [11]. Bremsstrahlung radiation is produced by the deceleration of charged particles as it is deflected by another charged particle. As the moving particle loses kinetic energy, this is converted into neutral radiation (Bremsstrahlung radiation), thus satisfying the law of conservation of energy. When the electrons leave the waveguide, they have a distribution of energies. The electron beam then travels through a series of electromagnets, with a current set to allow only electrons with the desired energy to pass. The selected electrons then directly hit the patient, or a target (usually Tungsted), to generate the correct energy range of photons. The energy of the electron beam is often given in units of electronvolts, eV, as the beam is monoenergetic. The photon beam consists of a heterogeneous energy spectrum because of Bremsstrahlung effects. Thus, the beam is rather described by the potential used to accelerate the electrons, in units of volts, V.

Conventional Treatment Planning

This technique is well established, and generally quick and reliable. The radiation field is shaped using blocks, wedges and multi-leaf collimators, to acquire the most conformal shape as possible to the target volume. Opposing beams, tangential beams, three-beam arrangements and four-field box-techniques are used to match the field in the best way possible.

3D-CRT

Three-dimensional conformal radiation therapy (3D-CRT) uses CT images of the patient for the treatment planning, giving the physicians better knowledge about the true radiation dosage to the tissue [13]. The profile of each radiation beam is shaped to fit the profile of the target from the beam's eye view (BEV), to make the treatment profile more conform.

IMRT and VMAT

IMRT and VMAT are so-called inverse treatment planning techniques [13], in the sense that clinical goals are set, and a plan is made to meet those objectives. IMRT uses more gantry angles than conventional treatment delivery, and each of the beams have modulated intensity and field shape. This improves the ability to conform the treatment volume, as each field pattern of the different gantry angles are tailored for that BEV of the target volume. The VMAT technique further improves the conformity of radiation, as it irradiates during gantry movement. The intensity and collimator shape can be changed almost continuously.

2.4.7 Delivery of Protons

Acceleration of protons to the desired energies typically happens in a cyclotron or synchrotron. The major components of a cyclotron are a radio-frequency system, where the protons are accelerated, a constant magnetic field, that pushes the protons into a spiral-shaped orbit for repeated acceleration in the radio-frequency field, a proton source of hydrogen gas, and an extraction system [1]. In the extraction system, the protons of the desired energy is guided out from the cyclotron into a beam transport system. The synchrotron evolved from the cyclotron, but here the guiding magnetic field varies in strength in time [1]. Two proton beam delivery systems are available today; passive scattering and active scanning [1, 13].

Passive Scattering Beam Delivery

By placing a material in the beam path, the proton beam is spread in the lateral direction. A range modulator wheel is used for axial precision, and for obtaining the SOBP.

Active Scanning Beam Delivery

In scanning beam techniques, the lateral precision is obtained using magnets to deflect and steer the proton beam. The depth of penetration (axial control) of the Bragg peak is adjusted by varying the energy of the beam as it enters the gantry. The treatment target volume can in such a way be painted, voxel by voxel, in successive layers. IMPT implies this electromagnetic spatial control using so-called pencil-beams of protons of variable energy and intensity.

2.4.8 Treatment Planning of Breast Cancer

The major OARs in breast cancer radiotherapy are the lungs, the heart, the skin and the contralateral breast, which are shown in Figure 2.9. The aim of sparing these volumes is to reduce the risk of radiation pneumonitis, late cardiac toxicities, pericarditis, skin burns and radiation-induced cancer, among other things [26].

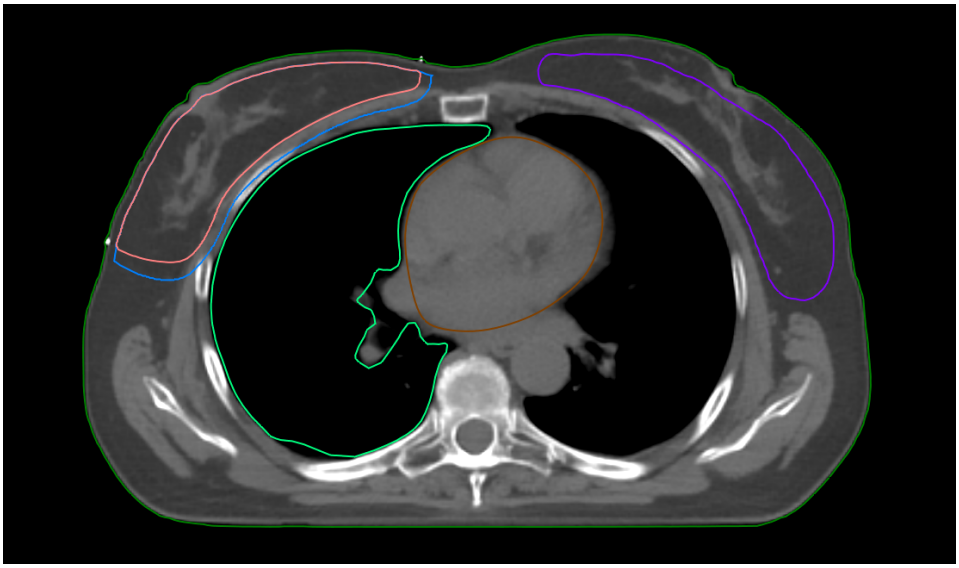

Figure 2.9: A CT image including the delineation of the most important regions of interest when irradiating a breast. Target volumes; the CTV ■, the PTV ■, and organs at risk; the right lung ■, the contralateral breast ■, and the heart ■. Also shown is the external contour ■.

National guidelines for breast cancer recommends a $D_{avg} \leq 2$ Gy to the heart, and a $V_{18\,\mathrm{Gy}} \leq 15\%$ to the lungs, for fractionation regime 2.67 Gy $\times$ 15, [27]. The minimum required dose to the PTV is 90% of the prescribed dose [27], but the 95% isodose is more commonly used in the clinic. In conventional photon treatment planning, the PTV may be expanded to include some air above the chest, to ensure robustness in that direction. If the breast swells or develops a seroma, causing the

CTV to expand away from the lungs, such a PTV will ensure coverage.

Sparing of the OARs is visualized in Figure 2.10, where the photon treatment plan delivers a higher dose to both the lung and heart than the proton plan. Breast cancer radiotherapy in Norway today is typically delivered in 15 or 25 fractions, with a prescribed dose to the CTV of 40 Gy or 50 Gy, respectively [27]. Today, 3D-CRT is considered the standard treatment technique for breast cancer patients in Norway. Hybrid plans consisting of tangential 3D-CRT fields with VMAT supplement arcs should be considered if the prescribed dose is not met in the deeper regions of the chest [27]. To adjust for chest movement due to breathing, it is today common to use gating when irradiating the left breast. This consists of a system where the patient has moving-sensors on the chest, which produces a respiratory diagram. The radiation is cut-off during exhalation, to reduce the dose to the OARs [13].

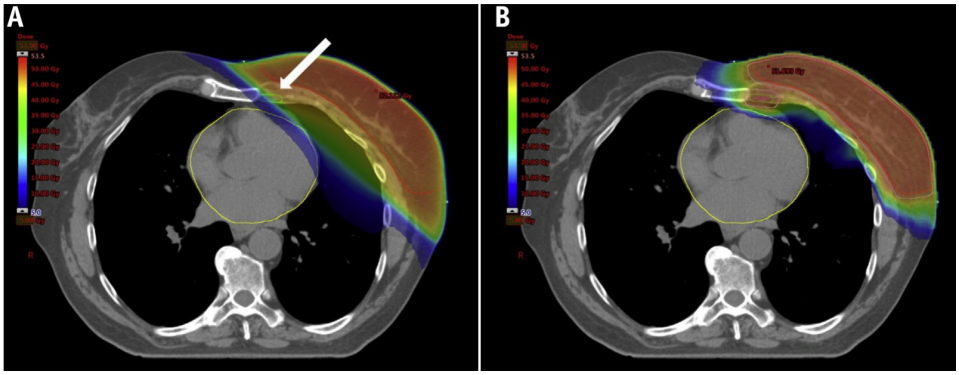

Figure 2.10: CT images with a photon treatment plan (A), and a comparative proton treatment plan (B), both including a dose wash from 10% (blue) to 107% (red) of the prescribed dose. The internal mammary node (white arrow in A) required a high dose, which was not obtained in the photon plan, because of restriction protocols for maximum dose to the heart (yellow contour). The dose to the CTV (red contour) is similar, but the photon plan failed to deliver adequate dose to the internal mammary node, and had a higher dose to the heart and lung. Courtesy of [28].

Chapter 3

Methods

3.1 Study

This retrospective, *in silico*, comparative study looked at ten patients diagnosed with right-sided breast cancer. They all received external photon beam radiotherapy at St. Olavs hospital, using respiratory gating. The delineation of target volumes and OAR done by physicians for these patients, together with their pCTs and CBCTs, were exported to RayStation Research and anonymized. The same delineated volumes and fractionation regimens were used to retrospectively plan photon and protons plans. Proton plans were made by a spot scanning technique with two beams, and compared with 3D-CRT photon treatment plans, in terms of target coverage and sparing of OARs. 3D-CRT was used as it is considered the standard treatment for breast cancer patients in Norway today [27]. By using the CBCTs taken at each fraction one can visualize changes in borders and volumes throughout the treatment course. The method of studying accumulated dose on deformed fraction CBCTs was scripted in the previous project thesis [16], using RayStations functions for deformed image registrations (DIRs). Thus, individual fraction doses could be compared with the planned dose on the pCT, and accumulated for evaluation of the delivered total dose.

For further investigation of robustness and to separately evaluate the sensitivity against an isocenter shift, a script was made to incrementally change the position of the isocenter of the treatment plan, and recalculate the doses. This was done in two-dimensions, in the lateral (x) and posterior-anterior (y) direction of the transverse plane, to assess the sensitivity to change/robustness in those directions.

3.1.1 Patient Selection

Breast cancer patients are eligible for proton therapy because OARs lie close to the target volume, as explained in Chapter 2.3.1. 31 breast cancer patients were considered and ten was selected (patient A-J), to be apart of this retrospective treatment planning study, with pCTs and CBCTs. Eligibility criteria were

- right sided breast cancer,
- no lymph node metastasis at the time of radiotherapy,
- CBCT field of view large enough to cover photon field from all directions,
- a prescribed dose of 40.05 Gy to the CTV, given in 15 fractions,
- no image artifacts on the CBCT.

3.2 Treatment Planning

The radiation treatment planning system used in this project was RayStation 6 Research, a software system designed for treatment planning and analysis of radiation therapy. The program modules for Patient Data Management, Patient Modeling, Plan Design, Plan Optimization, Plan Evaluation and Treatment Adaptation were used. In addition, RayStation supports scripting, and scripts were written in Python for additional use of the data available in the standard modules, and for automation and connectivity. Proton and photon plans were made for all patients, based on the pCT taken for treatment. The delineated ROIs made for the treatment by physicians was used in this study. The contour for the contralateral breast was missing from one patient, patient G. As this contour was only used for dose-statistics, and not included in the treatment optimization, the patient was not withdrawn from the study. All patients had a head first supine treatment position, and all treatment plans were made by the same person.

3.2.1 Proton Plans

The pencil beam scanning treatment technique was used in all simulations. The proton plans were made with two fields, one from the front (0 degrees) and one from the right side of the patient (between 270-310 degrees), the latter depended on the anatomy of the patient. A representative proton treatment plan is shown in Figure 3.1.A.

Optimization Criteria

The same optimization objectives were used on all patients, but weighted to fit the individual patients. The objectives included, but were not limited to

- a uniform dose coverage of 40.05 Gy to the CTV,

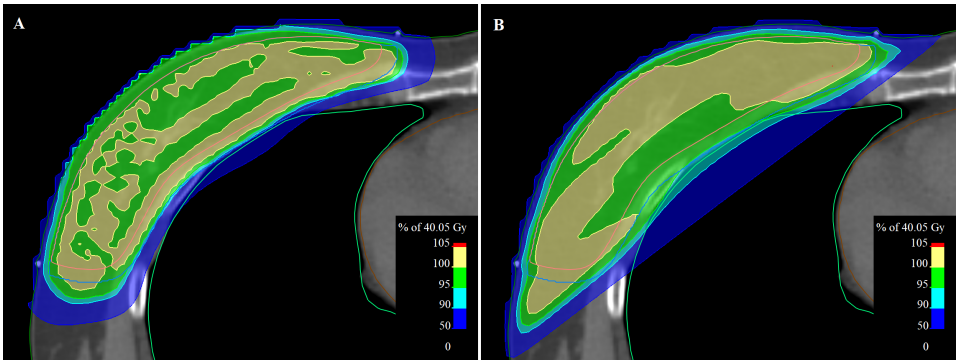

Figure 3.1: Representative treatment plans made with protons (A) and photons (B), shown on CT images. The CTV ■ is well covered with both modalities, with at least 95% of the prescribed dose. The proton plan has a sharper dose fall-off towards the right lung ■.

- a minimum dose of 39 Gy to the CTV (robust demand),
- a dose of at least 38 Gy to at least 90% of the PTV volume,
- 0 Gy to the heart and the contralateral breast,
- pushing the dose lower to the right lung, using appropriate DVH points.

The robust criteria used the minimax method explained in Section 2.4.2. The positioning of a patient was assumed to fluctuate randomly during the treatment course, following a three dimensional normal distribution with zero mean and a 1.96 $\times$ standard deviation = 5 mm in all three directions. Hence the 95% confidence interval of dose metrics was estimated, using the approximate value of the 97,5 percentile point of the normal distribution. The calibration error for density conversion was held constant at 3.5%. This accounts for the conversion from HU to electron density needed for the proton plan simulations, and was treated as a systematic error. It was assumed to follow a normal distribution with zero mean and 1.96 $\times$ standard deviation = 3.5% (95% confidence interval). These robust settings were chosen after consulting with medical physicists at the St. Olavs hospital and literature [23].

3.2.2 Photon Plans

Tangential fields were given to all the patients, using the 3D-CRT treatment technique. Two main fields were given in opposite directions, with 3-4 cm coverage to the air above the chest, giving robustness in the anterior direction. Additional fields (between 3 and 6) were added from the same directions, to obtain a satisfactory homogeneous dose coverage to the target volumes. The 3D-CRT modality

thus has an intrinsic robustness, as the dose distribution will not deviate much with change in the direction of the tangential fields or with swelling/enlargement of the breast. All the beams were generated using a 6 MV potential. A representative photon treatment plan is shown in Figure 3.1.B.

3.3 Robustness Evaluation

3.3.1 Mann-Whitney U Test of Treatment Plans

The Mann-Whitney U test was used to test whether sample means were equal or not. This non-parametric test was chosen over the more commonly used paired Student's t-test, as the sample size was small and the test statistics could not be assumed to follow a normal distribution. To determine whether parametric or non-parametric statistical test should be used, the one-sample Kolmogorov-Smirnov test was used on the data, to test the normality of the test parametrics. The null hypothesis (normal distributed data) was rejected at the 5% significance level, hence the non-parametric Mann-Whitney U test was preferred. The test was executed on values for the right lung (D_{avg}, $V_{20\text{Gy}}$ and $V_{8\text{Gy}}$), the heart (D_{avg}), the contralateral breast (D_{avg}), the external contour (D_{02} and $D_{2\text{cm}^3}$), the PTV (D_{avg}) and for the CTV (D_{98}, HI and CI). The test evaluated the total dose, for all patients. The HI was considered at 98% of the volume of the CTV, giving a $\text{HI}_{\text{RS}} = D_{98}/D_{02}$ as explained in Chapter 2.3.3. The CI was considered at the 95% isodose, 38.05 Gy. The two-sided hypothesis test was used, with a significance threshold set to 5%. At this point it was considered more interesting to further investigate $V_{8\text{Gy}}$ than $V_{20\text{Gy}}$ for the right lung. As protons gave lower doses to the lung, it was decided to investigate the less common values in the clinic, $V_{5\%}$ and $V_{20\%}$, which corresponds to $V_{2\text{Gy}}$ and $V_{8\text{Gy}}$, respectively, of the total dose.

3.3.2 Colormap

To visualize differences of a variable, the programming language Matlab has a built-in function called *imagesc()*. The code *imagesc(C)*, where C is a two-dimensional matrix, will display the data using a range of colors. One pixel in the resultant image will be specified by one element from C, and be given a color relative to the other elements of C. If m is the number of the rows, and n the number of the columns in C, the resulting image will be an m-by-n grid of pixels.

3.3.3 Perturbation Scenarios

To assess the robustness of the radiotherapy plans, perturbed doses were computed in RayStation's evaluation module. The DVHs of the original plan and the perturbed plans were exported to excel, and plotted in Matlab.

Normal Distribution

First, worst case scenarios of a big perturbations both in density and all the isocenter directions, were evaluated. It was considered not likely that all these events would occur at the same time. Further assessment of perturbed doses with isocenter and density changes drawn from a gaussian normal distribution was then considered, to randomly select a realistic perturbed dose. A script was written with guidance from developers at RaySearch, to run 1000 perturbed scenarios, with a density change drawn from a gaussian curve with 0 as mean and 2% change as the standard deviation, and isocenter shift in all three directions drawn from a gaussian curve with 0 as mean and 0.25 cm as the standard deviation. The various scenarios were then plotted in a DVH, and the spread gave an indication of the robustness of the plans.

After further consultation with RaySearch, it came to our attention that this type of evaluation is being incorporated in the new version of RayStation. As this tool could not be considered novel, other ideas for robustness evaluation techniques was considered. It was also of interest to separately investigate isocenter shift and density changes in regards to robustness of the treatment plans.

Isocenter Shift

If the isocenter of the treatment plan is shifted during treatment, the given dose distribution will differ from the planned. By studying changes of the given dose distribution depending on isocenter position, one can show in which directions the treatment plan is sensitive/robust. This methodology represents a setup error and/or patient positioning error. A script was developed that incrementally changed the position of the isocenter in the axial plane, including $\pm$ 1 cm in the x- and y-directions. With a step length of 0.1 cm, this gave in total 441 various perturbed scenarios, with (0,0) being the unperturbed dose, (1,1) being the perturbed dose with the isocenter moved 1 cm to the right (left in patient) and 1 cm in the posterior direction. A schematic figure of the isocenter shifts is shown in Figure 3.2.

Whilst perturbation settings drawn from a gaussian distribution gave an indication of how robust the overall plan was, it gave no indication of where the plan was sensitive to change. The incremental method of isocenter shifts was scripted in Python, for evaluation of various parameters, to evaluate the robustness in two dimensions. Each of the parameteres investigated was plotted in Matlab using the colopmap function. Running the script was time-consuming (up to 12 hours for one treatment plan), as 441 values had to be calculated for each parameter investigated. The choice of including an isocenter shift of $\pm$ 1 cm, was to include extreme scenarios, and the step length of 0.1 cm was chosen to get a good resolution in the colormaps explained in Section 3.3.2. The script calculated fraction doses. The

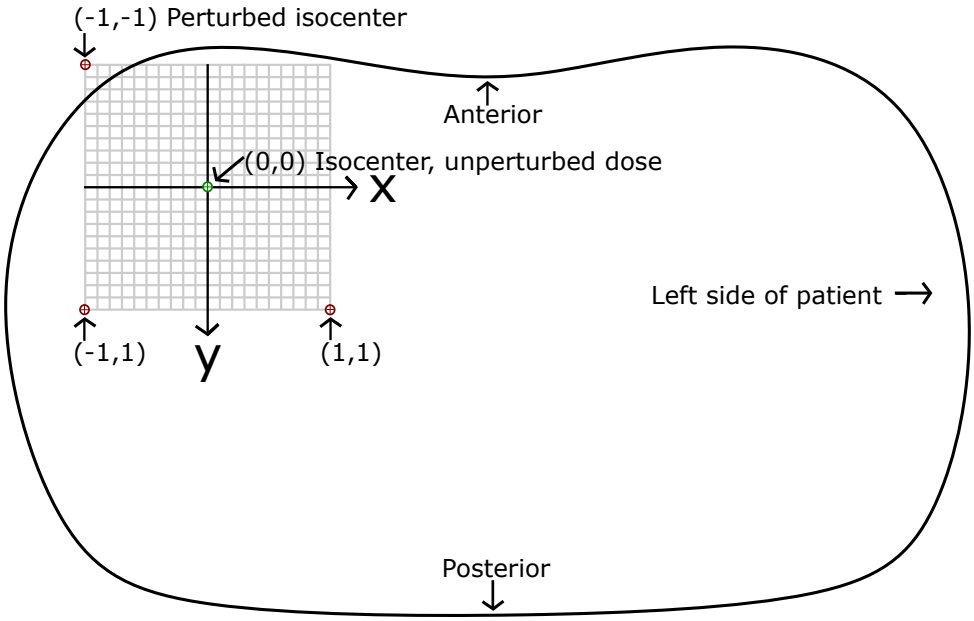

Figure 3.2: A graphic representation of the isocenter shift, with exaggerated dimensions of the x- and y-axis. The grid graphically represents the 441 isocenter positions evaluated for each patient.

parameters chosen for evaluation was

- for the CTV; D_{avg}, D_{50}, D_{min}, D_{98}, D_{02} and $V_{95\%}$,
- for the external contour; D_{max},
- for the right lung; D_{avg}, $V_{20\%}$ and $V_{05\%}$,
- for the heart; D_{avg} and D_{max}.

These parameters were chosen as they describe the coverage of the CTV and critical OARs. D_{98} is more commonly used in the clinic to evaluate the minimum dose to the CTV, than D_{min}, as the latter represents a single pixel. The D_{min} was chosen to be included to thoroughly investigate the lowest doses to the CTV, and how these colormaps changed relative to the D_{98}. The script is attached in Appendix B.a. It was considered to plot the colormaps in percentage difference from unperturbed value, instead of absolute values, as this gives a nice representation of robustness in terms of absolute fluctuation. As some of the absolute values were close to 0, a small change gave an extreme change in percent difference. This gave room for misinterpretation and thus it was decided to plot the colormaps in

absolute values. As percent change does give a good indication of robustness, the parameters from all patients were also plotted in boxplots as the percent difference from unperturbed value.

Hybrid Based Deformed Registrations

RayStation has many built-in functions in Python. As a comprehensive analysis of many images was the goal, a script doing the appropriate image deformations was made. The CBCTs acquired were not in Hounsfield units and dose calculation was not possible based on these image sets. To evaluate the planned dose actually delivered to the patient, it was desirable to view the fraction doses in the CBCT geometry. This methodology was developed in the previous project thesis [16], and represents the realistic perturbed dose distributions, including both isocenter and density perturbations.

The ANACONDA algorithm was used to create the displacement field between the CBCTs and the pCT. The density field was then deformed, creating DIRs with correct Hounsfield units which could be used for dose calculations. In this project the reference image was the CBCT and the target image was the pCT, with the external contour as a controlling structure, as explained in Section 2.4.3. When using controlling ROIs in the ANACONDA algorithm, it was considered important that they were well defined and were consistent between slices. Fusion view of the pCT and the CBCT was used to give an overview of the overall fit of the hybrid, deformable registrations. For evaluating the result of the deformed registration, each registration was visually inspected, and ROI geometry statistics and DVHs were compared. Specific interest was given to the dice similarity, which is the overlap between the geometry in the reference image and the target image after being deformed to the reference image, and the geometry in the target and reference image after being deformed to the target image. The value was between 0 and 1, with a higher value representing greater overlap. Dice similarities less than 0.80 were given special consideration, as this most often meant than the patient external geometry had changed significantly from the pCT external geometry. The volume of ROIs were also examined both in the target and the reference image sets, and considerable differences were checked in their consecutive original image sets. The resultant DIRs had the external contour from the CBCTs and the densities from the pCT, as shown in Figure 3.3.C, and could be used for dose calculations.

The function *CreateDeformedRegistration* was identified after consulting with RayStation developers in Sweden. A script was written implementing this and other functions, to extrapolate all the data available, and to create deformed image registrations between the pCT and the CBCTs. The script makes CBCT image sets appropriate for fraction dose calculations, by deforming the HU from the pCT to the individual CBCTs. The script is attached in Appendix B.b. In short, the script

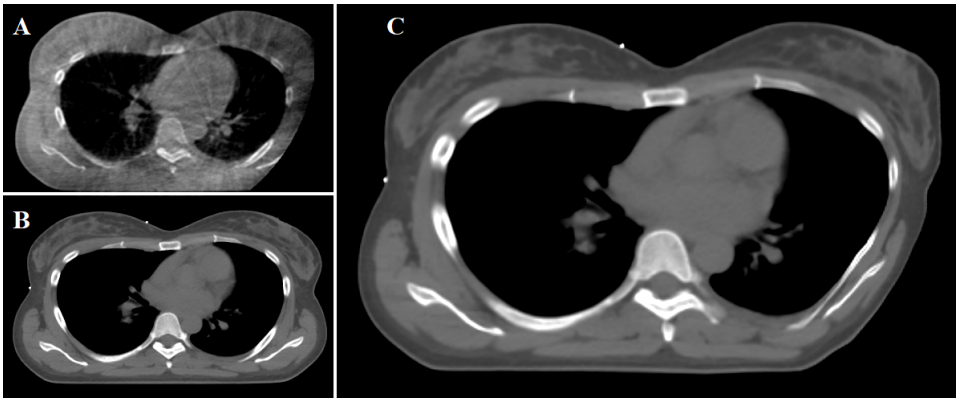

Figure 3.3: A CBCT (A), a pCT (B), and a DIR (C) of the same slice from the same patient. The limited field of view in the CBCT gives a similar cut-off in the DIR contour in the resultant image set.

can be summarized to:

1. Make a hybrid, deformable registration between the CBCT and the pCT. This aligned the two image sets and was used as input in step 3, where the densities were deformed.

2. Map ROIs from the pCT to the CBCT, using the ANACONDA algorithm, explained in Section 2.4.3.

3. Create deformed examinations, using the ANACONDA algorithm again. This correctly deformed the densities from the pCT to the CBCT, and created a new image set.

4. Copy ROIs from the CBCT to the new examination. This was satisfactory as the new examination had the same geometry as the CBCT.

5. Make a new hybrid registration between the pCT and the new examination. This was to correlate the two image sets, so that the dose could be deformed from the new deformed image sets back to the pCT. This step was needed for dose tracking of the individual fractions, to get the accumulated total dose.

Chapter 4

Results

4.1 Treatment Planning

Comparing the dose distributions from the treatment plans on the pCTs, gave an indication of target coverage and sparing of OAR. Initial statistical tests were run on data from the DVHs of these treatment plans. The planned accumulated dose (PAD) is the planned dose on the pCT. Representative DVHs of PADs for a photon and proton treatment plan are shown in Figure 4.1, and test statistics from all ten patients are shown in Table 4.1.

Table 4.1: Mann-Whitney U test results of the PADs, including data from all ten patients, except for the ■ contralateral breast (nine patients). U is the test statistic. The $D_{2\text{cm}^2}$ is the dose received by a 2 cm^3 region in the external contour. p = proton, γ = photon.

PAD	Median; p	Median; γ	U	p-value
■ CTV HI_{RS}	0.97	0.93	152.0	$< .001$
■ CTV CI	0.58	0.57	110.5	.705
■ CTV D_{98}	39.62 Gy	38.64 Gy	143.0	.005
■ PTV D_{avg}	40.08 Gy	40.01 Gy	47.0	.221
■ Heart D_{avg}	0.001 Gy	0.49 Gy	55.0	$< .001$
■ Left Breast D_{avg}	0.00 Gy	0.45 Gy	45.0	$< .001$
■ Right Lung D_{avg}	1.99 Gy	5.96 Gy	55.0	$< .001$
■ Right Lung $V_{20\text{Gy}}$	1.39%	12.22%	55.0	$< .001$
■ Right Lung $V_{8\text{Gy}}$	8.42%	18.32%	55.0	$< .001$
■ External D_{02}	40.03 Gy	40.04 Gy	101.5	.821
■ External $D_{2\text{cm}^3}$	42.02 Gy	42.22 Gy	52.5	.111

It was decided, that since the dose to the contralateral breast was so low, it would not be considered in the isocenter shift analysis. The CTV was the only

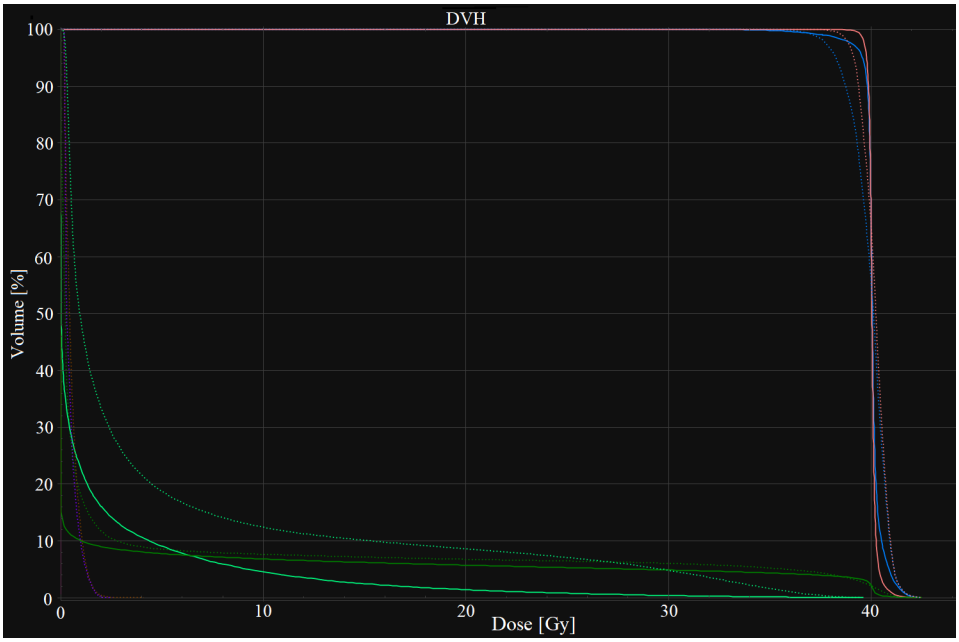

Figure 4.1: A representative DVH including both a proton plan (solid line), and photon plan (dotted line). The CTV ■, the PTV ■, the external contour ■ and the right lung ■ are clearly visible for both modalities, whilst the heart ■, and contralateral breast ■ lies close to 0 Gy for the proton plan, and in close proximity for the photon plan. Patient H.

target volume considered further. To more thoroughly investigate the robustness of the low-dose regions, it was decided to include the $V_{05\%}$, corresponding to $V_{2\text{Gy}}$ for the total dose, for the lung as well. After having planned photon and proton plans for all ten patients, with a focus on both sparing OARs and covering the CTV, the robustness of these plans were tested.

4.2 Isocenter Shift

The perturbed doses were calculated as explained in Section 3.3.3. The parameters were plotted in Matlab as colormaps, to visualize the change in absolute value with regards to isocenter shifts. Each parameter showed obvious trends. Only representative examples are included in this section, but all colormaps of all parameters investigated are available in Appendix A.a. Each parameter are shown for both the proton and photon modality, with a colorbar representing the interval of absolute values for that parameter from both modalities. The unperturbed values from the pCT are indicated in the (0,0) position, and the directions are as presented in Figure 3.2. Each parameter were also plotted in boxplots as percent difference from the unperturbed value. The boxplots are shown both for isocenter shifts up to

± 1 cm (441 values per patient) and isocenter shifts up to $\pm$ 0.5 cm (121 values per patient). The latter was used to exclude the most extreme values, which occured at isocenter shifts above 0.5 cm. All patients had a prescribed fraction dose of 2.67 Gy to the CTV.

4.2.1 CTV Coverage

Both modalities had good coverage of the CTV in the original plans. The D_{min} to the CTV gives an indication of where the DVHs start to drop from 100% coverage, and relating this to the D_{98} indicates how fast they are dropping. Figures 4.2 and 4.3 show representative colormaps for the minimum dose and the D_{98} of the CTV, respectively. Figure 4.4 shows the D_{02} of the CTV of a representative patient. The $V_{95\%}$ of the CTV is shown in Figure 4.5, for both modalities. The percentage difference from the unperturbed values for the CTV are shown in Figure 4.6, for all patients.

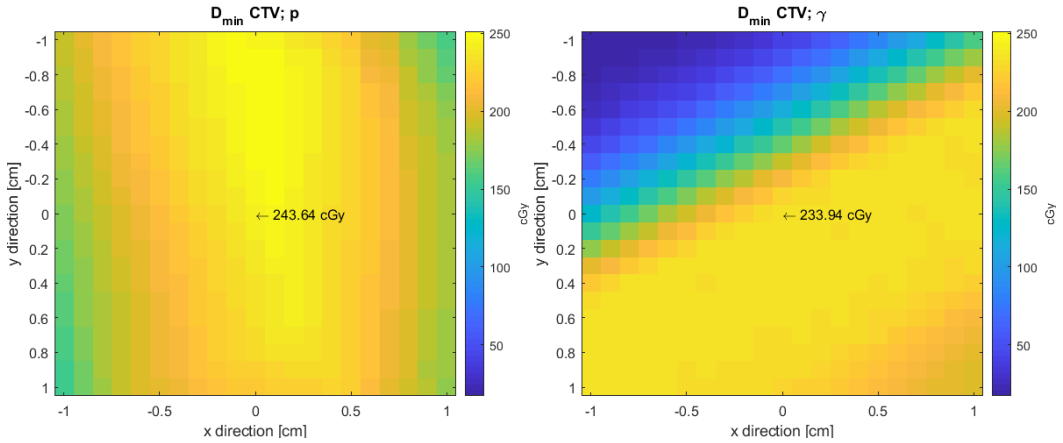

Figure 4.2: Representative colormaps of the D_{min} to the CTV. The axis represents the perturbation of the isocenter to the respective directions. Patient I, p = proton dose (left) with unperturbed value 2.44 Gy, γ = photon dose (right) with unperturbed value 2.34 Gy.

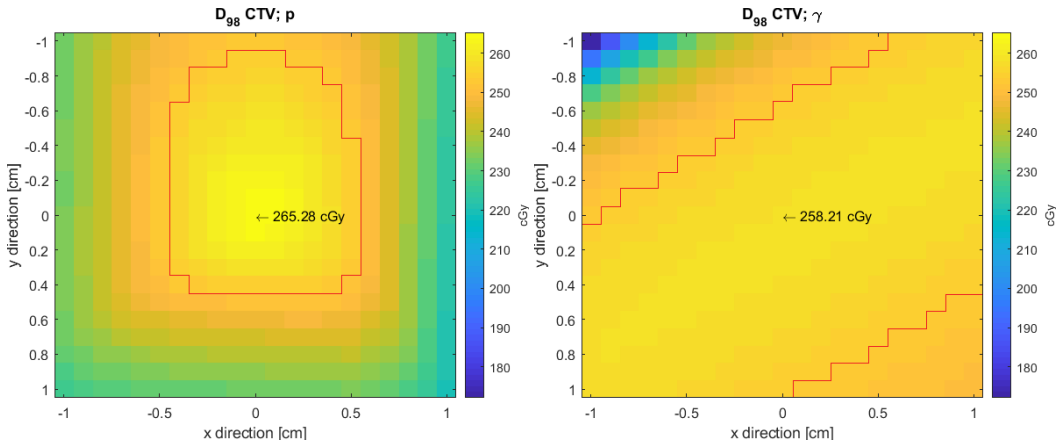

Figure 4.3: Representative colormaps of the D_{98} to the CTV, including the 95% isodose (red line). The axis represents the perturbation of the isocenter to the respective directions. Patient J, p = proton dose (left) with unperturbed value 2.65 Gy, γ = photon dose (right) with unperturbed value 2.58 Gy.

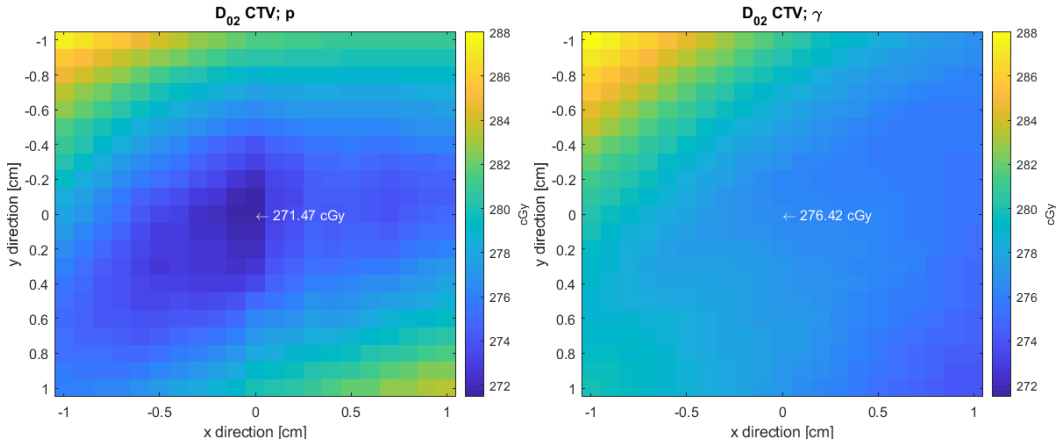

Figure 4.4: Representative colormaps of the D_{02} to the CTV. The axis represents the perturbation of the isocenter to the respective directions. Patient D, p = proton dose (left) with unperturbed value 2.72 Gy, γ = photon dose (right) with unperturbed value 2.76 Gy.

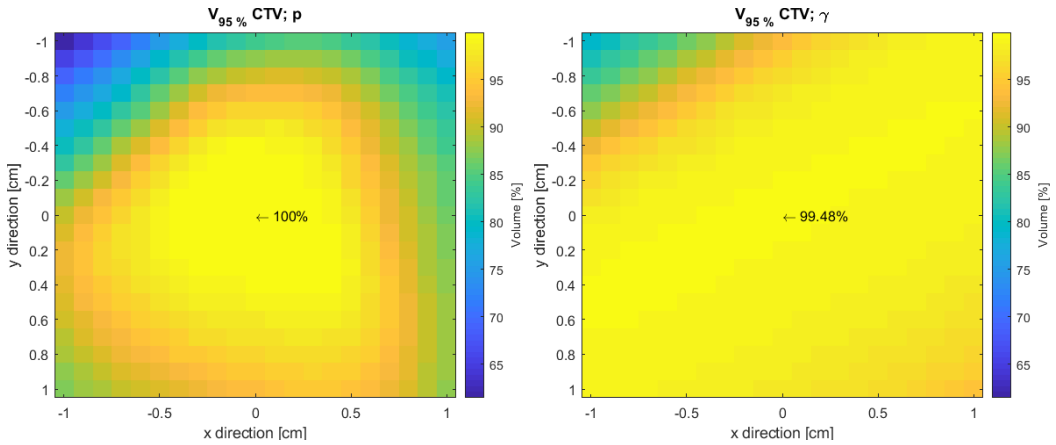

Figure 4.5: Representative colormaps of the $V_{95\%}$ to the CTV. The axis represents the perturbation of the isocenter to the respective directions. Patient C, p = proton dose (left) with unperturbed value 100%, γ = photon dose (right) with unperturbed value 99.5%.

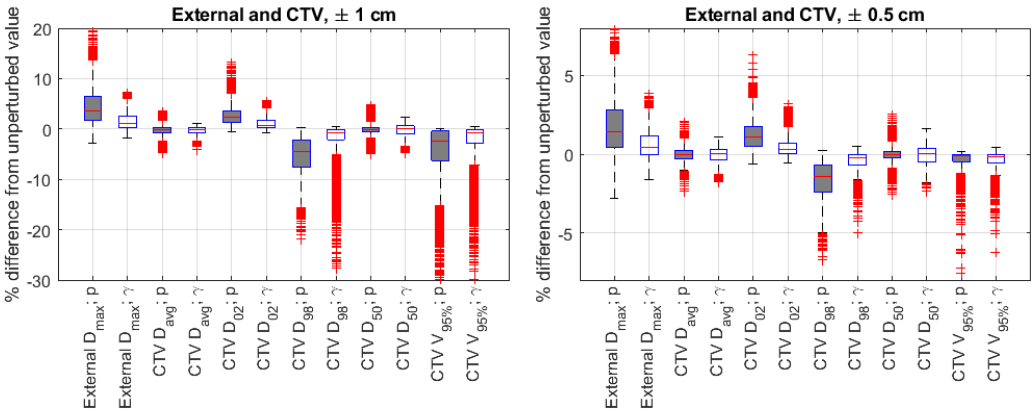

Figure 4.6: Boxplots of all values acquired for the external contour and the CTV with isocenter shift in the axial plane, represented as percentage change from the unperturbed value. To the left, perturbations $\in$ [-1, 1] cm are included, meaning that each boxplot has 441 $\times$ 10 values. To the right, perturbations $\in$ [-0.5, 0.5] cm are included, meaning that each boxplot has 121 $\times$ 10 values. The different intervals for the y-axis indicate that the plans were significantly more robust for isocenter shifts $\in$ [-0.5, 0.5] cm. p = proton (grey box), γ = photon (white box).

4.2.2 OAR Sparing

The colormaps for all the parameters of the right lung showed similar trends for each modality. Figure 4.7 shows the $V_{20\%}$ to the right lung, which equals the volume that received 0.53 Gy in each fraction, or 8 Gy of the total dose. Figure 4.8 shows the $V_{05\%}$ to the right lung, which equals the volume that received 0.13 Gy in each fraction, or 2 Gy of the total dose. As all patients had right-sided breast cancer, all received a very low dose to the heart, as shown in Figure 4.9. The colormaps from a representative patient, of the maximal dose received by the external contour is shown in Figure 4.10. The percentage difference from the unperturbed values for the right lung are shown in Figure 4.11, for all patients. All colormaps are attached in Appendix A.a.

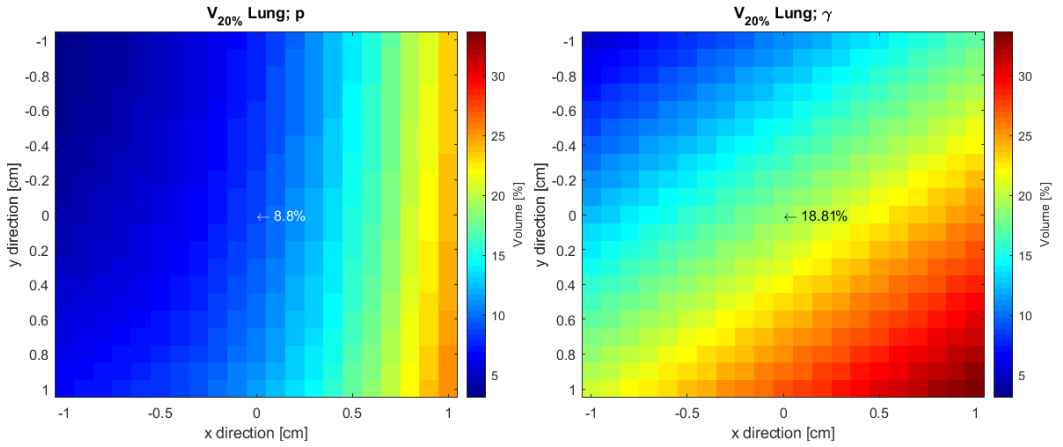

Figure 4.7: Representative colormaps of the $V_{20\%}$ to the right lung. The axis represents the perturbation of the isocenter to the respective directions. Patient D, p = proton plan (left) with unperturbed value 8.80%, γ = photon plan (right) with unperturbed value 18.81%.

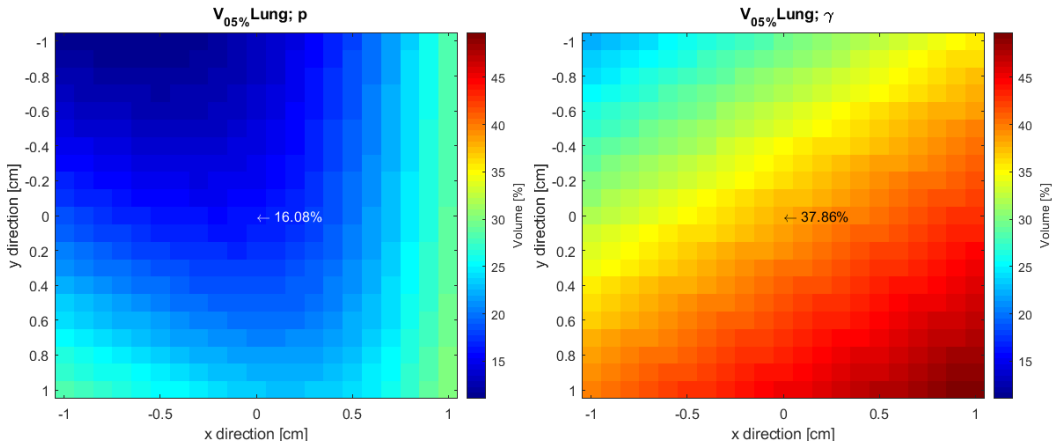

Figure 4.8: Representative colormaps of the $V_{05\%}$ to the right lung. The axis represents the perturbation of the isocenter to the respective directions. Patient G, p = proton dose (left) with unperturbed value 16.08%, γ = photon dose (right) with unperturbed value 37.86%.

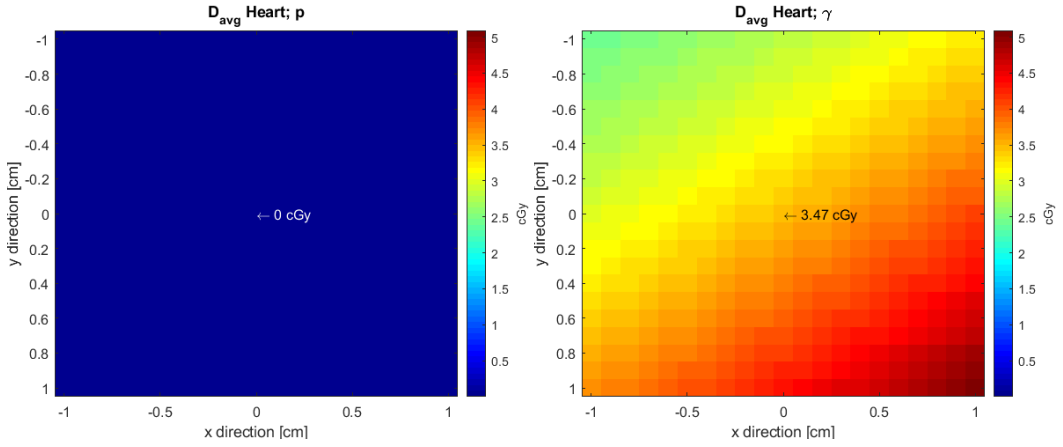

Figure 4.9: Representative colormaps of the D_{avg} to the heart. The axis represents the perturbation of the isocenter to the respective directions. Patient G, p = proton dose (left) with unperturbed value 0.0003 cGy, γ = photon dose (right) with unperturbed value 3.47 cGy.

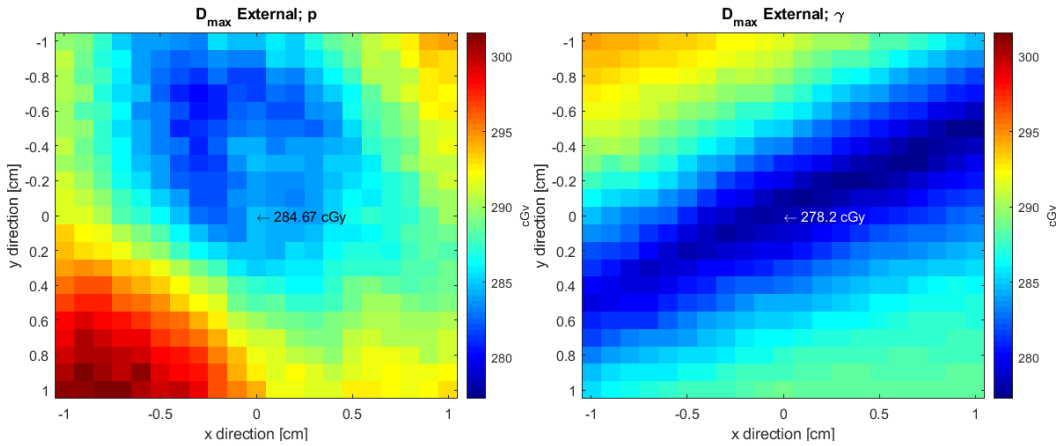

Figure 4.10: Representative colormaps of the D_{max} to the external contour. The axis represents the perturbation of the isocenter to the respective directions. Patient I, p = proton dose (left) with unperturbed value 2.85 Gy, γ = photon dose (right) with unperturbed value 2.78 Gy.

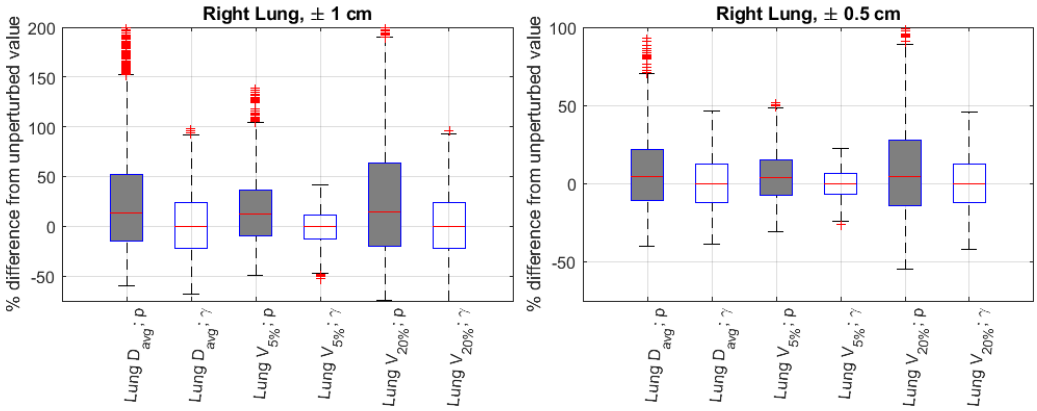

Figure 4.11: Boxplots of all values acquired for the right lung in the isocenter shift analysis. To the left, perturbations $\in$ [-1, 1] cm are included, meaning that each boxplot has 441 $\times$ 10 values. To the right, perturbations $\in$ [-0.5, 0.5] cm are included, meaning that each boxplot has 121 $\times$ 10 values. The different intervals for the y-axis indicate that the plans were significantly more robust for isocenter shifts $\in$ [-0.5, 0.5] cm. p = proton (grey box), γ = photon (white box).

4.3 DIR Analysis

After all DIRs between the pCTs and CBCTs were made, the accumulated delivered dose (ADD) could be calculated and compared to the planned accumulated dose. Figures 4.12 and 4.13 show representative DVHs for the two dose distributions. DVHs from all PADs and ADDs are shown in Appendix C. Table 4.2 shows median values and the results from a Mann-Whitney U test calculated on the ADDs, and is later compared with the similar table for the PADs, Table 4.1.

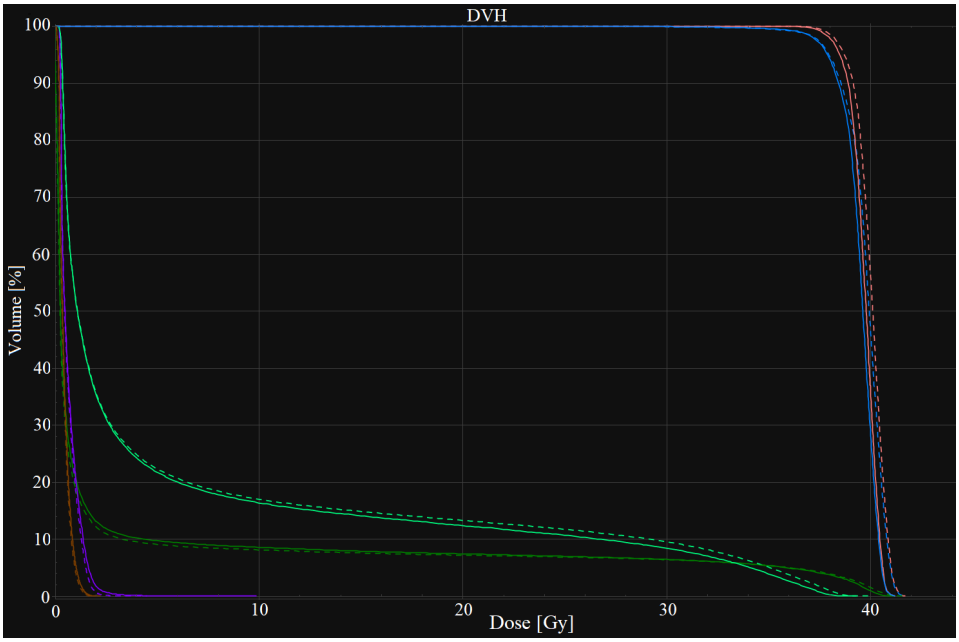

Figure 4.12: A representative DVH that includes the PAD (dotted line) and ADD (solid line) for a photon plan. The ROIs included are the CTV ■, the PTV ■, the right lung ■, the external contour ■, the heart ■, and the contralateral breast ■. Patient I.

The values from these two tables are plotted in absolute values as boxplots shown in Figures 4.14 and 4.15. The relative percentage changes in dose from the PAD to the ADD for selected organs and doselevels, are shown in Table 4.3.

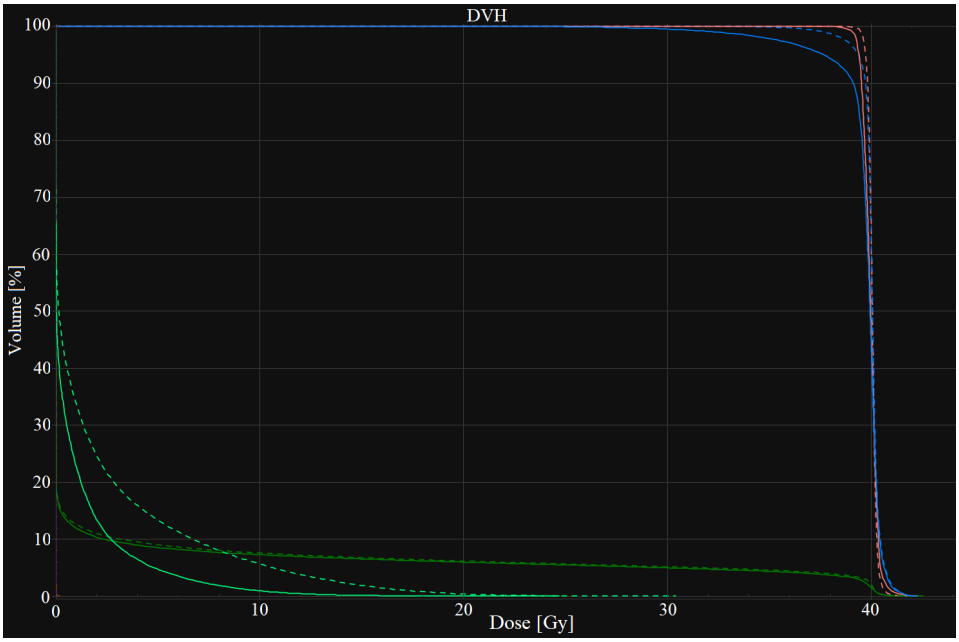

Figure 4.13: A representative DVH that includes the PAD (dotted line) and ADD (solid line) for a proton plan. The ROIs included are the CTV ■, the PTV ■, the right lung ■, and the external contour ■. The heart ■, and the contralateral breast ■ lie close to 0 Gy. Patient I.

Table 4.2: Mann-Whitney U test results of the ADD, including data from all ten patients, except for the ■ contralateral breast (nine patients). U is the test statistic. The $D_{2\text{cm}^2}$ is the dose received by a 2 cm^3 region in the external contour. p = proton, γ = photon.

ADD	Median; p	Median; γ	U	p-value
■ CTV HI_{RS}	0.96	0.93	139.0	.011
■ CTV CI	0.61	0.59	113.5	.545
■ CTV D_{98}	39.26 Gy	38.50 Gy	133.0	.038
■ PTV D_{avg}	39.95 Gy	39.94 Gy	39.5	.985
■ Heart D_{avg}	0.00 Gy	0.51 Gy	55.0	$< .001$
■ Left BreastD_{avg}	0.00 Gy	0.46 Gy	45.0	$< .001$
■ Right Lung D_{avg}	0.92 Gy	5.61 Gy	55.0	$< .001$
■ Right Lung $V_{20\text{Gy}}$	0.14%	11.54%	55.0	$< .001$
■ Right Lung $V_{8\text{Gy}}$	2.58%	17.57%	55.0	$< .001$
■ External D_{02}	39.97 Gy	40.00 Gy	103.0	.910
■ External $D_{2\text{cm}^3}$	41.99 Gy	41.86 Gy	65.0	.798

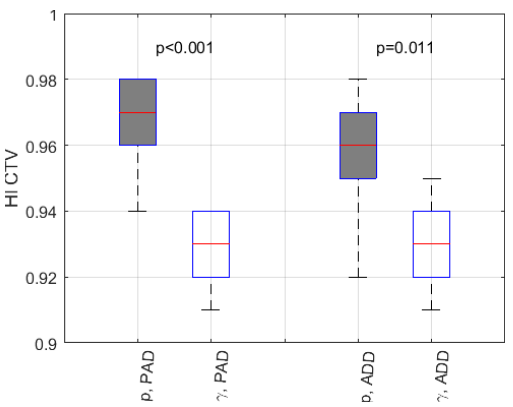

(a) HI of the CTV.

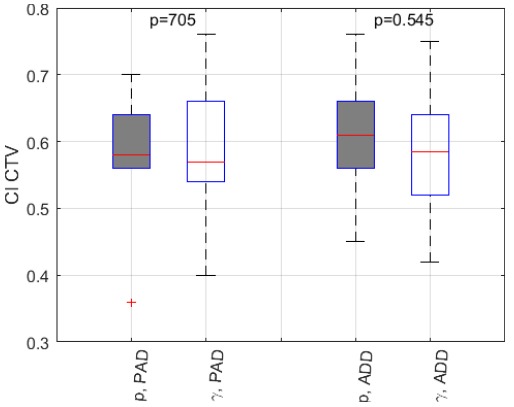

(b) CI of the CTV.

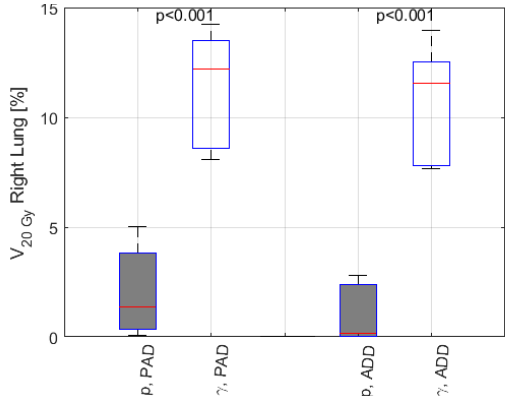

(c) The V_{20Gy} to the right lung.

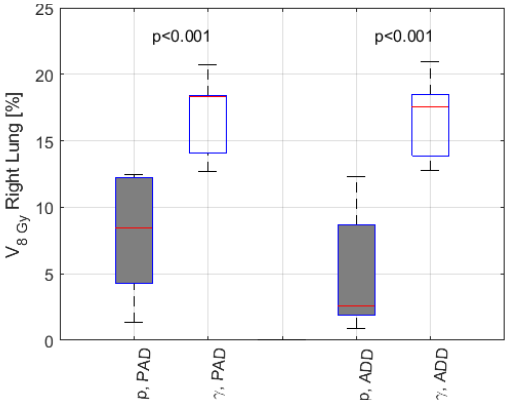

(d) The V_{8Gy} to the right lung.

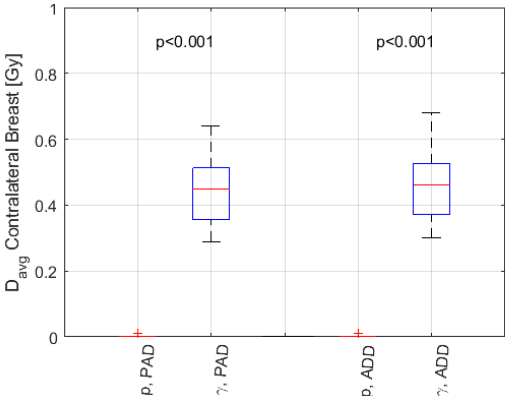

(e) The D_{avg} to the left breast (nine patients).

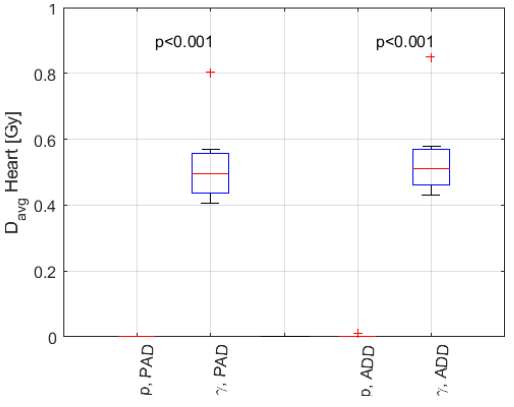

(f) The D_{avg} to the heart.

Figure 4.14: Parameters from the PADs and ADDs for both treatment plans, of all ten patients, plotted in absolute values. P-values were calculated with the Mann-Whitney U test. p = proton (grey box), γ = photon (white box).

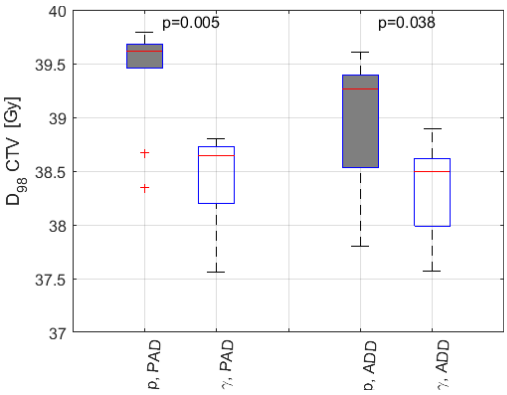

(a) The D_{98} to the CTV.

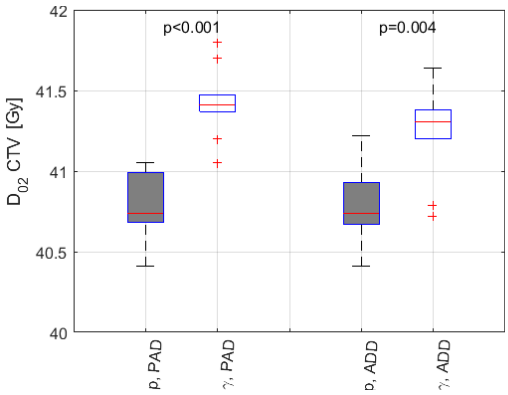

(b) The D_{02} to the CTV.

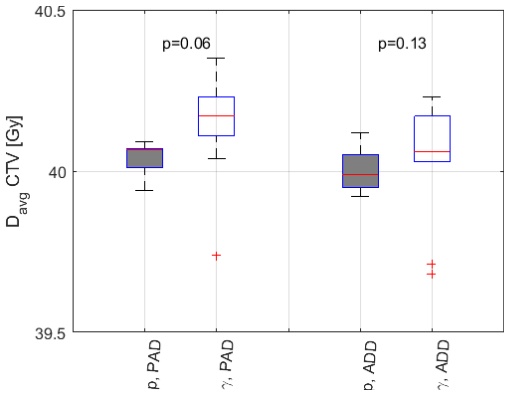

(c) The D_{avg} to the CTV.

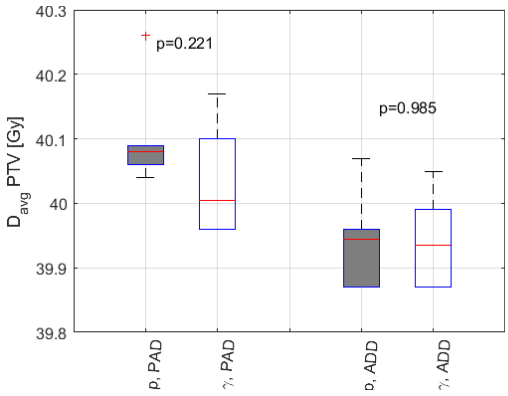

(d) The D_{avg} to the PTV.

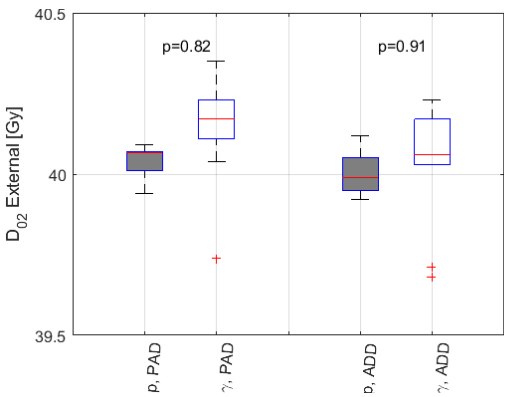

(e) The D_{02} to the external contour.

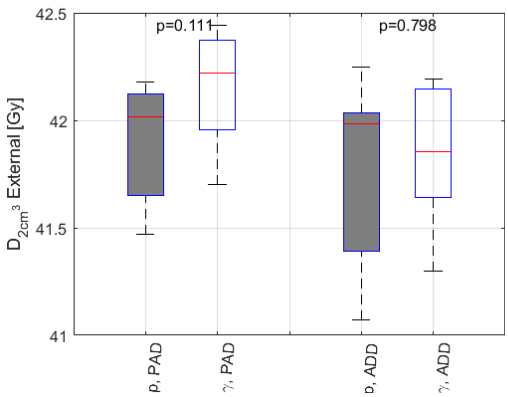

(f) The D_{2cm^3} to the external contour.

Figure 4.15: Parameters from the PADs and ADDs for both treatment plans, of all ten patients, plotted in absolute values. P-values were calculated with the Mann-Whitney U test. p = proton (grey box), γ = photon (white box).

Table 4.3: The average relative percentage change in dose for all patients, from the PAD to the ADD. p = proton, γ = photon. The average PAD value is given in parenthesis behind the relative change, all in the unit Gy.

Plan, organ	ΔD_{98} [%]	ΔD_{avg} [%]	ΔD_{50} [%]	ΔD_{02} [%]
p, CTV	-1.24 (39.41)	-0.37 (40.05)	-0.29 (40.16)	+0.07 (40.77)
γ, CTV	-0.31 (38.45)	-0.26 (40.14)	-0.24 (40.20)	-0.45 (41.43)
p, Right Lung	0 (0)	-30.10 (1.97)	-24.59 (0.10)	-29.09 (17.98)
γ, Right Lung	-0.20 (0.26)	-3.17 (5.57)	+1.20 (1.10)	-1.77 (36.29)
p, Heart	0 (0)	0 (0)	0 (0)	+48.61 (0.013)
γ, Heart	+8.92 (0.15)	+3.59 (0.47)	+1.58 (0.39)	+5.02 (1.25)
p, External	0 (0)	-0.42 (2.89)	0 (0.01)	-0.70 (39.92)
γ, External	0 (0)	+3.37 (3.48)	+1.42 (0.25)	-0.34 (39.87)

Chapter 5

Discussion

5.1 Trends

The goal of radiotherapy is to cure the cancer with the lowest cost, illustrated in Figure 5.1. The question at hand for this analysis is if a robust treatment plan is only obtained at the expense or sacrifice of OAR sparing. This analysis has investigated an isolated isocenter shift on treatment outcome, and the accumulated delivered dose on deformed image registrations between the pCT and CBCTs. The latter includes both isocenter positioning and anatomical changes, as it represents the realistic setup at each fraction given to the ten patients.

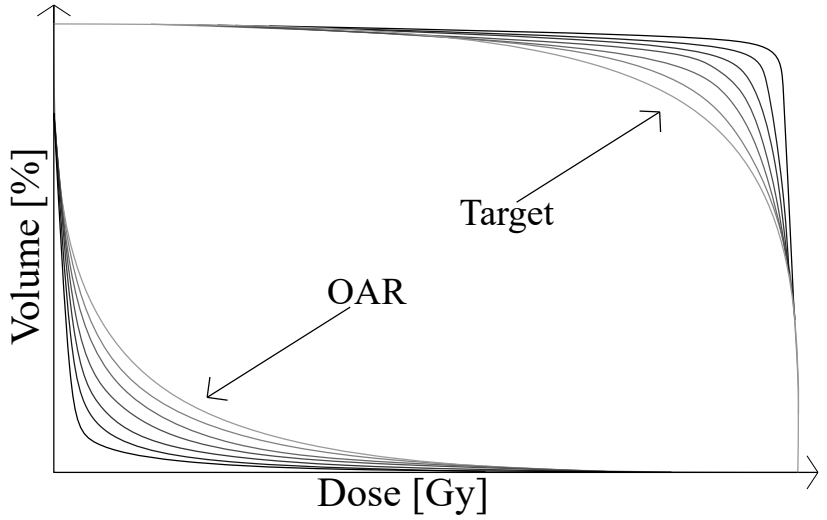

Figure 5.1: DVHs visualizing the overall goals of radiotherapy, which is to obtain good coverage of the target volumes, while reducing the dose to OARs as much as possible.

The isocenter shifts evaluated in this study include deviations up to $\pm$ 1 cm, which may be considered nonrealistic. Setup and range uncertainties are in the literature often dealt with using (0.3-0.6) cm margins for proton plans [8, 23]. Including the full range of $\pm$ 1 cm isocenter shifts, may thus be considered an exaggeration, but it does give a good indication of which directions the beam setup is robust/sensitive against, visualized in this thesis as colormaps. Density/anatomy changes is the other perturbation that may be hypothesized to play the most important role in dose deposition, particularly for protons. This statement is based on the stopping mechanism of protons, as explained in section 2.2.2. Future studies will follow, looking separately at simulations of density changes.

5.1.1 Target Coverage

Isocenter Perturbations

When comparing Figures 4.2 and 4.3 of the D_{min} and D_{98} to the CTV respectively, it is evident that the proton plans deliver doses closer to the prescribed dose (2.67 Gy) in the unperturbed scenario. The proton plans were as robust as the photon plans within $\pm$ 0.45 cm isocenter shifts for all ten patients, with regards to target coverage. As the proton plans were optimized to have a robust CTV coverage against displacements of 0.5 cm in all directions, our results supports that this critera was met. Beyond these isocenter shift, the protons plans did still cover the target volume, often to a greater degree than the photon plans up to $\pm$ 0.7 cm, except for patient B which is discussed later. Figure 4.3 shows the D_{98} of the CTV, including the 95$\%$ isodose curve, which is an absolute value above 2.54 Gy. These lines clearly show the robustness of the photon plan, in that the target coverage is insensitive to isocenter shifts in the direction of the tangential fields, as explained in Section 3.2.2. The two photon main fields were planned with an extra margin above the chest, which can explain the robustness of isocenter shifts to the right-posterior direction (worst case with isocenter in (1,1), isocenter shift to the patient's left). The photons plans are on the other hand not robust against isocenter shifts in the left-anterior direction (worst case with isocenter in (-1,-1), isocenter shift to the patient's right). This is clearly visible in the colormaps of the D_{98} shown for all patients in Appendix A.a, and Boxplot 4.6, where the values reach a 27$\%$ decrease when including perturbations $\in$ [-1, 1] cm. This coincides with expectations as the tangential photon fields are limited in the posterior, right (patient's left) direction, because of the lungs.

The 95$\%$ isodose for the proton plan in Figure 4.3 shows the trend for the D_{98} of the CTV, under isocenter perturbations. The proton plans were robust against movement of the isocenter in the anterior direction, and least robust against movement in the posterior direction. This might partly be explained by the fact that when the beams isocenter is moved closer to the lung, in the posterior direction,

one looses coverage to the front of the CTV. This is because of the field setup for these patients, as explained in Section 3.2.1, where the beam from the side might loose some coverage to the anterior, right (patient's left) part of the CTV when moved in the posterior direction.

The D_{02} of the CTV was for 9/10 patients lower for the proton plans in the unperturbed dose scenario. For patient C, the two modalities gave the same dose. On the other hand, the D_{02} colormaps indicate that proton plans can potentially give a greater high-dose volume than photon plans when subjected to isocenter shifts. The dose increases more quickly in these colormaps for the proton plans, and this occurs at isocenter perturbations that are smaller than for the photon plans, in 6/10 cases. Still, the dose does not exceed 2.80 Gy, 105% of the fraction dose, until a perturbation of at least $\pm$ 0.4 cm. The only exception is patient C, who was the thinnest patient in the group, and received higher D_{02} values when the isocenter was shifted in the posterior direction. For all ten patients, the dose increase from the unperturbed scenarios, from the D_{98} to the D_{02} of the CTV, was greater for the photon plans, indicating a sharper dose fall-off for the proton plans. The colormaps for the D_{min}, D_{98} and $V_{95\%}$ of the CTV all showed similar trends, for the respective modalities. These values were in 29/30 cases worse for the photon modality than the proton modality in the unperturbed isocenter cases. The D_{min} to the CTV was in general more robust for the proton treatment plans, translating to a more stable dose, closer to the prescribed dose, in all isocenter shift scenarios. The unperturbed values were also, in 9/10 cases, closer to the D_{98}, indicating a slower drop from the 100% coverage in the DVHs for the CTV, for the proton plans. The lower D_{min} values for the photon plans, representatively shown in Figure 4.2, may partly be explained by the build-up region stretching into the CTV, causing some pixels to have lower values.

The boxplots in Figure 4.6 and 4.11 has to be read with caution, as the absolute value may be closer to the desired value, even though the relative percentage change may be large. The boxplots can indicate robustness by evaluation of how much the values fluctuate, and it is evident that when including extreme isocenter shifts, $\in$ [-1, 1] cm, they fluctuate more than when only including less extreme isocenter shifts, $\in$ [-0.5, 0.5] cm. This indicates that the values differ more as the isocenter shift increases, in agreement with what is expected for perturbations of a smooth function. The boxplots including $\pm$ 1 cm isocenter offset fluctuated between -30% and +20% from the unperturbed values. It was the D_{98} and $V_{95\%}$ of the CTV, that differed the most, with the most extreme value of a 30% loss for the $V_{95\%}$ for a photon plan. When only considering $\pm$ 0.5 cm isocenter changes, all values fluctuated less, between -7.7% and +8% difference from the unperturbed value. Here, the proton modality consistently had a slightly wider spread than the photon modality, implying that the proton plans were less robust. The box-

plots represent values as a percentage difference from the unperturbed value of that modality. Thus, one must consider the unperturbed value. Take for instance the D_{98} of the CTV, which consistently lies higher for the proton plans, but did fluctuate more in percentage difference from unperturbed value. Looking at Figure 4.3, a representative colormap of the D_{98}, or even the least robust proton case, Figure 5.2, it is shown that the proton modality values lie closer to the prescribed dose than the photon modality, with isocenter perturbations between $\pm$ 0.3 cm.

When optimizing patient B's DVHs, a very low dose to the OARs was obtained in the proton treatment planning, shown in Figure 4 in Appendix A.a, whilst giving a good coverage to the target volumes. This can explain why patient B was most sensitive to isocenter shifts, in coverage of the CTV as shown in Figure 3 in Appendix A.a. Looking at Figure 5.2 of the D_{98} of the CTV for patient B, one still has satisfactory coverage of the CTV within $\pm$ 0.45 cm isocenter change.

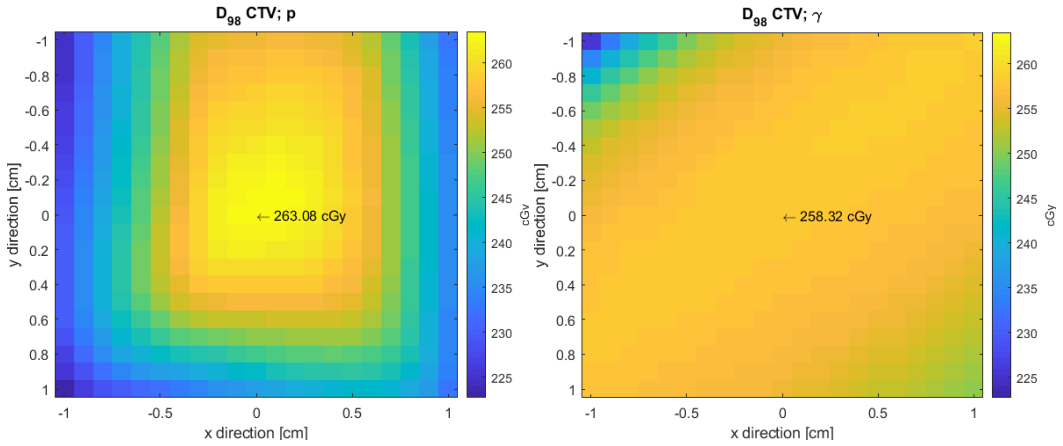

Figure 5.2: Colormaps of the D_{98} of the CTV, of the least robust patient treatment plan. The axis represents the perturbation of the isocenter to the respective directions. Patient B, p = proton dose (left) with unperturbed value 2.63 Gy, γ = photon dose (right) with unperturbed value 2.58 Gy.

The D_{avg} and D_{50} to the CTV were for both modalities well within $\pm$ 5% of the prescribed dose, for all perturbations scenarios, visualized in the colormaps in Appendix A.a.

DIR Analysis

When looking at Figures 4.12 and 4.13, and the remaining figures in Appendix C, of DVHs showing both the PAD and ADD for both modalities, some trends are evident. The proton plans does on average loose more coverage to the CTV from the PAD to the ADD, than the photon plans, but it should be noted that for all patients, the final accumulated CTV coverage is still on average better with

the proton modality. Figure 4.15a shows that the absolute value for the D_{98} of the CTV with the proton modality was significantly different from the photon modality (p = .038), with a mean value closer to the prescribed dose. The DVHs for the CTV with the photon modality showed a higher degree of consistency from the PAD to the ADD, emphasizing the robustness of the treatment planning.

Table 4.3 shows the average values for all ten patients, and the percentage difference from the PADs to the ADDs. Both modalities show satisfactory coverage of the CTV in both the PADs and ADDs, being above 95% of the prescribed dose (38.05 Gy) on average. The photon modality gave the worse result, with an ADD of D_{98} = 37.57 Gy to the CTV, seen in DVHs 27a in Appendix C. The results show that the coverage to the target volume was robust against the changes that these patients underwent during the course of the treatment, for both modalities.

5.1.2 OAR Dose Sparing

By evaluation of the isocenter shift colormaps (Figures 4.7, 4.8, 4.9 and 4.10) and the DIR analysis (Boxplots 4.14c, 4.14d, 4.14e and 4.14f), the proton plans did not sacrifice its beneficial OAR sparing. Though the proton plans did fluctuate more in percentage difference in OAR dose in the isocenter study, seen for the right lung in Figure 4.11, the doses were consistently lower than the photon doses to the same organs, for isocenter perturbation $\in$ [-1, 0.9].

The ADDs from the DIRs showed a lower delivered than planned dose to the right lung, for the protons. Taking a closer look at the percentage difference from the PAD to the ADD for the OARs, Table 4.3, there is a substantial drop in the average right lung dose with the proton modality, -30.10% from 1.97 Gy. What is interesting to see is that the drop for the photon plans is much smaller, -3.17% from 5.57 Gy. The same trend was seen for the D_{98}, D_{50}, D_{02} of the right lung. When looking at Figures 4.12 and 4.13, and the remaining figures in Appendix C, it is evident that the dose to the right lung on average decreased from the PADs to the ADDs for both modalities, for all dose levels. This might be explained by a patient setup deviation, movement of the isocenter in the right-anterior direction, or swelling of the breast, or an overestimation of lung dose for the proton PADs. Another contribution to this result may be the production of the CBCTs, which are generated over some time, without respiratory gating. This can produce some HU deviation in the image set due to respiratory motion, affecting the range calculations of protons, causing an underestimation of dose to the lungs for the ADDs. The DVHs from the photon DIR analysis for the right lung showed a higher degree of consistency throughout the dose levels from the PADs to the ADDs. This emphasizes the robustness of the photon treatment planning, which in terms of sparing of OARs is not beneficial. The robustness of the photon plans in the tangential field plane limits the sparing of the lungs.

The patients in this study did have lower dose values to the OARs with the proton modality than the photon modality. All results presented indicates that the sparing of the OARs is not lost even if the proton plans are made robust. This statement is based on a limited patient selection, and can not be generalized without further investigations. The dose to the right lung increases for both modalities with isocenter perturbations to the right (patiens left), as shown in Figures 4.7 and 4.8, which coincides with expectations. The results from the isocenter perturbation scenarios indicates that the proton plans are as robust as the photon plans in regard to sparing of OAR. The colormaps for all patients are attached in Appendix A.a, and by visual inspection of these, it is evident that for the proton treatment, the percentage difference might fluctuate more, but the delivered dose to the OARs are on average much lower than for the photon treatment. An exception is for patient C, with an isocenter shift 1 cm to the right in the colormap (patient's left), where the lung dose is higher for the proton plan. Patient C was the thinnest patient in the group, which might explain this larger dose increase than for the other patients. In contrast to this was patient F, the thickest patient in the group, who had more stable low doses to the OARs even with $\pm$ 1 cm isocenter perturbations for the proton modality.

The p-values $<$ .001 for average dose to heart, contralateral breast and lung, and V_{20Gy} and V_{8Gy} of the right lung, indicate that by the Mann-Whitney U test one can reject the null hypothesis of equal medians between the two modalities for these values, at the 5% significance level. This is shown in Boxplots 4.14c, 4.14d, 4.14e and 4.14f, and the results persists from the PADs to the ADDs. This show that all parameters investigated for the right lung, the heart and contralateral breast received a significantly lower dose from the proton plans than the photon plans (p $<$ .001). To investigate the high-dose volumes, a 2 cm^3 region of the external contour was evaluated. Boxplot 4.15f shows that the median value for the ADDs were higher for the proton plans than the photon plans, but this result was not significant (p = .798). By comparing the DVHs presented in Figures 4.12 and 4.13 it is evident that the external contour received a lower average dose from the proton plans than from the photon plans. All these factors may contribute to lower risks of secondary malignancies.

A study analyzing radiation doses to the heart and the risk of ischemic heart disease showed that there exists no lower dose limit for risk, but that the relative risk increased with 7.4% per Gy in average dose to the heart [29]. This estimation was done using a logistic regression model. The average dose to the heart ranged from 0.41 Gy to 0.80 Gy for the photon PADs (mean, 0.49 Gy), and were all below 0.003 Gy for the proton PADs (mean, 0.001 Gy). The ADDs showed a small increase in heart dose for the photons, ranging from 0.43 Gy to 0.85 Gy (mean, 0.51 Gy), as shown in Boxplot 4.14f. The PADs and ADDs for the average

heart dose for both modalities, were well below the national recommendation of a maximum 2 Gy D_{avg} to the heart, as explained in Section 2.4.8. As the rate of heart disease increases proportional with the mean dose to the heart, decreasing the exposure will also decrease the probability of later complications.

An article studying the potential reduction of dose to the OARs for left-sided breast cancer patients, found that IMPT plans pose a greater potential in reduction of the risk of late-toxicities than comparative IMRT and 3D-CRT. The risk of lung and cardiac toxicity is especially worrying in the long term for young patients, because of their long-life expectancy. The study showed that the mean lung dose was reduced from (15.0 $\pm$ 2.0) Gy for IMRT photon plans to (7.0 $\pm$ 3.0) Gy for proton plans, and the mean heart dose was reduced from (12.0 $\pm$ 2.0) Gy for the IMRT photon plans to (1.0 $\pm$ 1.0) Gy for the proton plans [30]. These results were from ten left-sided breast cancer patients, who received local radiotherapy limited to the breast. This thesis investigated right-sided breast cancer patients, but the results still coincide with expectations.

Figures 4.7, 4.8, and 4.9 show that proton radiation spare the low dose regions more than with photon radiation. This was confirmed in the DIR analysis, where the D_{20Gy} of the right lung ranged from 0% to 2.82% for the proton ADDs (mean, 0.14%), and from 7.65% to 13.97% for the photon ADDs (mean, 11.54%), shown in Boxplot 4.14c. As explained in Section 2.4.8, the recommendation for a 2.67 Gy $\times$ 15 fractionation regime is a $V_{18\text{Gy}} \leq 15\%$ for the lungs. As $V_{20\text{Gy}}$ is more commonly used in the clinic, it was the parameter investigated in this work. Still, our results clearly shows that the proton modality were well below the national recommendations. The D_{8Gy} of the right lung ranged from 0.92% to 12.28% for the proton ADDs (mean, 2.58%), and from 12.77% to 20.93% for the photon ADDs (mean, 17.57%), shown in Boxplot 4.14d. Long term follow-up studies are needed to assess the benefit of this reduction. A study following 558 patients treated with proton radiation and 558 patients treated with photon radiation for various types of cancers, concluded that proton therapy is not associated with a significantly higher risk of radiotherapy induced secondary cancers compared to photon therapy [3]. They found 29 incidents in the patients treated with proton radiation and 42 incidents in the patients treated with photon radiation of second malignancies, and called for longer follow-up studies to determine if proton therapy poses a significant reduction in risk of radiotherapy induced cancer.

The theoretical advantage of protons is supported in this project, obtaining a lower dose to OAR, while fulfilling the coverage of target volumes. In a study investigating cardiac toxicity after delivered photon plans vs. simulated proton plans [28], they found that the predicted risk of cardiac toxicity was reduced by 2.9%, and the risk of breast cancer recurrence was reduced by 0.9% with the proton plans. Cardiotoxicity risk was in this study estimated with the logistic regression

model mentioned above [29]. Tables 4.1 and 4.2 showed that the average dose to the heart was significantly lower for the proton treatment, with $p < .001$, at the 5% significance level. This was a study of right-sided breast cancer patients, and neither modalities delivered high doses to the heart. Still, in radiation therapy, one should always strive for reduction of dose to the OARs. For left-sided breast cancer patients, and more complex patients with parasternal node involvement, the potential benefit of proton therapy will perhaps be more evident in the sparing of dose to the heart.

In Appendix A.b the boxplots of the isocenter shifts of the heart are included. These gave room for misinterpretation as the absolute value for the heart from the proton plans were extremely low, as discussed in Section 5.1.1.

5.1.3 HI and CI

The p-value below .001 for the HI by the Mann-Whitney U test indicates that one should reject the null hypothesis of equal HI medians at the 5% significance level for the PADs. Boxplot 4.14a of the CTV's HI for both modalities, showed that the HI was still significantly higher in the ADD evaluation, but to a lower degree. The HIs ranged from 0.94 to 0.98 for the proton PADs (mean, 0.97), and from 0.91 to 0.94 for the photon PADs (mean, 0.93). For the ADDs the HIs ranged from 0.92 to 0.98 for the protons (mean, 0.96) and from 0.91 to 0.95 for the photons (mean, 0.93). The median HI values for the photons were in the PAD and ADD lower than the protons, but were also more robust in the sense that the median value did not change much and fluctuated less. The same comparison between the CI gave less conclusive results, with a p-value of .71 for the PADs and .55 for the ADDs, shown in Boxplot 4.14b. The CIs ranged from 0.45 to 0.76 for the proton ADDs (mean, 0.61), and from 0.42 to 0.75 for the photon ADDs (mean, 0.59). Neither modality achieved ideal conformation, and there was only a marginal advantage of using protons. Using more conform photon delivery methods, such as IMRT or VMAT, or using more beams for the proton setup, could have increased the CI.

5.2 Parameter Choice

CTV and OAR

Section 3.3.3 explains how the program for calculating perturbed doses with isocenter shifts works. The parameters selected for the target volume and OARs were chosen based on what is commonly used in the clinic, and additional parameteres were chosen as they gave good indications of robustness, either alone or in relation to other values. The $V_{20\%}$ was chosen to be written this way, as the isocenter script analyzed fraction doses, thus giving small doses. Future developments of this script should ideally include three dimensions, and a summation of all the fractions. The user could then choose an isodose they want to observe for a target

or OAR volume, and evaluate the three dimensional figure. This would give information about how big deviation in all directions the plan is robust against isocenter shifts, for a given isodose.

Other dose levels could have been investigated in the isocenter analysis, such as the $V_{20\text{Gy}}$ and $V_{18\text{Gy}}$ for the lung. As the initial results from the PAD on the pCTs gave low volumes for the $V_{20\text{Gy}}$, it was decided to further investigate only lower doses in the isocenter analysis. Thus, the $V_{05\%}$ and the $V_{20\%}$ was included to evaluate the low dose regions. As the volume that receives 20 Gy is much used, it was studied in the DIR analysis. It could have been prioritized in the isocenter analysis as well. The maximum dose to the heart could have been excluded from the isocenter perturbations, as this value is not commonly used in the clinic, and only represents a single pixel. The $D_{2\text{cm}^3}$ to the heart could have been included instead, but as the dose levels were relatively low, it was considered sufficient to investigate the D_{avg}. The initial results for the contralateral breast also showed very low doses, and was decided not to be included in the isocenter shift analysis.

HI and CI

Future studies should investigate various isodose levels for the CI, and various dose levels for the HI. Geometric and dosimetric data is incorporated in the two indices. With improving algorithms for tumor control probabilities, normal tissue complication probability and equivalent uniform doses in treatment planning systems, future homogeneity studies could perhaps incorporate such radiobiological parameters. Such an integration would give qualitative indicators of the probabilistic data, and could give better quantitative data of a HI based on radiobiologic characteristics, and not merely from doses and volumes.

External contour

The only value drawn from the external contour in the isocenter shift analysis was the maximal dose. This is in fact only one pixel, and not of high clinical relevance. The colormaps still paints a picture indicating a higher, and perhaps larger high-dose region with proton compared to photon radiation. The drawback of investigating a pixel value was realized after all simulations had run. Thus the investigation of the maximum dose to a 2 cm^3 region was only included in the DIR analysis. Boxplots 4.15e showed that the proton plans actually delivered a lower D_{02} than the photon plans to the external contour, but these result were not significant at the 5% significance level with the Mann-Whitney U test. The protons gave in the ADDs a D_{cm^3} ranging from 41.07 Gy to 42.25 Gy (mean, 41.99 Gy), while the photons in the ADDs gave between 41.3 Gy and 42.19 Gy (mean, 41.86 Gy), as shown in Boxplot 4.15f, but neither of these result were significant at the 5% significance level with the Mann-Whitney U test. This was a change from the PADs, where the proton plans gave a lower mean D_{cm^3} of the external contour

than the photon plans. The proton plans fluctuated more between fractions than the photon plans, but all values were close to 105% of the prescribed dose. Further analysis of the high-dose regions are needed, and could include an analysis of the 105% isodose, and its change after impact of perturbations.

5.3 Scripting

Isocenter Perturbed Doses

As stated in Section 5.2 future developments for the isocenter evaluation tool of robustness are thought of. The robustness of proton dose distribution does depend on the precision of setup in regards to the planned isocenter as investigated in this study. Future studies could include a weighting of isocenter shift in the different directions, perhaps drawn from a normal distributed probability curve, as discussed in Section 3.3.3. The sharp distal fall-off does give the considerable benefit of sparing normal tissues, but increases the dependency of density heterogeneities within a patient. With IMPT, the varying patterns of proton fluence may get even higher delivery-uncertainties than passive scanning techniques.

Future work could include a similar model as the one presented here for the isocenter shift, to separately address the sensitivity of density changes. By incrementally adding and removing tissue in front of the tumor, under the skin, one can simulate seromas and swelling. Such a tool can be used to evaluate what density deviation is allowed to still give satisfactory doses both to target volumes and OARs. Inclusion of the z-direction will give indications for the craniocaudal coverage, and a summation of all fraction doses will give dose levels that are easier to evaluate. By including all perturbations in the same script, one can assess worst case scenarios for both modalities, and compare this with DIRs between pCTs and CBCTs. Such evaluation tools can be used for robustness analysis, but also as a guidance tool prior to treatment. By running the script, with a larger step-length to decrease simulation time, one could visualize in which directions the treatment plan is sensitive, and pay special attention to these regions when positioning the patient.

DIR

The methodology described in this thesis of making deformed pCT-CBCT registrations, is also well suited for post- and intermediate-evaluation of treatment plans. The procedure of treatment adaption is time consuming, and not necessary for all patients. By assessing DIRs between pCTs and CBCTs, patients that can benefit from an adapted plan can be identified. If, after some fractions, the OAR constraints or the target coverage criterions are not met, changes in the treatment plan should be considered to avoid discrepancies. Further investigations of breast cancer patients will give an indication of how often, and in which cases, re-planning

should be used. Creating the DIRs is relatively fast (minutes), and should be incorporated in cases where the physician/radiotherapist finds significant change in the geometry in the CBCT from the pCT.

Evaluation of the quality of the DIR must always be addressed. J. Pukala *et al.* [31] assess the performance of five different deformable image registration algorithms, and conclude that the uncertainties of these image sets should be considered for clinical cases. As more treatment planning systems get deformable image registration modules integrated, there is a need for caution and acknowledgement of risk for deviations. Evaluation procedures, briefly explained in Chapter 3.3.3 should be standardized and extended.

5.4 Patients and Treatment Planning

The outline of the remaining sections are partly based on a project thesis done prior to this master thesis [16]. The patient group of this study were all right-sided breast cancer patient. The potential benefit of proton treatment would perhaps have been more profound if studying left-sided breast cancer patients, where the heart is more exposed. As an initial incorporation of robustness evaluation tools, only 10 similar patients were investigated. It will be interesting to follow similar robustness analyses of more complex cases and larger patient groups. This study included no patients with dramatic seromas or swelling. Proton plans may in such extreme cases not deliver satisfactory doses to the target volumes, in the sense that the tumor cells might not all be killed, while photon plans are more robust against such changes. The benefit from proton therapy over photon therapy is evident for breast cancer patients, in the sparing of critical OARs, but long term follow-ups are needed to evaluate the side effect frequency and late effects [9].

Tumor positions that are highly dependent on internal movements will inevitably decrease the robustness of treatment plans with sharp dose gradients. Advancements in organ delineation, robust optimization and patient immobilization as discussed in this section, can further improve the outcome of radiation therapy, and the benefit from protons may then become more profound.

It should be noted that all plans were made by an untrained student, but were approved by a medical physicist.

5.4.1 Beam Angles and Patient Positioning

Two separate proton beam angles were used on all patients. Loma Linda University Medical Center uses 2-4 beam angles for breast cancer patients [6]. Future simulations could investigate the use of more beam angles, to further increase tumor control and decrease normal tissue doses.

The standard patient position for breast cancer patients at St. Olavs hospital is the supine position. By changing to the prone position, gravity will allow the breast

to be pulled away from the chest wall and OARs. This could, for both proton and photon therapy, keep the radiation in front of the ribs to a larger extent, as shown in Figure 5.3. This position would also decrease the effect of respiratory motion [7].

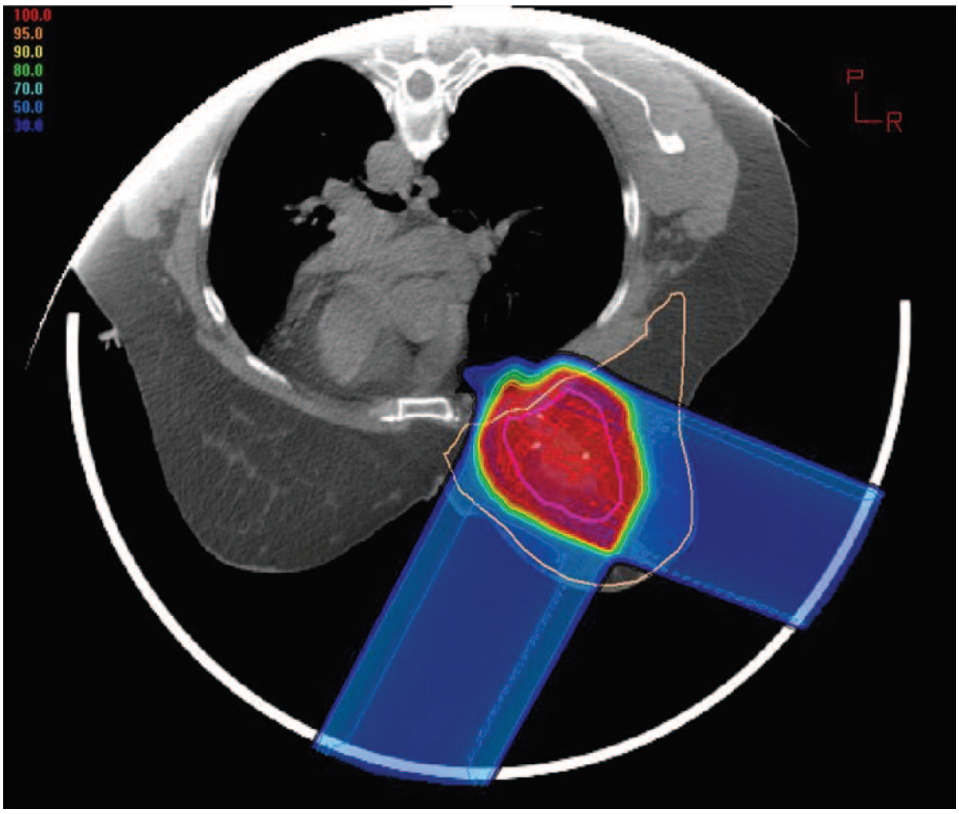

Figure 5.3: The advantage of a prone patient position for breast cancer radiotherapy is demonstrated by a proton treatment plan, with very little dose to the OARs. The dose-wash ranges from 30% (dark blue) to 100% (red) of the prescribed dose. The pink contour inside the red isodose is the GTV. Courtesy of [7].

5.4.2 Volume Delineation

It can be argued that treatment plans with sharp dose gradients are particularly dependent on precise volume delineations. With improving radiation techniques, the image guiding and organ delineation must follow its phase of development. Volume delineation today is associated with a high degree of uncertainty. The target volume itself has uncertainties which include, but are not limited to, inter- and intraobserver variability, organ motion, patient setup and movements. A review of

119 articles, studying delineations of GTVs and CTVs, showed a lack of consistency in conducting and reporting analyses, between observers [32]. A need for a standardized framework is acknowledged. Tumor delineation may be considered the weakest link in the search for accuracy in radiation therapy [33]. Other limitations lies for instance in the accuracy of analytical dose calculations and in the density accuracy of the planning CTs. Magnetic resonance (MR) imaging gives a better soft tissue contrast than CTs. MR-LINAC systems are in development, and will enable physicians to visualize structures during treatment, with perhaps the ulimate objective to adapt the plan in realtime for precise dose depositions. MRI-only workflow eliminates the need for CTs, and gives greater confidence and accuracy in delineation and intrafraction assessment [33]. Intra- and interobserver variability are today considered in the internal target volume, as described in Section 2.3.1. It will be interesting to follow the technology of automated organ segmentation, using machine learning algorithms and deep neural networks. This development has the potential of giving more precise organ delineation, and eliminating the errors of observer variability [34].

PTV Concept

The ADDs of the proton plans in Figure 4.13 and in Appendix C, shows that the proton plans loose coverage to the PTV compared with the PADs. This was not at the compromise of CTV coverage. This fact emphasizes that the ADDs for the PTV have no clinical relevance, as the volume is defined for treatment planning to ensure CTV coverage during the course of the treatment. Future investigations could include robust demands on the PTV as well, which would perhaps compromise the OAR sparing.

Planning with margins outside the CTV is the traditional way to handle motion and setup uncertainties in radiotherapy [9]. There are several limitations of the margin treatment planning concept described in Section 2.3.1. The approach may be suboptimal in terms of normal tissue sparing for conform treatment fields, if even peripheral parts of the PTV is given the prescribed dose. For non-conformal plans there will be inherent dosimetric margins and additional margins beyond the GTV should be unisotropic [23]. When using IMRT and proton therapy with a high degree of conformity, the definition of a PTV itself becomes obsolete, because of robust treatment planning. The advancement of computer programming, robust optimization and imaging technology, poses the question if planning with PTVs may be an excess, and should perhaps not be used in the future.

Skin Dose

As explained in Section 2.2.3, the photon modality has an inherent skin sparing characteristic, because of the build-up region of the dose deposition. Though the dose to the skin was not subject of this thesis, it is important to note that proton

radiation may deliver a higher skin dose. By rigid immobilization of patients, and optimization with a skin contour, one can strive to shape the proton beams in a way to keep the 90% isodose line below the surface of the skin, and in that way limit the skin toxicities to an acceptable level. A clinical investigation following 100 breast cancer patients treated with proton therapy, showed that by using such skin-sparing techniques one could protect the skin from serious acute toxicities, and reduce the occurrence of telangiectasia compared to photon therapy [6].

5.5 RBE

One can not discuss protons without mentioning the ongoing debate of the RBE value, defined in Section 2.1.3. Clinical use of proton beam therapy uses a constant RBE value of 1.1 [1, 4]. The LET of protons are relatively low, up until the Bragg peak where it will increase as the energy deposited to the medium increases. Hence, the discussion revolves around the constant value of the RBE, and whether or not it should be increased at the end of the SOBP. The impact of an error in the RBE value is most critical on the normal tissue complication probability. The problem lies perhaps in that the magnitude of RBE variation is small relative to the ability to determine RBE values. However, *in vivo* experiments and clinical data indicate that employing the constant 1.1 RBE value is reasonable [1, 4]. Nonetheless, further investigations of the biological effect, especially including the dose range of clinical use, and RBE variation with physical and biological parameters, are needed.

5.6 Protons versus Photons

The impact of the principles stated in Chapter 2.2.3 is that the same tumor dose may be delivered by protons as by photons, while simultaneously delivering a lower dose to a smaller volume of normal tissue. The lack of compelling evidence from randomized clinical trials to prove protons superiority in patient outcomes, may be the reason why protons are not only considered, but are “exotic” in some countries. Further comparisons of clinical results between proton therapy, VMAT, IMRT, and conventional conformal photon radiotherapy are needed, but this is not without complications. As phase III clinical trials are designed to assess the effectiveness of a new intervention, in comparison with current “gold standard” treatments, it may be considered unethical to give some patients a less conformal technology when protons are in fact available. The more complex issue of cost versus benefit is even more difficult to address; in other words, protons may be better, but are they worth the cost? With increasing radiation treatment survivors, long-term sequelae most follow. This chapter started with the statement that the goal of radiotherapy is to cure with the lowest cost. In regards to patient quality of life, this cost can be interpreted as side-effects of treatment. The upfront financial

costs of proton therapy may be higher than photon therapy. However, because of fewer long-term toxicities, proton therapy can perhaps have a lower cost than photon therapy, both in terms of finance and quality of life [3, 4].

Chapter 6

Conclusions

In this thesis, a number of relatively simple tools for robustness analysis prior to radiation treatment, and evaluation tools during treatment, have been introduced. With advancement in treatment planning and delivery methods that can deliver exquisite dose distributions in the treatment planning system, it is important to account for the practicalities of the delivery process. This study looked at a small patient group, but the methodology developed could be used for future, bigger studies. A demonstration of deformed image registrations and dose tracking showed that these are useful and valuable tools to confirm the delivered doses, and evaluate the need for adaptive planning. Isocenter perturbations were investigated separately, and showed that the proton plans were as robust as the photon plans for perturbations under 4.5 mm, both in regards to target coverage and OARs sparing.

It can be reiterated that proton dose distributions are, due to the characteristics of proton energy deposition, more sensitive to various forms of changes than photon dose distributions. This was evident in the deformed image registration analysis, where the proton plan values had a higher relative change than the photon plan values. However, the absolute values from the proton plans, were still superior to those from the photon plans in regards to OARs sparing, without loosing acceptable target doses. Isocenter shifts were separately investigated in this thesis, and the same tools can be further developed to assess range and robustness due to density changes.

Although this work was concentrated to only ten patients, it does imply, at least from the point of reasonable isocenter shifts, that proton plans can be made as robust as photon plans, without sacrificing the beneficial dose sparing to OARs. I acknowledge that the isocenter perturbed scenarios investigated in this thesis have limitations, especially in the sense that a realistic accumulated delivered dose does depend on several uncertainties simultaneously. More sophisticated approaches

including three dimensional perturbation of isocenter and density should be investigated, requiring more computational resources. The results from this work indicate that breast cancer patients have a potential to benefit from proton radiotherapy over photon radiotherapy, in terms of OARs sparing. Future developments of automated organ delineation, adaptive treatment and patient immobilization will further improve the outcome of radiotherapy, and perhaps make the gain of the proton modality over the photon modality even more profound.

There is a fine line between the clinical benefit of a highly conform dose distribution and the uncertainties of its delivery. Decisions must be made on a patient-by-patient basis. The methods demonstrated in this thesis can aid in this decision making.

Bibliography

[1] H. Paganetti, *Proton Therapy Physics*. CRC Press, Taylor & Francis Group, 2012.

[2] *Penger til ELTE-Studenter, Kreft og Rus i Revidert Budsjett*. Dagens Medisin. Accessed 2018-05-06. Available at https://www.dagensmedisin.no/artikler/2018/05/15/penger-til-elte-studenter-kreft-og-rus-i-revidert-budsjett/.

[3] C. Chung *et al*, *Incidence of Second Malignancies Among Patients Treated With Proton Versus Photon Radiation*. International Journal of Radiation Oncology, vol. 87, pp. 46-52, 2013.

[4] V. Gondi *et al*, *Proton Therapy for Paediatric CNS Tumours - Improving Treatment-Related Outcomes*. Nature Reviews, Neurology, vol. 12, pp. 334-345, 2016.

[5] *PTCOG Patient Statistics*. Accessed 2018-10-14. Available at https://www.ptcog.ch/index.php/ptcog-patient-statistics.

[6] J. D. Slater *et al*, *Partial Breast Radiation Therapy With Proton Beam: 5-Year Results With Cosmetic Outcomes*. International Journal of Radiation Oncology, vol. 90, pp. 501-505, 2014.

[7] A. J. Wroe, *et al*, *Clinical Immobilization Techniques for Proton Therapy*. Technology in Cancer Research and Treatment, vol. 14, pp. 71-79, 2015.

[8] W. Liu *et al*, *Robust Optimization of Intensity Modulated Proton Therapy*. Medical Physics, vol. 39, pp. 1079-1091, 2012.

[9] J. Unkelbach *et al*, *Robust radiotherapy planning (review paper)*. Mathematics Magazine, Physics in Medicine & Biology, vol. 63:22TR02, 2018.

[10] D. Yan *et al*, *Adaptive Radiation Therapy*. Physics in Medicine and Biology, vol. 42, pp. 123-132, 1997.

[11] E. J. Hall *et al*, *Radiobiology for the Radiologist*. Wolters Kluwer Health, 2011.

[12] *Report 85: Fundamental Quantities and Units for Ionizing Radiation (Revised)*. Journal of the International Commission on Radiation Units and Measurements, vol. 11, p. 85, 2011.

[13] S. Danielsen and A. B. L. Marthinsen, *FY8409 Radiation Therapy Physics*. Course, NTNU, Fall Semester 2017.

[14] *The 2007 Recommendations of the International Commission on Radiological Protection. ICRP Publication 103.* Journal of the International Commission on Radiological Protection, vol. 37, p. 31, 2007.

[15] V. P. Singh *et al*, *Effective atomic numbers of some tissue substitutes by different methods: A comparative study*. Journal of Medical Physics / Association of Medical Physicists of India, vol. 39, pp. 24-31, 2014.

[16] A. Høeg, *Proton Therapy for Breast Cancer*. Project thesis, NTNU, 2018.

[17] H. Bethe *et al*, *Experimental Nuclear Physics*. ed. E. Segré, J. Wiley, vol. 1, p. 253, 1953.

[18] J. E. Leeman *et al*, *Proton therapy for head and neck cancer: expanding the therapeutic window*. The Lancet Oncology, vol. 18, pp. 254-265, 2017.

[19] S. Levernes, *Volumes and doses for external radiotherapy - Definitions and recommendations*. Østerås: Norwegian Radiation Protection Authority, Language: Norwegian. StrålevernRapport, 2012:9.

[20] *Report 83: Prescribing, recording, and reporting photon-beam IMRT (Revised)*. Journal of the International Commission on Radiation Units and Measurements, vol. 10, pp. 25-35, 2010.

[21] *RAYSTATION 6 User Manual*. RaySearch Laboratories AB, Stockholm, 2016.

[22] L. A. Feldkamp *et al*, *Practical Cone-Beam Algorithm*. Optical Society of America, vol. 1, pp. 612-619, 1984.

[23] A. Fredriksson *et al*, *Minimax optimization for handling range and setup uncertainties in proton therapy*. Medical Physics, vol. 38, pp. 1672-1684, 2011.

[24] S.Svensson *et al*, *The ANACONDA algorithm for deformable image registration in radiotherapy*. Medical Physics, vol. 42, p. 40, 2015.

[25] *RAYSTATION 6 RayPhysics Manual*. RaySearch Laboratories AB, Stockholm, 2017.

[26] M. T. Milano *et al*, *Normal Tissue Tolerance Dose Metrics for Radiation Therapy of Major Organs*. Seminars in Radiation Oncology, Elsevier, vol. 17, pp. 131-140, 2007.

[27] B. Naume *et al*, *Nasjonalt handlingsprogram med retningslinjer for diagnostikk, behandling og oppfølging av pasienter med brystkreft. Nasjonale faglige retningslinjer, IS-2736*. Helsedirektoratet, vol. 11, pp. 79-100, 2018.

[28] L. B. Stick *et al*, *Joint Estimtion of Cardiac Toxicity and Recurrence Risks After Comprehensive Nodal Photon Versus Proton Therapy for Breast Cancer*. International Journal of Radiation Oncology, vol. 97, pp. 754-761, 2016.

[29] S.C. Darby *et al*, *Risk of Ischemic Heart Disease in Women after Radiotherapy for Breast Cancer*. New England Journal of Medicine, vol. 386, pp. 987-998, 2013.

[30] C. Ares *et al*, *Postoperative Proton Radiotherapy for Localized and Locoregional Breast Cancer: Potential for Clinically Relevant Improvements?* International Journal of Radiation Oncology, vol. 76, pp. 685-697, 2007.

[31] J. Pukala *et al*, *Benchmarking of five commercial deformable image registration algorithms for head and neck patients*. Journal of Applied Clinical Medical Physics, vol. 17, pp. 25-40, 2016.

[32] S. K. Vinod *et al*, *Uncertainties in volume delineation in radiation oncology: A systematic review and recommendations for future studies*. Radiotherapy and Oncology, vol. 121, pp. 169-179, 2016.

[33] M. Alsaker *et al*, *Seminar: MRI in Radiotherapy*. NTNU and St. Olavs hospital, Kunnskapssenteret, 2018-12-5.

[34] S. Trebeschi *et al*, *Deep Learning for Fully-Automated Localization and Segmentation of Rectal Cancer on Multiparametric MR*. Scientific Reports, Published Online, vol. 7:5301, 2017.

Appendix A

A.a. Colormaps, Perturbed Isocenter

In the following section all colormaps from the perturbed isocenter analysis will follow. All colormaps have x- and y-axis that represents the isocenter shift in the x- and y-direction respectively, in centimeters. The colorbars to the left of the photon colormaps corresponds to the interval of the value for that parameter, for both the proton and photon plan.

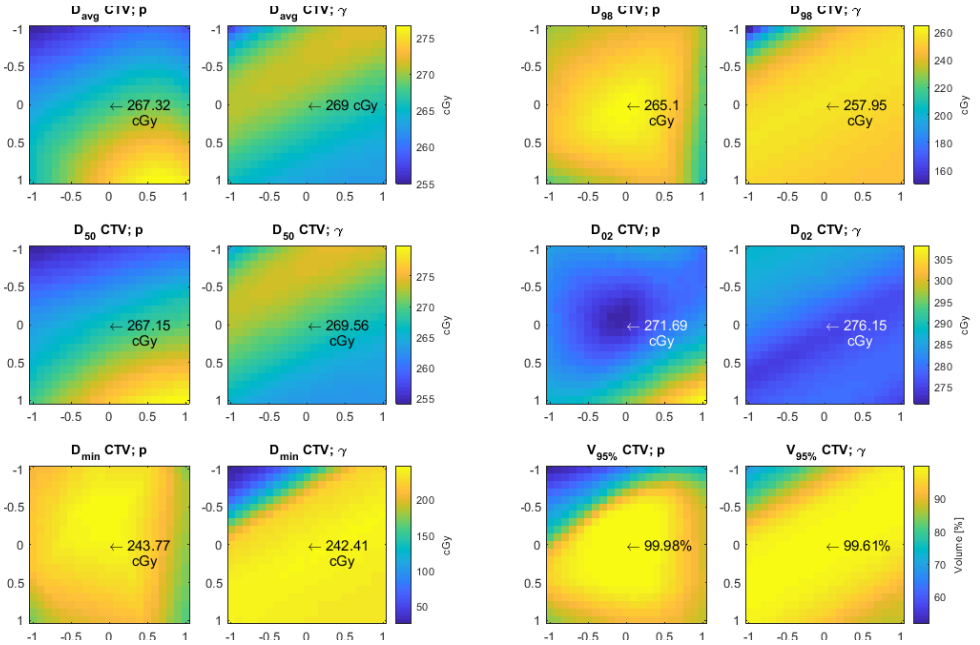

Figure 1: Patient A, CTV

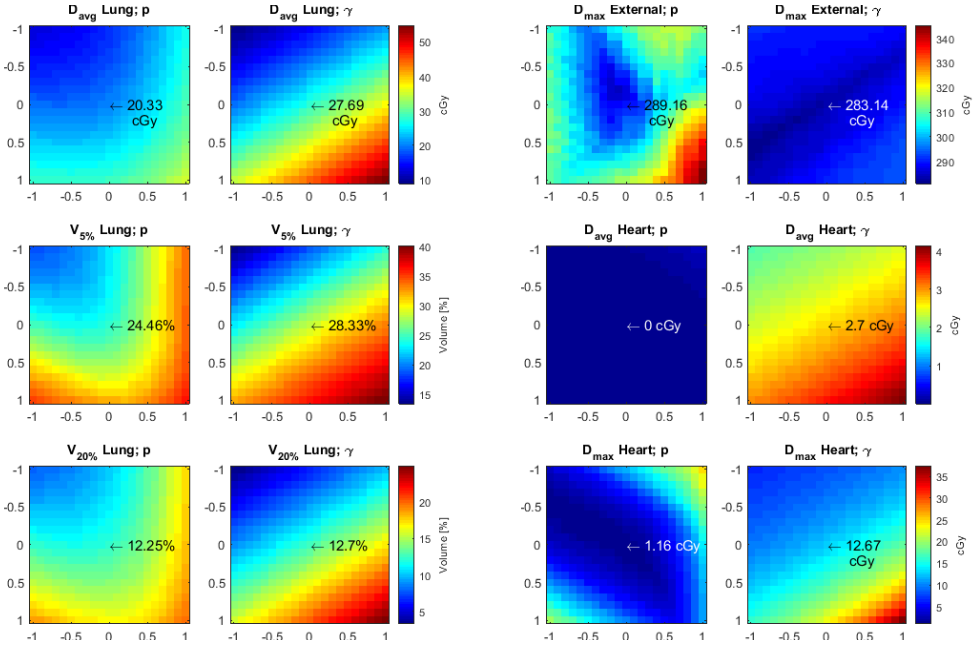

Figure 2: Patient A, OAR

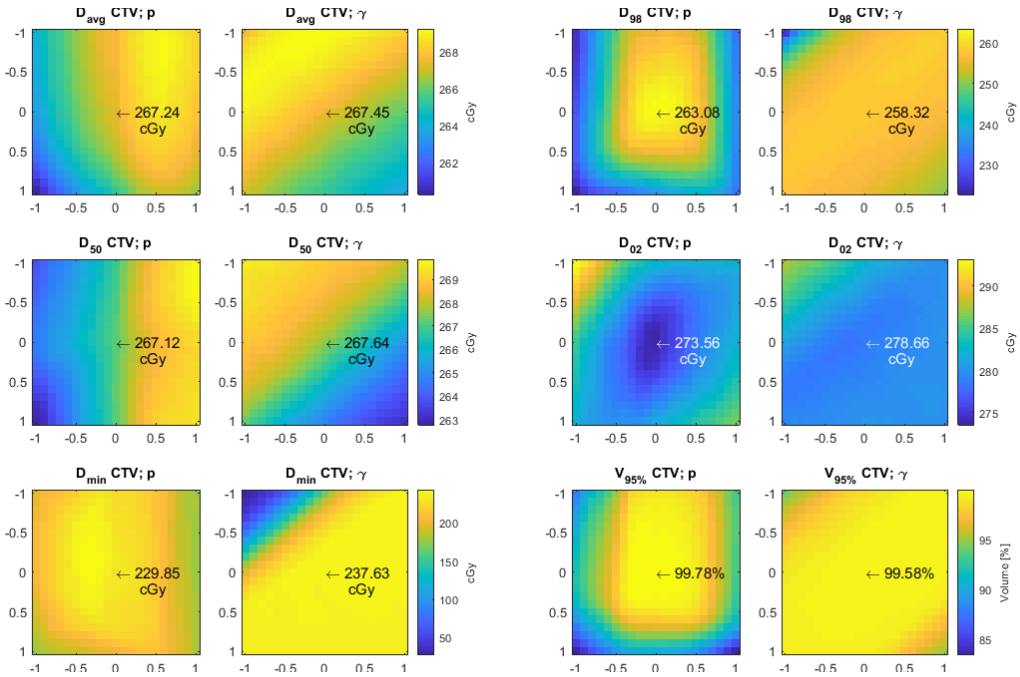

Figure 3: Patient B, CTV

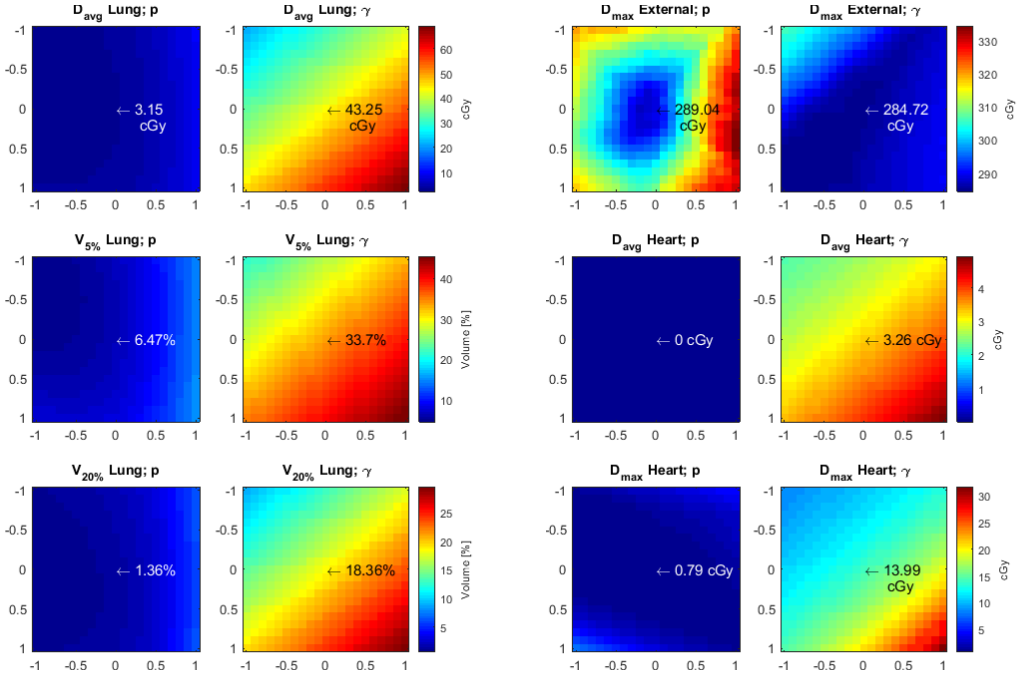

Figure 4: Patient B, OAR

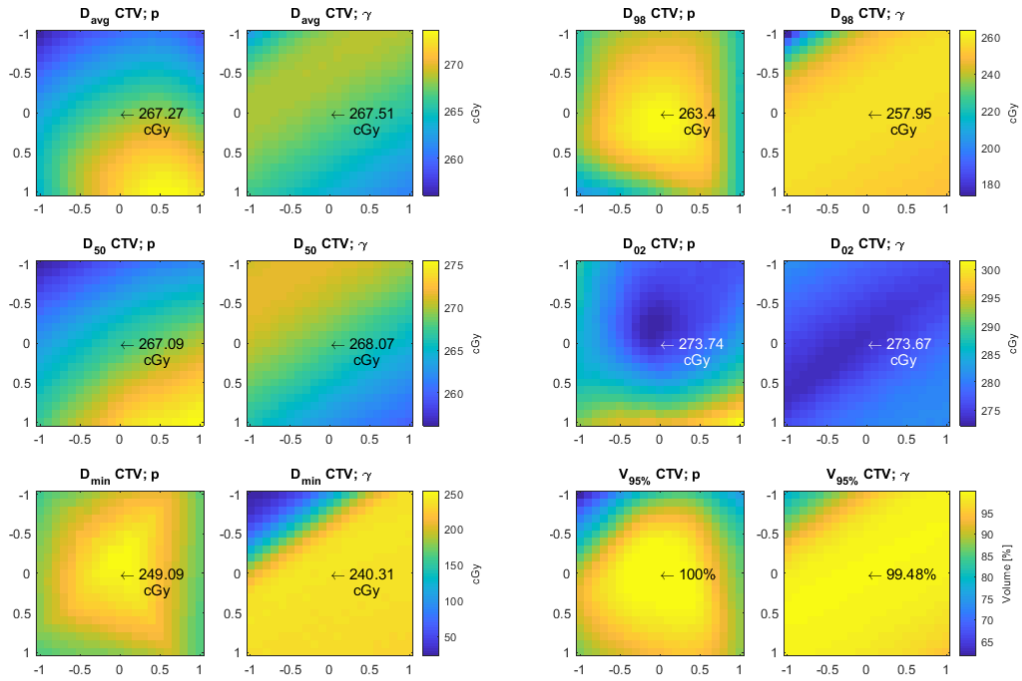

Figure 5: Patient C, CTV

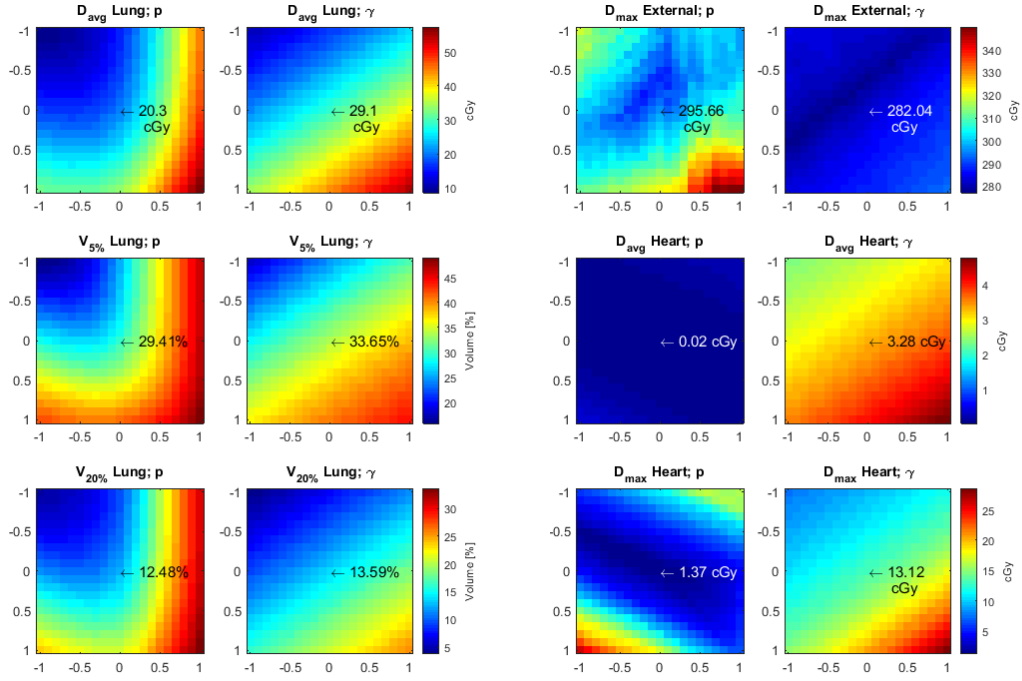

Figure 6: Patient C, OAR

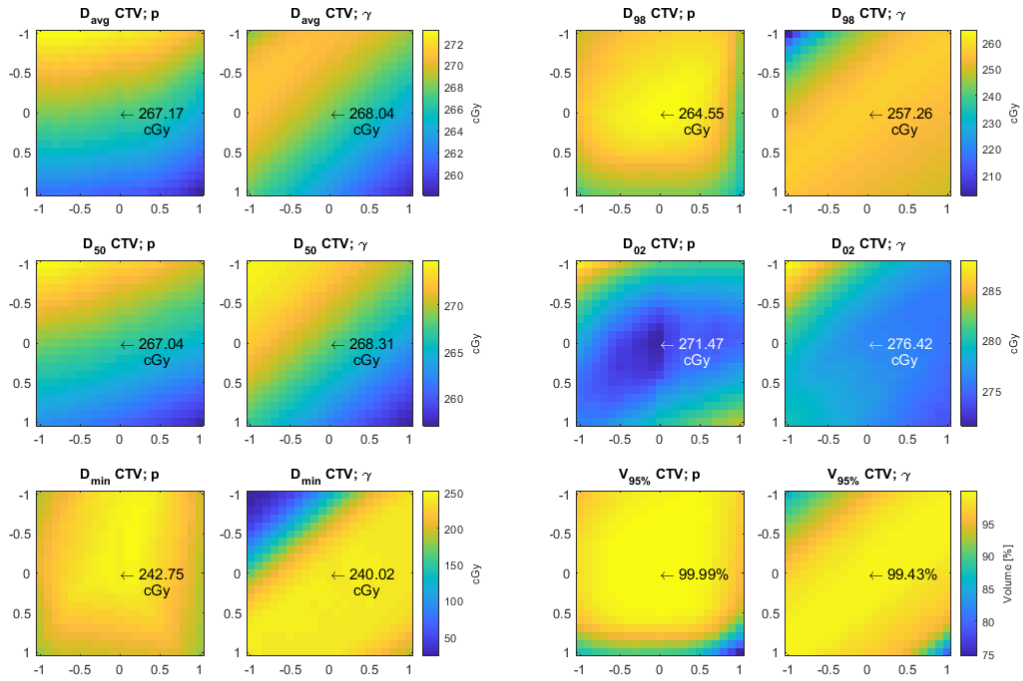

Figure 7: Patient D, CTV

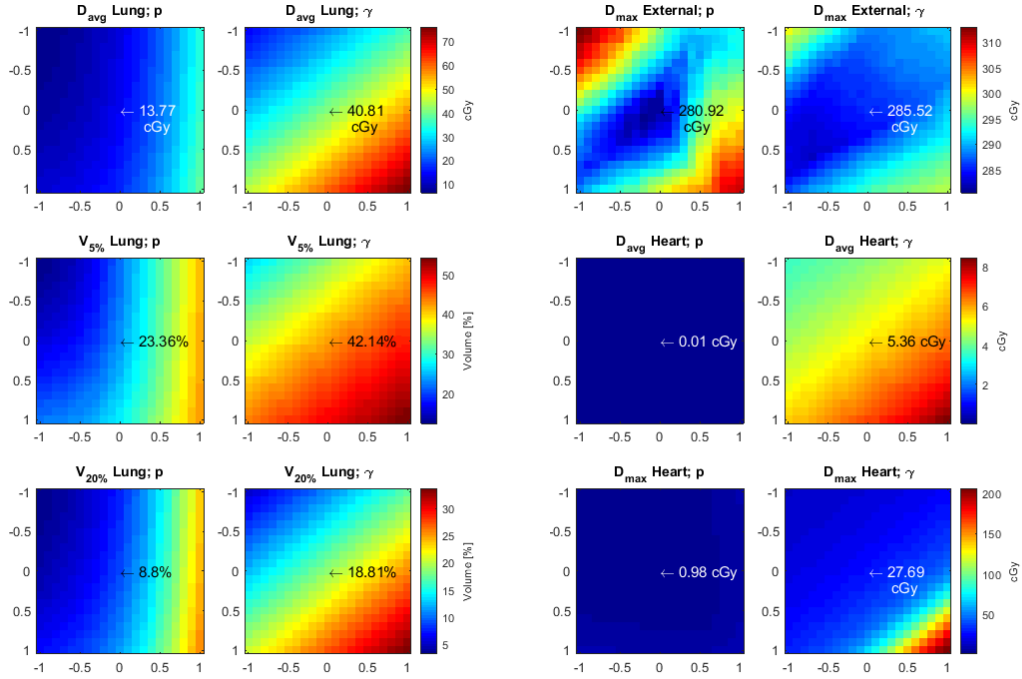

Figure 8: Patient D, OAR

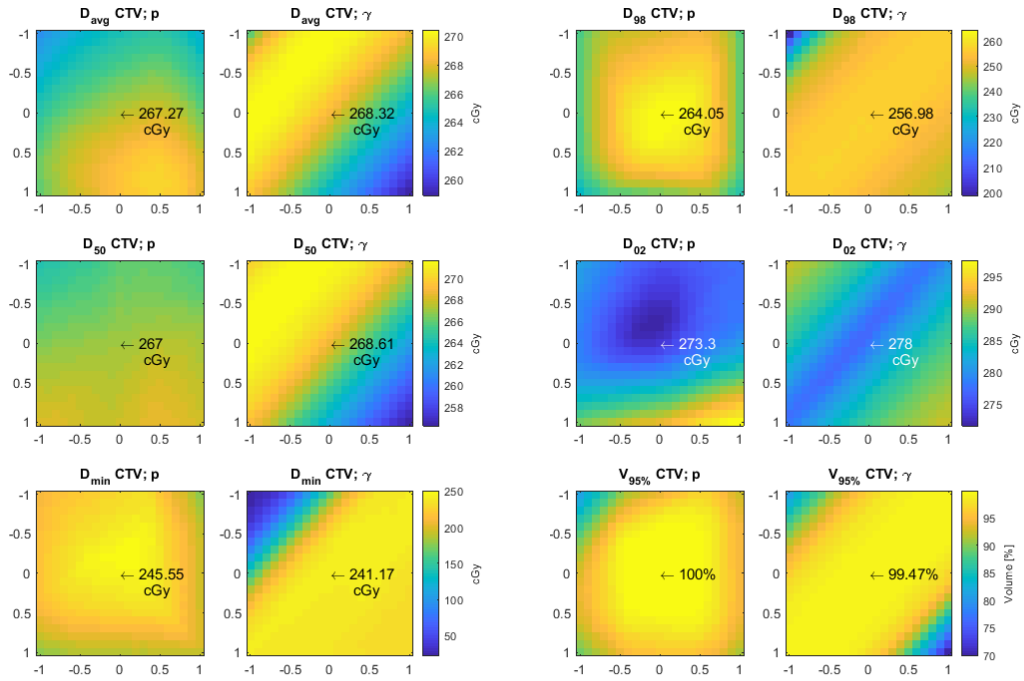

Figure 9: Patient E, CTV

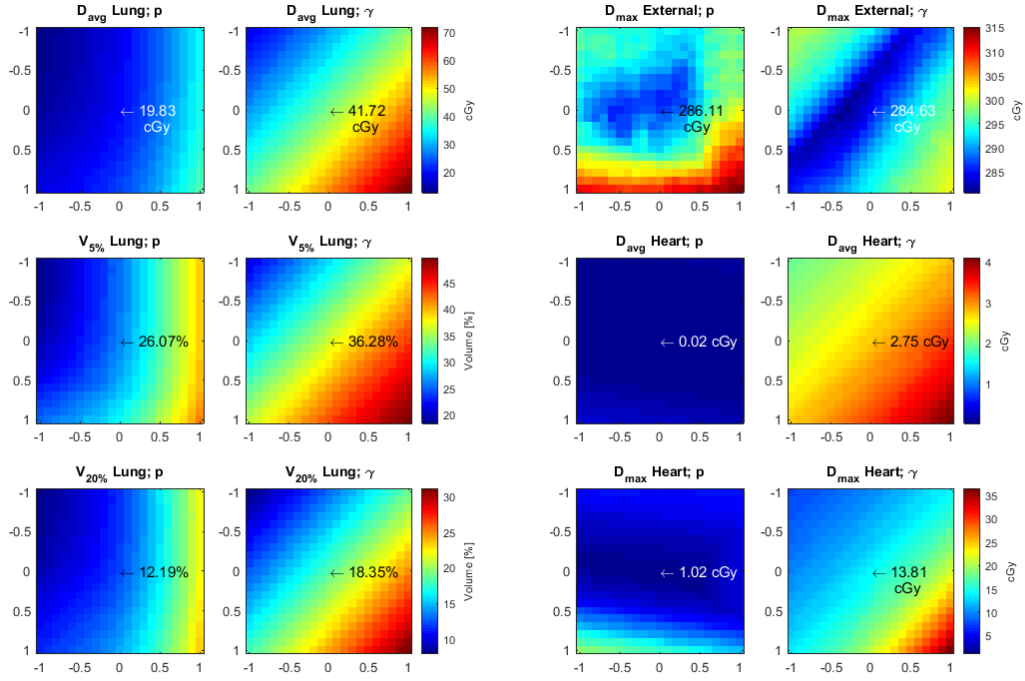

Figure 10: Patient E, OAR

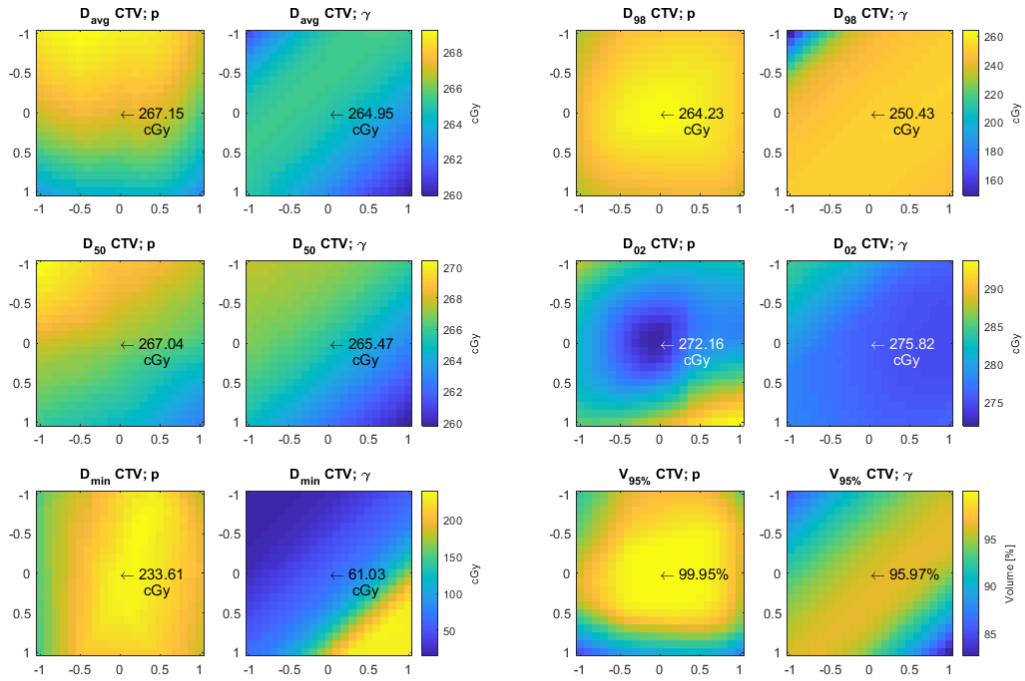

Figure 11: Patient F, CTV

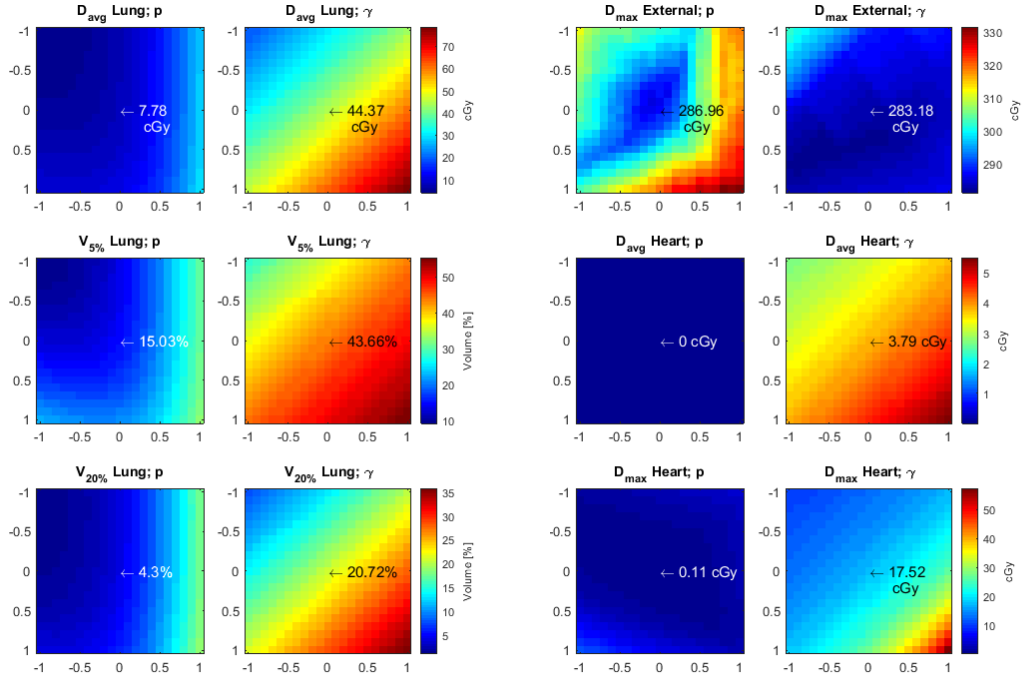

Figure 12: Patient F, OAR

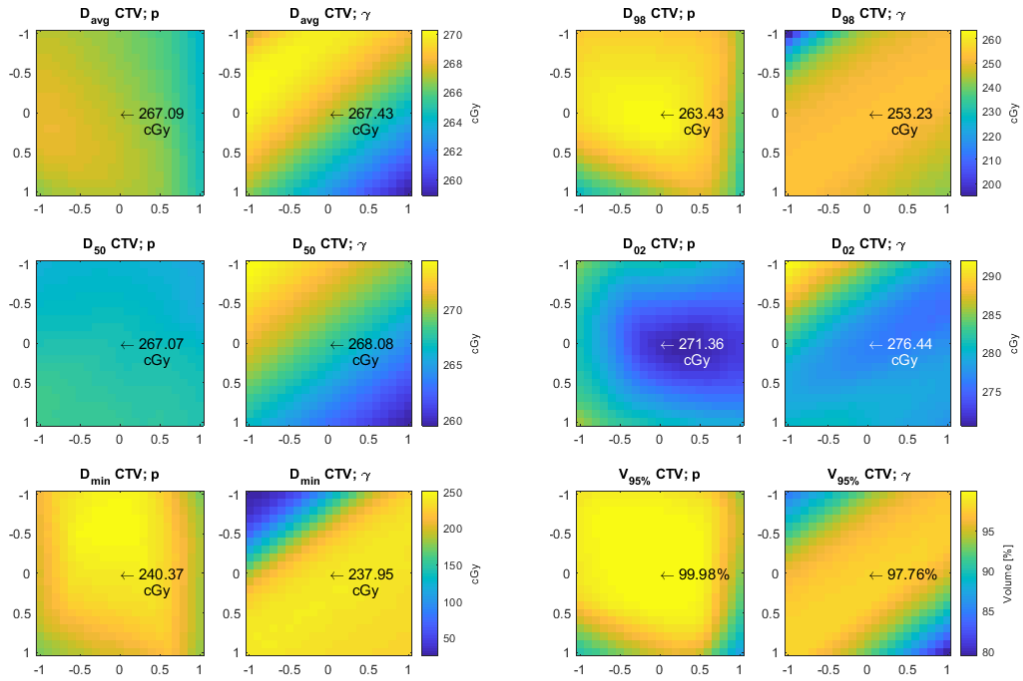

Figure 13: Patient G, CTV

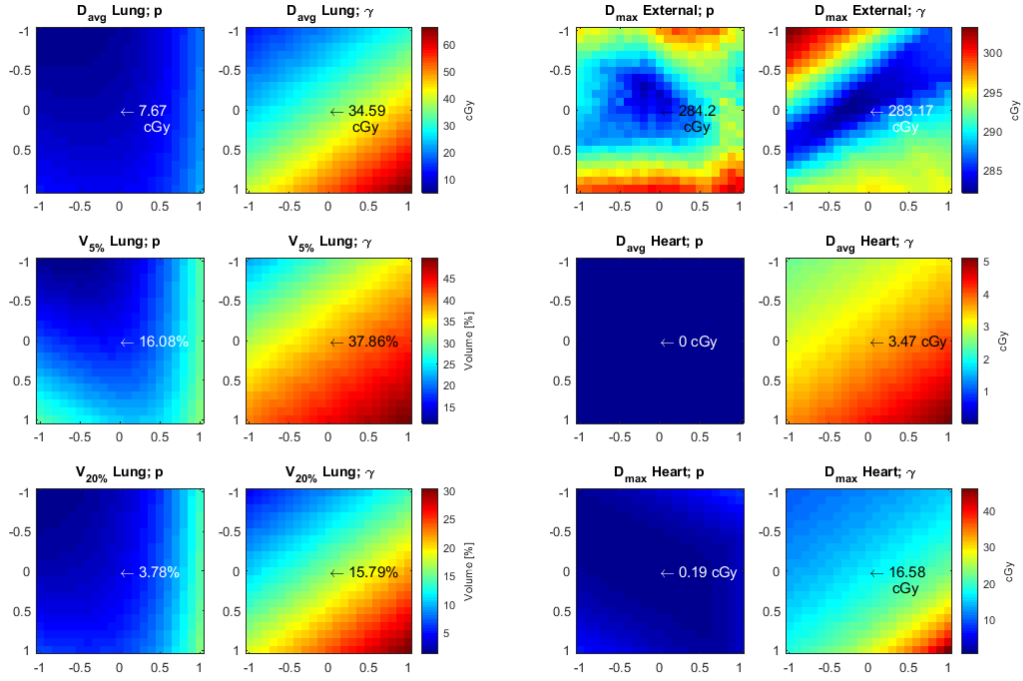

Figure 14: Patient G, OAR

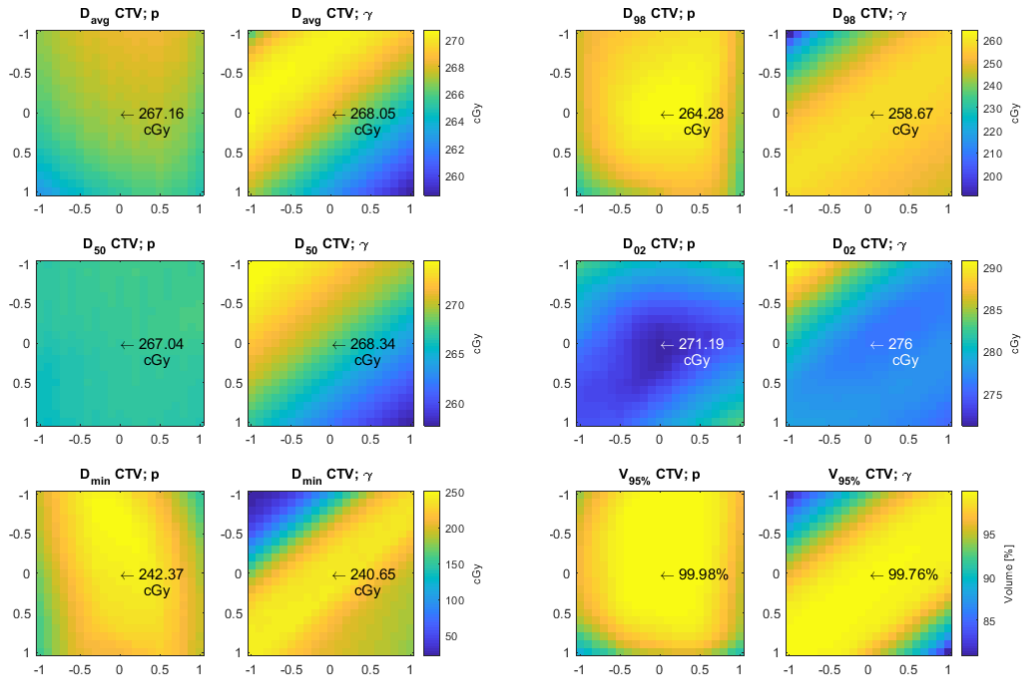

Figure 15: Patient H, CTV

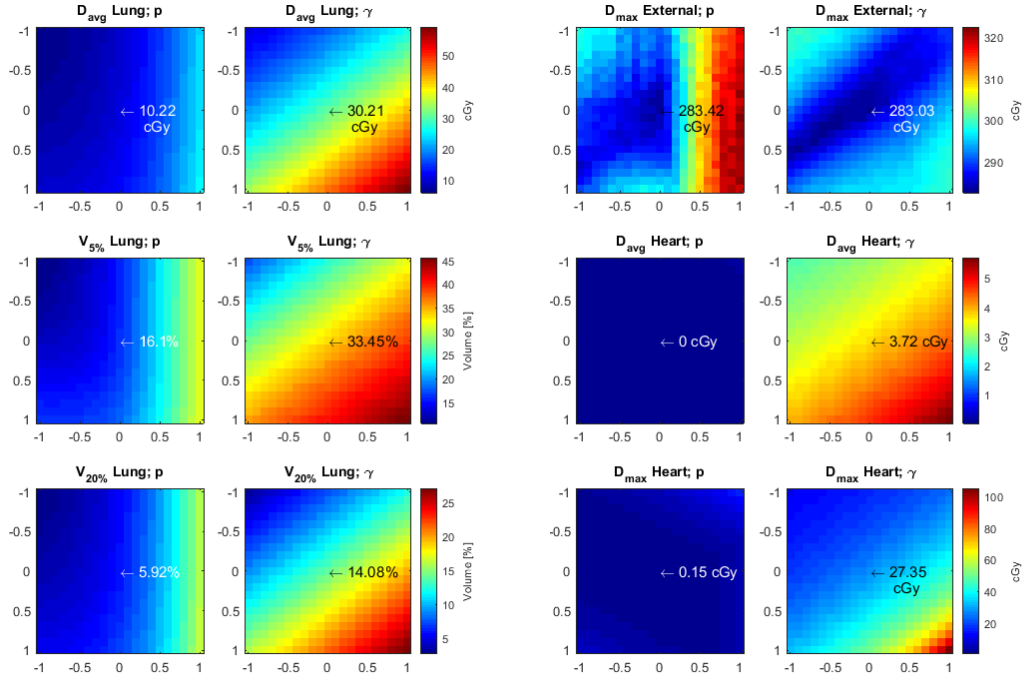

Figure 16: Patient H, OAR

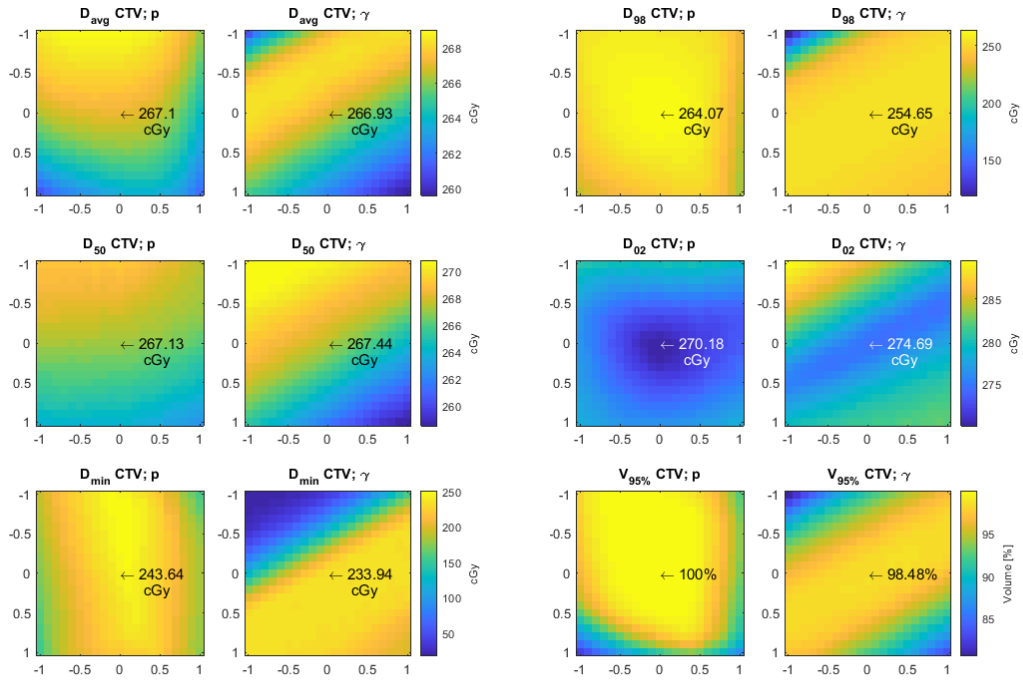

Figure 17: Patient I, CTV

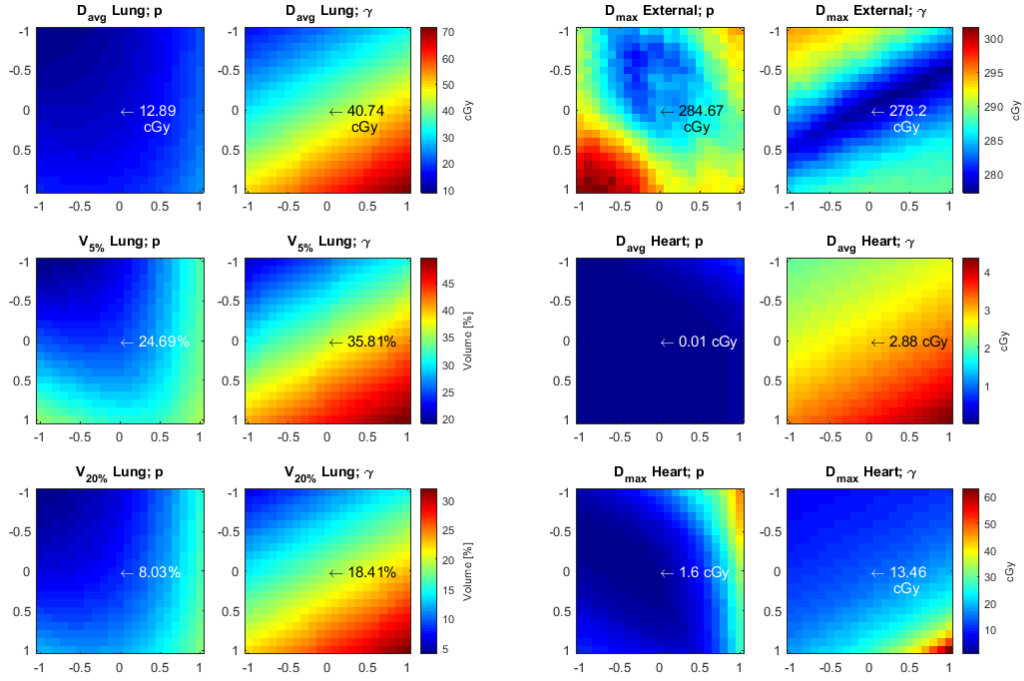

Figure 18: Patient I, OAR

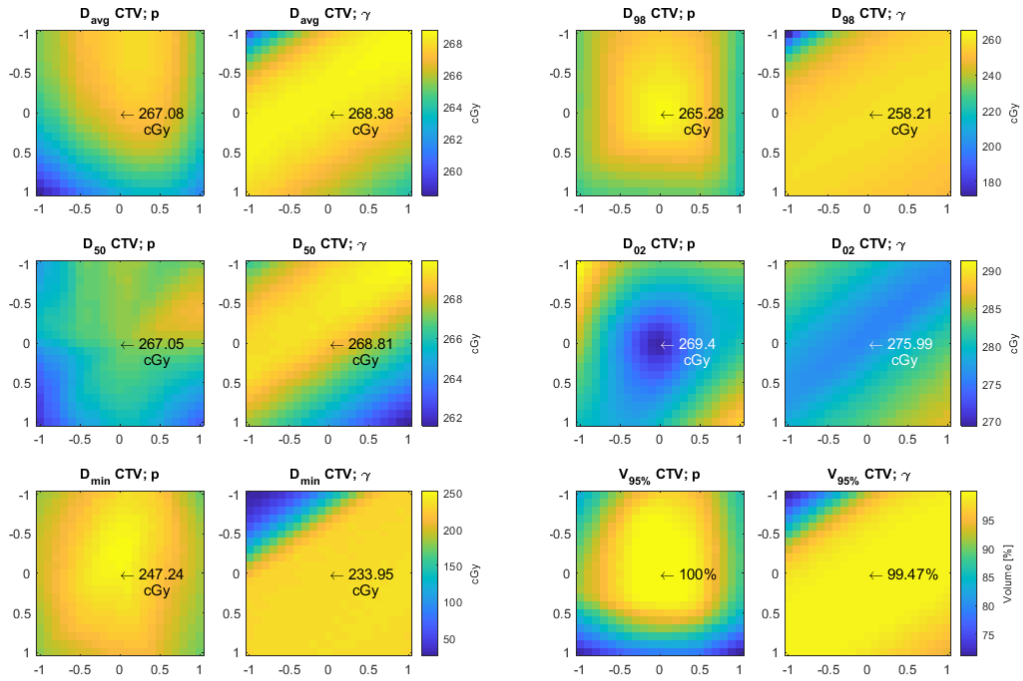

Figure 19: Patient J, CTV

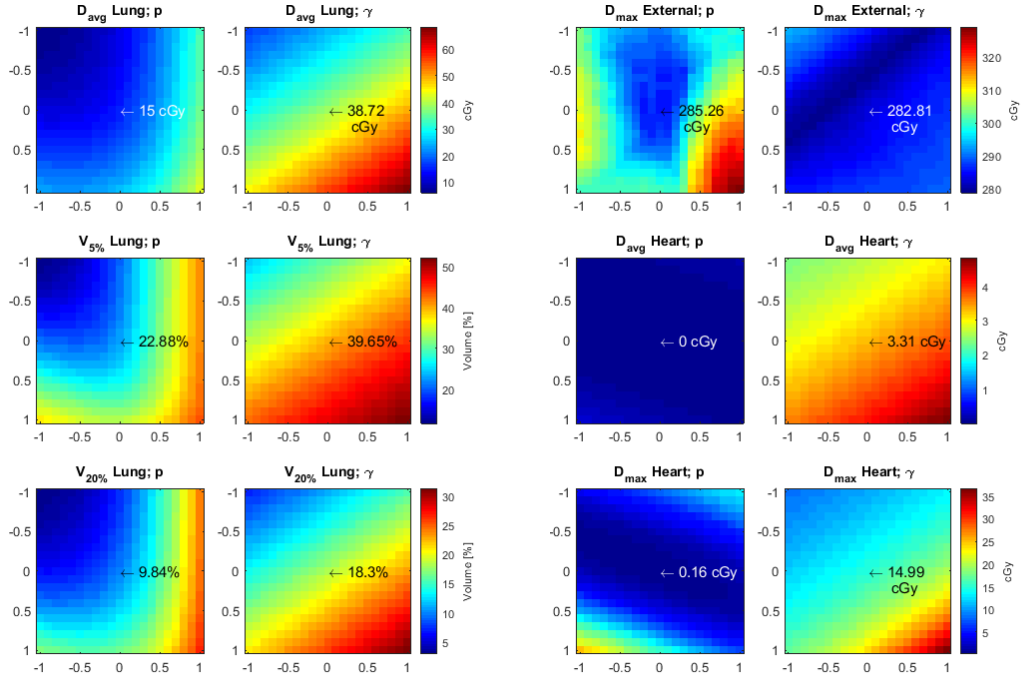

Figure 20: Patient J, OAR

A.b. Boxplots of OAR, Isocenter Shifts

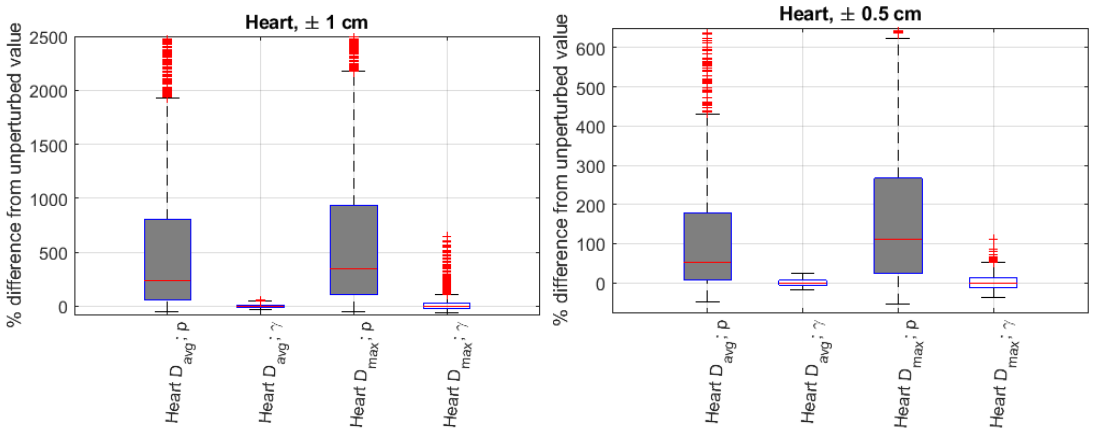

Figure 21: Boxplots of all values acquired for the heart in the isocenter shift analysis. To the left, perturbations ∈ [-1, 1] cm are included, meaning that each boxplot has 441 × 10 values. To the right, perturbations ∈ [-0.5, 0.5] cm are included, meaning that each boxplot has 121 × 10 values. The different intervals for the y-axis indicate that the plans were significantly more robust for isocenter shifts ∈ [-0.5, 0.5] cm. p = proton (grey box), γ = photon (white box).

Appendix B

B.a. Perturbed Isocenter Script

```
#Made by Andrea Hoeg
import wpf, os, sys, System, clr, random
from System import Windows
from System.Windows import *
from System.Windows.Input import Key
clr.AddReference("System.Windows.Forms")
clr.AddReference('System.Drawing')
from System.Windows.Forms import *
from System.Drawing import *
clr.AddReference("Office")
clr.AddReference("Microsoft.Office.Interop.Excel")
from Microsoft.Office.Interop.Excel import ApplicationClass,
    XlWBATemplate, XlChartType
import Microsoft.Office.Interop.Excel as Excel
from System import Array
from connect import *

beam_set = get_current("BeamSet")
plan = get_current("Plan")
patient = get_current("Patient")
case = get_current("Case")
#First; gather user input about variables that change between
    patients
# Create a Class Form
class CreateWindow(Form):
    def __init__(self):
        # Create the Form
        self.Name = "Create Window"
        self.Text = "Deviation length"
```

```
        self.Size = Size(500, 100)
        self.CenterToScreen()
        # Create Label = label
        label = Label(Text = "Cm in one direction")
        label.Parent = self
        label.Location = Point(30, 20)
        # Create TextBox = textbox
        self.textbox = TextBox()
        self.textbox.Parent = self
        self.textbox.Text = "1"
        self.textbox.Location = Point(150, 20)
        self.textbox.Width = 150
        # Create Button = button
        button = Button()
        button.Parent = self
        button.Text = "Apply"
        button.Location = Point(400, 20)
        # Register event
        button.Click += self.ButtonClicked
    # Create button event
    def ButtonClicked(self, sender, args):
        if sender.Click:
            self.value = self.textbox.Text
            self.Close()
form = CreateWindow()
Application.Run(form)
DevOneDim = float(form.value)

# Create a Class Form
class CreateWindow1(Form):
    def __init__(self1):
        # Create the Form
        self1.Name = "Create Window"
        self1.Text = "Name your inputs"
        self1.Size = Size(500, 100)
        self1.CenterToScreen()
        # Create Label = label
        label1 = Label(Text = "Name of planning CT")
        label1.Parent = self1
        label1.Location = Point(30, 20)
        # Create TextBox = textbox
        self1.textbox1 = TextBox()
        self1.textbox1.Parent = self1
        self1.textbox1.Text = "CT 1"
        self1.textbox1.Location = Point(150, 20)
        self1.textbox1.Width = 150
        # Create Button = button
        button1 = Button()
        button1.Parent = self1
```

```
        button1.Text = "Apply"
        button1.Location = Point(400, 20)
        # Register event
        button1.Click += self1.ButtonClicked
    # Create button event
    def ButtonClicked(self1, sender, args):
        if sender.Click:
            self1.value = self1.textbox1.Text
            self1.Close()
form1 = CreateWindow1()
Application.Run(form1)
PlanningCT = form1.value

# Create a Class Form
class CreateWindow2(Form):
    def __init__(self2):
        # Create the Form
        self2.Name = "Create Window"
        self2.Text = "Name your inputs"
        self2.Size = Size(500, 100)
        self2.CenterToScreen()
        # Create Label = label
        label2 = Label(Text = "Step length [cm]")
        label2.Parent = self2
        label2.Location = Point(30, 20)
        # Create TextBox = textbox
        self2.textbox2 = TextBox()
        self2.textbox2.Parent = self2
        self2.textbox2.Text = "0.1"
        self2.textbox2.Location = Point(150, 20)
        self2.textbox2.Width = 150
        # Create Button = button
        button2 = Button()
        button2.Parent = self2
        button2.Text = "Apply"
        button2.Location = Point(400, 20)
        # Register event
        button2.Click += self2.ButtonClicked
    # Create button event
    def ButtonClicked(self2, sender, args):
        if sender.Click:
            self2.value = self2.textbox2.Text
            self2.Close()
form2 = CreateWindow2()
Application.Run(form2)
StepLength = float(form2.value)

# Create a Class Form
class CreateWindow3(Form):
```

```
    def __init__(self3):
        # Create the Form
        self3.Name = "Create Window"
        self3.Text = "Name your inputs"
        self3.Size = Size(500, 100)
        self3.CenterToScreen()
        # Create Label = label
        label3 = Label(Text = "Name CTV")
        label3.Parent = self3
        label3.Location = Point(30, 20)
        # Create TextBox = textbox
        self3.textbox3 = TextBox()
        self3.textbox3.Parent = self3
        self3.textbox3.Text = "CTV_hudbarbert"
        self3.textbox3.Location = Point(150, 20)
        self3.textbox3.Width = 150
        # Create Button = button
        button3 = Button()
        button3.Parent = self3
        button3.Text = "Apply"
        button3.Location = Point(400, 20)
        # Register event
        button3.Click += self3.ButtonClicked
    # Create button event
    def ButtonClicked(self3, sender, args):
        if sender.Click:
            self3.value = self3.textbox3.Text
            self3.Close()
form3 = CreateWindow3()
Application.Run(form3)
ROIName = form3.value

# Create a Class Form
class CreateWindow4(Form):
    def __init__(self4):
        # Create the Form
        self4.Name = "Create Window"
        self4.Text = "Name your inputs"
        self4.Size = Size(500, 100)
        self4.CenterToScreen()
        # Create Label = label
        label4 = Label(Text = "Name Lung")
        label4.Parent = self4
        label4.Location = Point(30, 20)
        # Create TextBox = textbox
        self4.textbox4 = TextBox()
        self4.textbox4.Parent = self4
        self4.textbox4.Text = "Lung_Right"
        self4.textbox4.Location = Point(150, 20)
```

```
        self4.textbox4.Width = 150
        # Create Button = button
        button4 = Button()
        button4.Parent = self4
        button4.Text = "Apply"
        button4.Location = Point(400, 20)
        # Register event
        button4.Click += self4.ButtonClicked
    # Create button event
    def ButtonClicked(self4, sender, args):
        if sender.Click:
            self4.value = self4.textbox4.Text
            self4.Close()
form4 = CreateWindow4()
Application.Run(form4)
LUNGName = form4.value

# Create a Class Form
class CreateWindow5(Form):
    def __init__(self5):
        # Create the Form
        self5.Name = "Create Window"
        self5.Text = "Name your inputs"
        self5.Size = Size(500, 100)
        self5.CenterToScreen()
        # Create Label = label
        label5 = Label(Text = "Name external")
        label5.Parent = self5
        label5.Location = Point(30, 20)
        # Create TextBox = textbox
        self5.textbox5 = TextBox()
        self5.textbox5.Parent = self5
        self5.textbox5.Text = "External_pasientkontur"
        self5.textbox5.Location = Point(150, 20)
        self5.textbox5.Width = 150
        # Create Button = button
        button5 = Button()
        button5.Parent = self5
        button5.Text = "Apply"
        button5.Location = Point(400, 20)
        # Register event
        button5.Click += self5.ButtonClicked
    # Create button event
    def ButtonClicked(self5, sender, args):
        if sender.Click:
            self5.value = self5.textbox5.Text
            self5.Close()
form5 = CreateWindow5()
Application.Run(form5)
```

```
NAMEExternal = form5.value

# Create a Class Form
class CreateWindow6(Form):
    def __init__(self6):
        # Create the Form
        self6.Name = "Create Window"
        self6.Text = "Name your inputs"
        self6.Size = Size(500, 100)
        self6.CenterToScreen()
        # Create Label = label
        label6 = Label(Text = "Fx dose")
        label6.Parent = self6
        label6.Location = Point(30, 20)
        # Create TextBox = textbox
        self6.textbox6 = TextBox()
        self6.textbox6.Parent = self6
        self6.textbox6.Text = "2.67"
        self6.textbox6.Location = Point(150, 20)
        self6.textbox6.Width = 150
        # Create Button = button
        button6 = Button()
        button6.Parent = self6
        button6.Text = "Apply"
        button6.Location = Point(400, 20)
        # Register event
        button6.Click += self6.ButtonClicked
    # Create button event
    def ButtonClicked(self6, sender, args):
        if sender.Click:
            self6.value = self6.textbox6.Text
            self6.Close()
form6 = CreateWindow6()
Application.Run(form6)
FxDose = float(form6.value)

# Create a Class Form
class CreateWindow7(Form):
    def __init__(self7):
        # Create the Form
        self7.Name = "Create Window"
        self7.Text = "Name your inputs"
        self7.Size = Size(500, 100)
        self7.CenterToScreen()
        # Create Label = label
        label7 = Label(Text = "Fx dose")
        label7.Parent = self7
        label7.Location = Point(30, 20)
        # Create TextBox = textbox
```

```
273         self7.textbox7 = TextBox()
            self7.textbox7.Parent = self7
275         self7.textbox7.Text = "Heart"
            self7.textbox7.Location = Point(150, 20)
277         self7.textbox7.Width = 150
            # Create Button = button
279         button7 = Button()
            button7.Parent = self7
281         button7.Text = "Apply"
            button7.Location = Point(400, 20)
283         # Register event
            button7.Click += self7.ButtonClicked
285     # Create button event
        def ButtonClicked(self7, sender, args):
287         if sender.Click:
                self7.value = self7.textbox7.Text
289             self7.Close()
form7 = CreateWindow7()
291 Application.Run(form7)
HeartNAME = form7.value
293

295 ####################################################
counter = 0
297 structure_set = plan.GetStructureSet()
examination_name = structure_set.OnExamination.Name
299 fraction_number = 0

301 ####################################################

303 xsize = int(round(DevOneDim/StepLength*2) +1)
ysize = int(round(DevOneDim/StepLength*2) +1)
305
lower=float(-DevOneDim)
307 upper=float(DevOneDim)
xval1D = [lower + x*(upper-lower)/(xsize-1) for x in range(xsize)]
    # tilsvarer linspace
309 yval1D = [lower + x*(upper-lower)/(ysize-1) for x in range(ysize)]


311
X2D = Array.CreateInstance(float, xsize, ysize)
313 for i in range(xsize):
    for j in range(ysize):
315         X2D[i, j] = 0
Y2D =  Array.CreateInstance(float, xsize, ysize)
317 for i in range(xsize):
    for j in range(ysize):
319         Y2D[i, j] = 0
OUT2D= Array.CreateInstance(float, xsize, ysize)
```

```
for i in range(xsize):
    for j in range(ysize):
        OUT2D[i, j] = 0
OUT22D= Array.CreateInstance(float, xsize, ysize)
for i in range(xsize):
    for j in range(ysize):
        OUT22D[i, j] = 0
OUT32D= Array.CreateInstance(float, xsize, ysize)
for i in range(xsize):
    for j in range(ysize):
        OUT32D[i, j] = 0
OUT42D= Array.CreateInstance(float, xsize, ysize)
for i in range(xsize):
    for j in range(ysize):
        OUT42D[i, j] = 0
OUT52D= Array.CreateInstance(float, xsize, ysize)
for i in range(xsize):
    for j in range(ysize):
        OUT52D[i, j] = 0
OUT62D= Array.CreateInstance(float, xsize, ysize)
for i in range(xsize):
    for j in range(ysize):
        OUT62D[i, j] = 0
OUT72D= Array.CreateInstance(float, xsize, ysize)
for i in range(xsize):
    for j in range(ysize):
        OUT72D[i, j] = 0
OUT82D= Array.CreateInstance(float, xsize, ysize)
for i in range(xsize):
    for j in range(ysize):
        OUT82D[i, j] = 0
OUT92D= Array.CreateInstance(float, xsize, ysize)
for i in range(xsize):
    for j in range(ysize):
        OUT92D[i, j] = 0
OUT102D= Array.CreateInstance(float, xsize, ysize)
for i in range(xsize):
    for j in range(ysize):
        OUT102D[i, j] = 0
OUT112D= Array.CreateInstance(float, xsize, ysize)
for i in range(xsize):
    for j in range(ysize):
        OUT112D[i, j] = 0
OUT122D= Array.CreateInstance(float, xsize, ysize)
for i in range(xsize):
    for j in range(ysize):
        OUT122D[i, j] = 0
# zeros
OUT = 0
```

```
OUT2 = 0
OUT3 = 0
OUT4 = 0
OUT5 = 0
OUT6 = 0
OUT7 = 0
OUT8 = 0
OUT9 = 0
OUT10 = 0
OUT11 = 0
OUT12 = 0


# Run simulations (start from last value, because next goes backwards in the end)
count=0
for ix,x in enumerate(xval1D[::-1]):
    for iy,y in enumerate(yval1D[::-1]):
        if x == 0 and y== 0:
            beam_set.ComputePerturbedDose(DensityPerturbation=0, IsocenterShift={ 'x': 0, 'y': 0.0000001, 'z': 0 }, OnlyOneDosePerImageSet=False, AllowGridExpansion=True, ExaminationNames=[PlanningCT], FractionNumbers=[0], ComputeBeamDoses=True)

        print count, ix,x,iy,y
        count+=1

        try:
            beam_set.ComputePerturbedDose(DensityPerturbation=0, IsocenterShift={ 'x': x, 'y': y, 'z': 0 }, OnlyOneDosePerImageSet=False, AllowGridExpansion=True, ExaminationNames=[PlanningCT], FractionNumbers=[0], ComputeBeamDoses=True)
        except:
            print 'Could not run simulation'

V95 = 100*FxDose*0.95
V05 = 100*FxDose*0.05
V20 = 100*FxDose*0.20

# Take out data
for ix,x in enumerate(xval1D):
    for iy,y in enumerate(yval1D):

        count-=1
        print count, ix,x,iy,y

        try:
```

```
            fe = next(f for f in case.TreatmentDelivery.
    FractionEvaluations if f.FractionNumber == fraction_number)
411         doe = next(d for d in fe.DoseOnExaminations if d.
    OnExamination.Name == examination_name)
            de = doe.DoseEvaluations[doe.DoseEvaluations.Count-1]
413         OUT = de.GetRelativeVolumeAtDoseValues(RoiName=ROIName
    , DoseValues=[V95])
            OUT2 = de.GetRelativeVolumeAtDoseValues(RoiName=
    LUNGName, DoseValues=[V05])
415         OUT3 = de.GetDoseStatistic(RoiName=NAMEExternal,
    DoseType = 'Max')
            OUT4 = de.GetDoseAtRelativeVolumes(RoiName=ROIName,
    RelativeVolumes=[0.50])
417         OUT5 = de.GetDoseStatistic(RoiName=ROIName, DoseType='
    Min')
            OUT6 = de.GetDoseStatistic(RoiName=HeartNAME, DoseType
    ='Max')
419         OUT7 = de.GetDoseAtRelativeVolumes(RoiName=ROIName,
    RelativeVolumes=[0.98])
            OUT8 = de.GetDoseAtRelativeVolumes(RoiName=ROIName,
    RelativeVolumes=[0.02])
421         OUT9 = de.GetRelativeVolumeAtDoseValues(RoiName=
    LUNGName, DoseValues=[V20])
            OUT10 = de.GetDoseStatistic(RoiName=ROIName, DoseType=
    'Average')
423         OUT11 = de.GetDoseStatistic(RoiName=LUNGName, DoseType
    ='Average')
            OUT12 = de.GetDoseStatistic(RoiName=HeartNAME,
    DoseType='Average')
425         de.DeleteEvaluationDose()
        except:
427         OUT = 6*(x+y)
            print 'Could not find simulation results'
429     X2D[ix,iy] = x
        Y2D[ix,iy] = y
431     OUT2D[ix,iy] = 100*OUT[0]
        OUT22D[ix,iy] = 100*OUT2[0]
433     OUT32D[ix,iy] = OUT3
        OUT42D[ix,iy] = OUT4[0]
435     OUT52D[ix,iy] = OUT5
        OUT62D[ix,iy] = OUT6
437     OUT72D[ix,iy] = OUT7[0]
        OUT82D[ix,iy] = OUT8[0]
439     OUT92D[ix,iy] = 100*OUT9[0]
        OUT102D[ix,iy] = OUT10
441     OUT112D[ix,iy] = OUT11
        OUT122D[ix,iy] = OUT12
443
#Print to excel
```

```
445 excel = Excel.ApplicationClass()
    excel.Visible = True
447 workbook = excel.Workbooks.Add()
    worksheet = workbook.Worksheets[1]
449 worksheet1 = workbook.Worksheets.Add()
    worksheet2 = workbook.Worksheets.Add()
451 worksheet3 = workbook.Worksheets.Add()
    worksheet4 = workbook.Worksheets.Add()
453 worksheet5 = workbook.Worksheets.Add()
    worksheet6 = workbook.Worksheets.Add()
455 worksheet7 = workbook.Worksheets.Add()
    worksheet8 = workbook.Worksheets.Add()
457 worksheet9 = workbook.Worksheets.Add()
    worksheet10 = workbook.Worksheets.Add()
459 worksheet11 = workbook.Worksheets.Add()
    worksheet12 = workbook.Worksheets.Add()
461 worksheet13 = workbook.Worksheets.Add()

463 xlrange = worksheet.Range["A1:AZ100"]
    xlrange1 = worksheet1.Range["A1:AZ100"]
465 xlrange2 = worksheet2.Range["A1:AZ100"]
    xlrange3 = worksheet3.Range["A1:AZ100"]
467 xlrange4 = worksheet4.Range["A1:AZ100"]
    xlrange5 = worksheet5.Range["A1:AZ100"]
469 xlrange6 = worksheet6.Range["A1:AZ100"]
    xlrange7 = worksheet7.Range["A1:AZ100"]
471 xlrange8 = worksheet8.Range["A1:AZ100"]
    xlrange9 = worksheet9.Range["A1:AZ100"]
473 xlrange10 = worksheet10.Range["A1:AZ100"]
    xlrange11 = worksheet11.Range["A1:AZ100"]
475 xlrange12 = worksheet12.Range["A1:AZ100"]
    xlrange13 = worksheet13.Range["A1:AZ100"]
477
    xlrange.Value2 = OUT2D
479 xlrange1.Value2 = X2D
    xlrange2.Value2 = Y2D
481 xlrange3.Value2 = OUT22D
    xlrange4.Value2 = OUT32D
483 xlrange5.Value2 = OUT42D
    xlrange6.Value2 = OUT52D
485 xlrange7.Value2 = OUT62D
    xlrange8.Value2 = OUT72D
487 xlrange9.Value2 = OUT82D
    xlrange10.Value2 = OUT92D
489 xlrange11.Value2 = OUT102D
    xlrange12.Value2 = OUT112D
491 xlrange13.Value2 = OUT122D
```

script/PerturbedIsocenter.py

B.b. DIR Script

```
#Made by Andrea Hoeg
from connect import *
import sys
Patient = get_current("Patient")
case = get_current("Case")
nameOfHybrid = 'HybridDefReg_Frac'
nameOfHybrid_dose = 'HybridDefReg_Frac_dose'
import clr
clr.AddReference('System.Windows.Forms')
clr.AddReference('System.Drawing')
import System
from System.Drawing import *
from System.Windows.Forms import *
#First; gather user input about variables that change between patients,
#and which fraction to evaluate
#Create a Class Form
class MultilineTextBoxForm(Form):
    def __init__(selfInfo):
        selfInfo.Text = "Information"
        selfInfo.Size = Size(500, 250)
        selfInfo.CenterToScreen()
        selfInfo.setupTextBox()
        selfInfo.button1 = Button()
        selfInfo.button1.Text = 'OK'
        selfInfo.button1.Location = Point(20, 125)
        selfInfo.AcceptButton = selfInfo.button1
        selfInfo.Controls.Add(selfInfo.textbox)
        selfInfo.Controls.Add(selfInfo.button1)
    def setupTextBox(selfInfo):
        textbox = TextBox()
        textbox.Text = "The initial conditions for this program"
        "to run is (1) that there exists an external contour defined"
        "for both the planning CT and the CBCT that you want to make"
        "a deformed registrion of,and (2) that there exists NO hybrid"
        "registration between these two image sets. If these "
        "conditions are not met, exit and edit, and run again."
        textbox.Location = Point(30, 25)
        textbox.Width = 300
        textbox.Height = 100
        textbox.Multiline = True
        textbox.ScrollBars = ScrollBars.Vertical
        textbox.AcceptsTab = True
        textbox.AcceptsReturn = True
```

```
            textbox.WordWrap = True
            selfInfo.textbox = textbox
formInfo = MultilineTextBoxForm()
Application.Run(formInfo)


# Create a Class Form
class CreateWindow(Form):
    def __init__(self):
        # Create the Form
        self.Name = "Create Window"
        self.Text = "Name your inputs"
        self.Size = Size(500, 100)
        self.CenterToScreen()
        # Create Label = label
        label = Label(Text = "Name of planning CT")
        label.Parent = self
        label.Location = Point(30, 20)
        # Create TextBox = textbox
        self.textbox = TextBox()
        self.textbox.Parent = self
        self.textbox.Text = "CT 1"
        self.textbox.Location = Point(150, 20)
        self.textbox.Width = 150
        # Create Button = button
        button = Button()
        button.Parent = self
        button.Text = "Apply"
        button.Location = Point(400, 20)
        # Register event
        button.Click += self.ButtonClicked
    # Create button event
    def ButtonClicked(self, sender, args):
        if sender.Click:
            self.value = self.textbox.Text
            self.Close()
form = CreateWindow()
Application.Run(form)
TargetExamination = form.value

class CreateWindow1(Form):
    def __init__(self1):
        # Create the Form
        self1.Name = "Create Window"
        self1.Text = "Name your inputs"
        self1.Size = Size(500, 100)
        self1.CenterToScreen()
        # Create Label = label
        label1 = Label(Text = "Name of CBCT")
```

```
93          label1.Parent = self1
            label1.Location = Point(30, 20)
95          # Create TextBox = textbox
            self1.textbox = TextBox()
97          self1.textbox.Parent = self1
            self1.textbox.Text = "CT 3"
99          self1.textbox.Location = Point(150, 20)
            self1.textbox.Width = 150
101         # Create Button = button
            button1 = Button()
103         button1.Parent = self1
            button1.Text = "Apply"
105         button1.Location = Point(400, 20)
            # Register event
107         button1.Click += self1.ButtonClicked1
        # Create button event
109     def ButtonClicked1(self1, sender, args):
            if sender.Click:
111             self1.value = self1.textbox.Text
                self1.Close()
113 form1 = CreateWindow1()
Application.Run(form1)
115 ReferenceExamination = form1.value

117 class CreateWindow2(Form):
        def __init__(self2):
119         # Create the Form
            self2.Name = "Create Window"
121         self2.Text = "Name your inputs"
            self2.Size = Size(500, 100)
123         self2.CenterToScreen()
            # Create Label = label
125         label2 = Label(Text = "Fraction number")
            label2.Parent = self2
127         label2.Location = Point(30, 20)
            # Create TextBox = textbox
129         self2.textbox = TextBox()
            self2.textbox.Parent = self2
131         self2.textbox.Text = "1"
            self2.textbox.Location = Point(150, 20)
133         self2.textbox.Width = 150
            # Create Button = button
135         button2 = Button()
            button2.Parent = self2
137         button2.Text = "Apply"
            button2.Location = Point(400, 20)
139         # Register event
            button2.Click += self2.ButtonClicked2
141     # Create button event
```

```
    def ButtonClicked2(self2, sender, args):
        if sender.Click:
            self2.value = self2.textbox.Text
            self2.Close()
form2 = CreateWindow2()
Application.Run(form2)
FractionNumber = form2.value

NameOfHyb = str(TargetExamination)+' deformed using '+str(nameOfHybrid)
            +str(FractionNumber)+str(1)
#Make the hybrid
case.PatientModel.CreateHybridDeformableRegistrationGroup(
    RegistrationGroupName=nameOfHybrid+str(FractionNumber),
    ReferenceExaminationName=ReferenceExamination,
    TargetExaminationNames=[TargetExamination],
    ControllingRoiNames=[], ControllingPoiNames=[],
    FocusRoiNames=[], AlgorithmSettings={
        'NumberOfResolutionLevels': 3,
        'InitialResolution': { 'x': 0.5, 'y': 0.5, 'z': 0.5 },
        'FinalResolution': { 'x': 0.25, 'y': 0.25, 'z': 0.3 },
        'InitialGaussianSmoothingSigma': 2,
        'FinalGaussianSmoothingSigma': 0.333333333333333,
        'InitialGridRegularizationWeight': 400,
        'FinalGridRegularizationWeight': 400,
        'ControllingRoiWeight': 0.5,
        'ControllingPoiWeight': 0.1,
        'MaxNumberOfIterationsPerResolutionLevel': 1000,
        'ImageSimilarityMeasure': "CorrelationCoefficient",
        'DeformationStrategy': "Default",
        'ConvergenceTolerance': 1E-05 })
#Map the ROI  geometries from CT1 to CBCT
case.MapRoiGeometriesDeformably(RoiGeometryNames=[
    "CTV_hudbarbert", "PTV_hudbarbert", "Heart",
    "Breast_contralateral", "Lung_Right", "Lung_Left",
    "Above104", "Skin over CTV", "Pasientkontur"],
    CreateNewRois=False,
    StructureRegistrationGroupNames=[nameOfHybrid+str(
    FractionNumber)],
    ReferenceExaminationNames=[ReferenceExamination],
    TargetExaminationNames=[TargetExamination],
    ReverseMapping=True, AbortWhenBadDisplacementField=False)

#Check that there is a hybrid registration.
#For this script to run, you need to register a hybrid,
#with the CBCT as the REFERENCE, and the planCT as the TARGET.
try:
Patient.Cases['CASE 1'].PatientModel.
    StructureRegistrationGroups[NameOfHyb]
```

```
except:
print 'No hybrid registration found.'
    sys.exit()

#This is the path to access the deformable structure registration.
Patient.Cases['CASE 1'].PatientModel.
StructureRegistrationGroups[nameOfHybrid+str(FractionNumber)].
DeformableStructureRegistrations[nameOfHybrid
+str(FractionNumber)+ str(1)].
CreateDeformedExamination(ExaminationName="")

#Copy the geometries from CBCT to the hybrid examination
#(same geometry, so OK to copy)
case.PatientModel.CopyRoiGeometries(
    SourceExamination=case.Examinations[ReferenceExamination],
    TargetExaminationNames=[NameOfHyb],
    RoiNames=["CTV_hudbarbert", "PTV_hudbarbert",
              "Breast_contralateral", "Heart",
              "Lung_Right", "Lung_Left", "Above104",
              "Skin over CTV", "External_pasientkontur",
              "Pasientkontur"])

#Make the next hybrid, input for Dose Tracking
case.PatientModel.
CreateHybridDeformableRegistrationGroup(
    RegistrationGroupName=nameOfHybrid_dose+str(FractionNumber),
    ReferenceExaminationName=TargetExamination,
    TargetExaminationNames=[NameOfHyb],
    ControllingRoiNames=[],
    ControllingPoiNames=[],
    FocusRoiNames=[],
    AlgorithmSettings={ 'NumberOfResolutionLevels': 3,
        'InitialResolution': { 'x': 0.5, 'y': 0.5, 'z': 0.5 },
        'FinalResolution': { 'x': 0.25, 'y': 0.25, 'z': 0.3 },
        'InitialGaussianSmoothingSigma': 2,
        'FinalGaussianSmoothingSigma': 0.333333333333333,
        'InitialGridRegularizationWeight': 400,
        'FinalGridRegularizationWeight': 400,
        'ControllingRoiWeight': 0.5,
        'ControllingPoiWeight': 0.1,
        'MaxNumberOfIterationsPerResolutionLevel': 1000,
        'ImageSimilarityMeasure': "CorrelationCoefficient",
        'DeformationStrategy': "Default",
        'ConvergenceTolerance': 1E-05 })
```

script/MakeDIR.py

Appendix C

DVHs from DIR Analysis

In the following section all DVHs from the DIR analysis will follow. Each subfigure contains the PADs and ADDs for the photon modality (a) and proton modality (b).

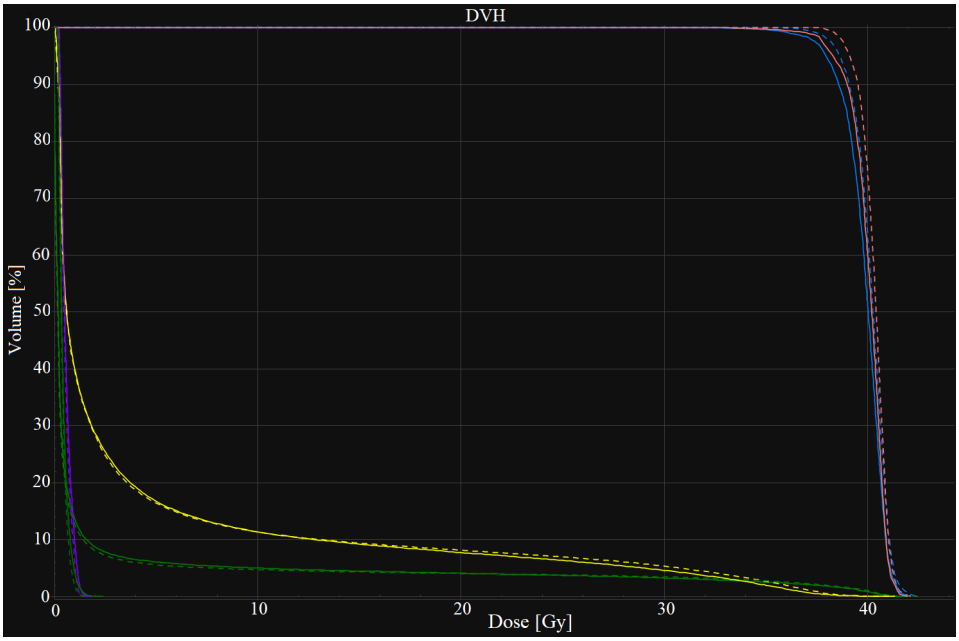

(a) Patient A, photon DVHs of the PAD (dotted line) and ADD (solid line).

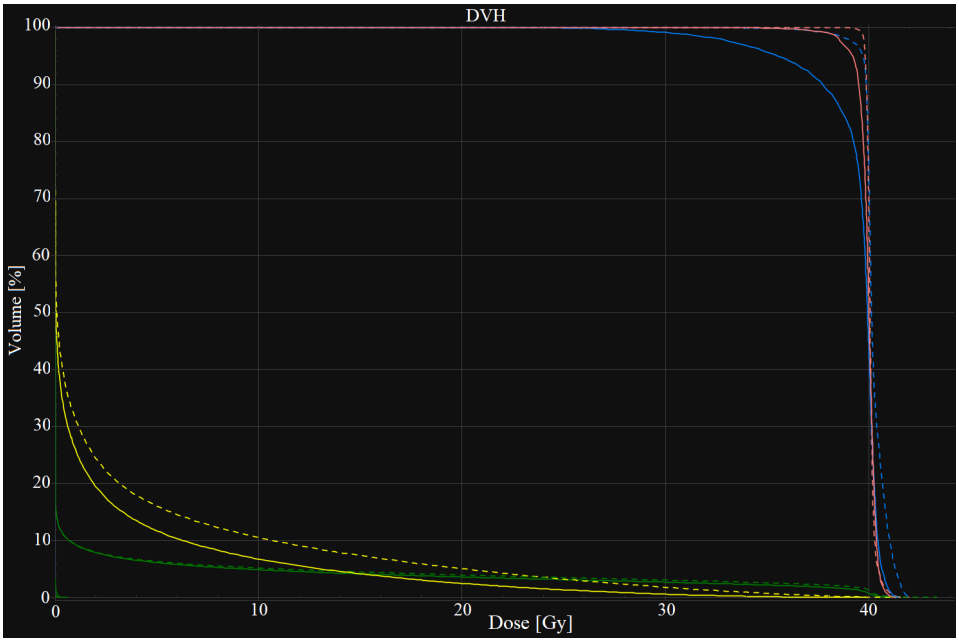

(b) Patient A, proton DVHs of the PAD (dotted line) and ADD (solid line).

Figure 22: DVHs of PAD (dotted line) and ADD (solid line) for photon (22a) and proton (22b) treatment plans. CTV ■, PTV ■, right lung ■, external contour ■, heart ■ (lower green line), and contralateral breast ■. Patient A.

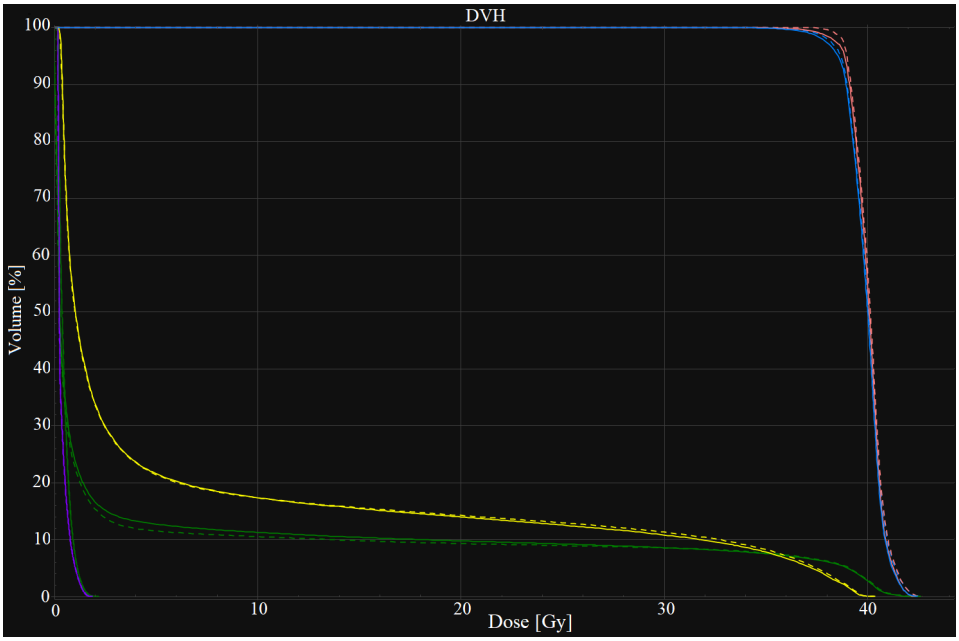

(a) Patient B, photon DVHs of the PAD (dotted line) and ADD (solid line).

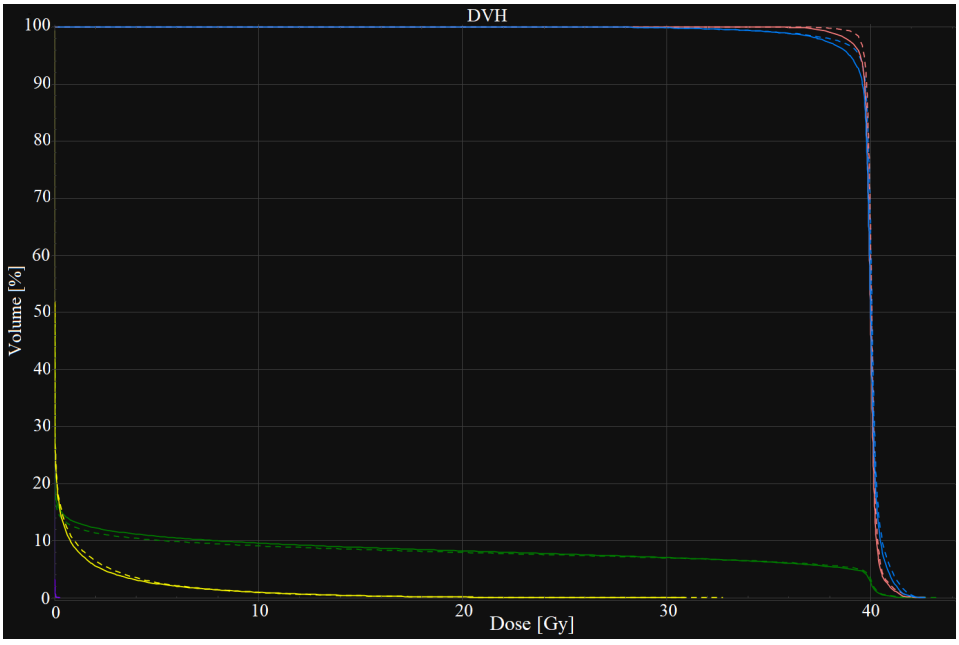

(b) Patient B, proton DVHs of the PAD (dotted line) and ADD (solid line).

Figure 23: DVHs of PAD (dotted line) and ADD (solid line) for photon (23a) and proton (23b) treatment plans. CTV ■, PTV ■, right lung ■, external contour ■, heart ■ (lower green line), and contralateral breast ■. Patient B.

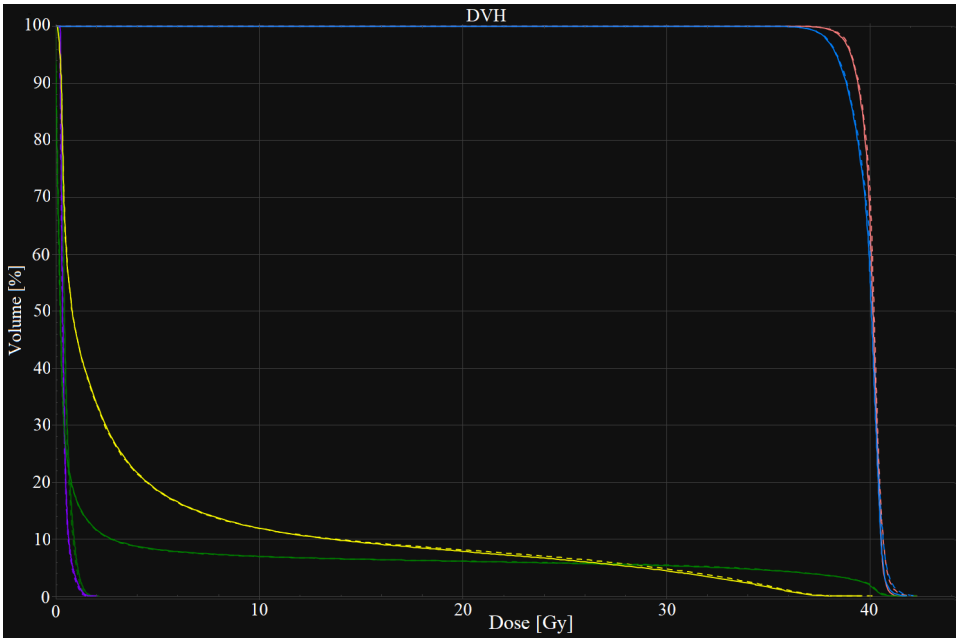

(a) Patient C, photon DVHs of the PAD (dotted line) and ADD (solid line).

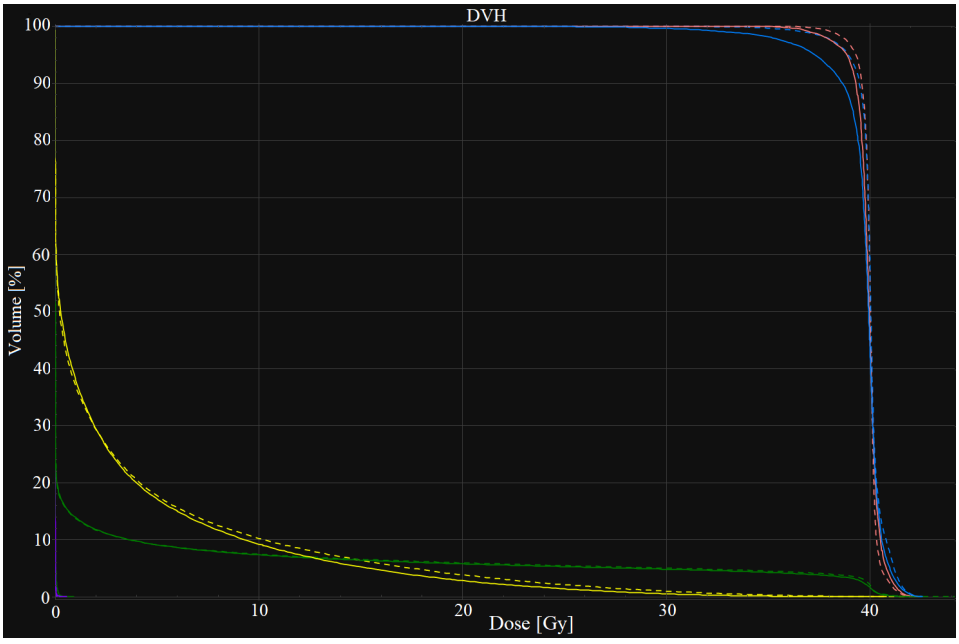

(b) Patient C, proton DVHs of the PAD (dotted line) and ADD (solid line).

Figure 24: DVHs of PAD (dotted line) and ADD (solid line) for photon (24a) and proton (24b) treatment plans. CTV ■, PTV ■, right lung ■, external contour ■, heart ■ (lower green line), and contralateral breast ■. Patient C.

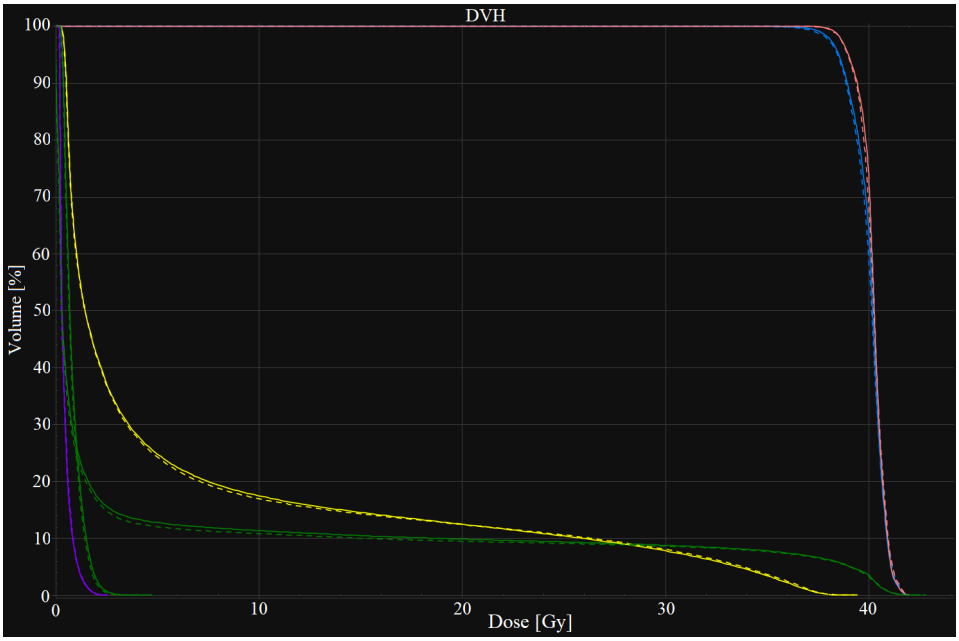

(a) Patient D, photon DVHs of the PAD (dotted line) and ADD (solid line).

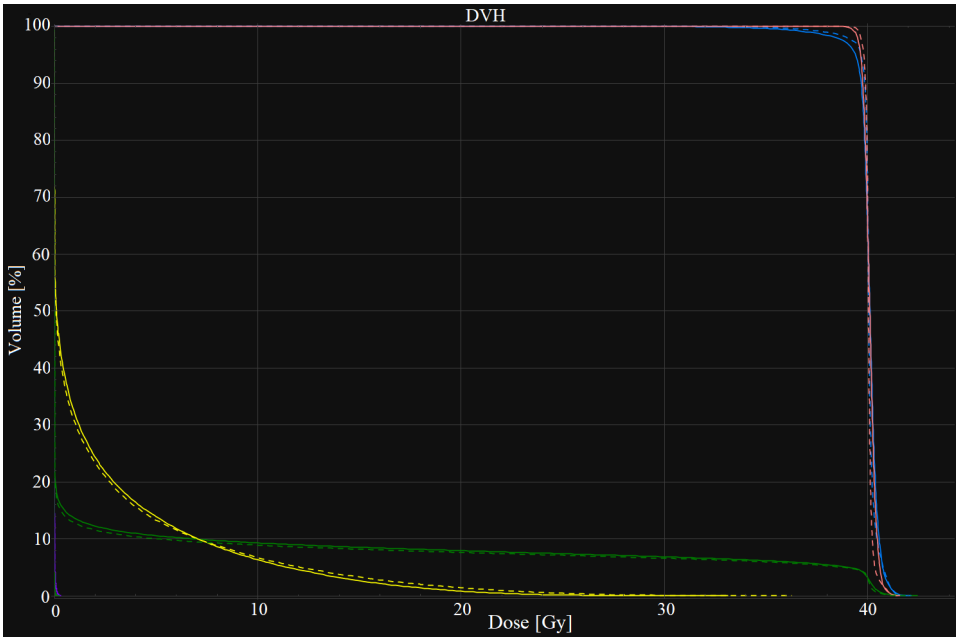

(b) Patient D, proton DVHs of the PAD (dotted line) and ADD (solid line).

Figure 25: DVHs of PAD (dotted line) and ADD (solid line) for photon (25a) and proton (25b) treatment plans. CTV ■, PTV ■, right lung ■, external contour ■, heart ■ (lower green line), and contralateral breast ■. Patient D.

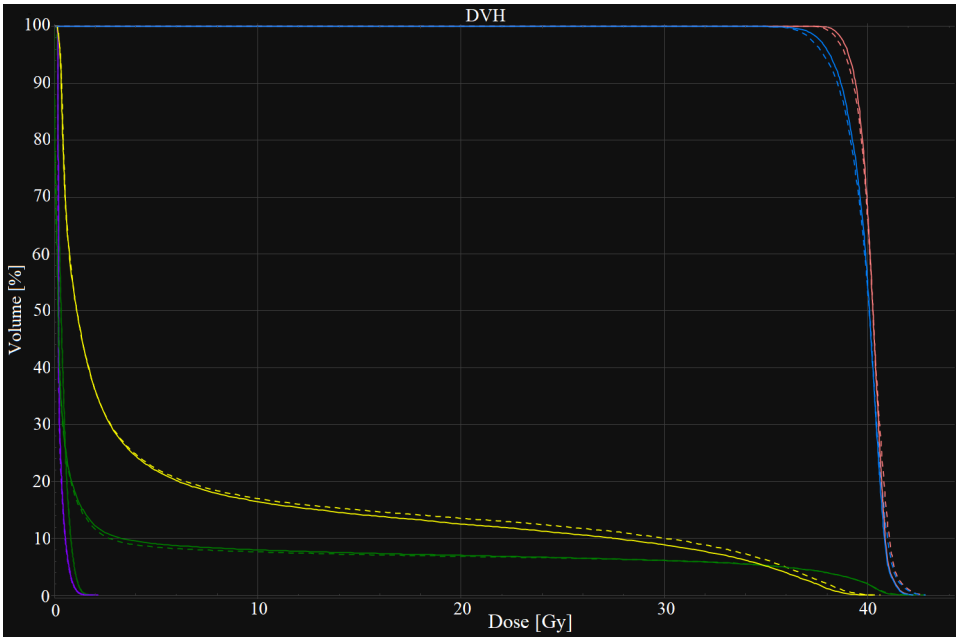

(a) Patient E, photon DVHs of the PAD (dotted line) and ADD (solid line).

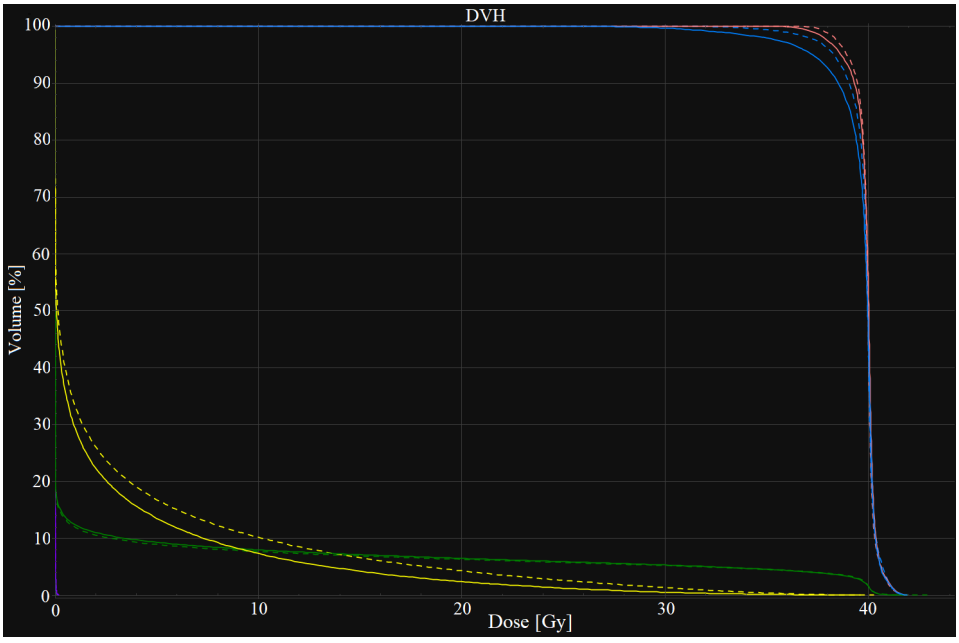

(b) Patient E, proton DVHs of the PAD (dotted line) and ADD (solid line).

Figure 26: DVHs of PAD (dotted line) and ADD (solid line) for photon (26a) and proton (26b) treatment plans. CTV ■, PTV ■, right lung ■, external contour ■, heart ■ (lower green line), and contralateral breast ■. Patient E.

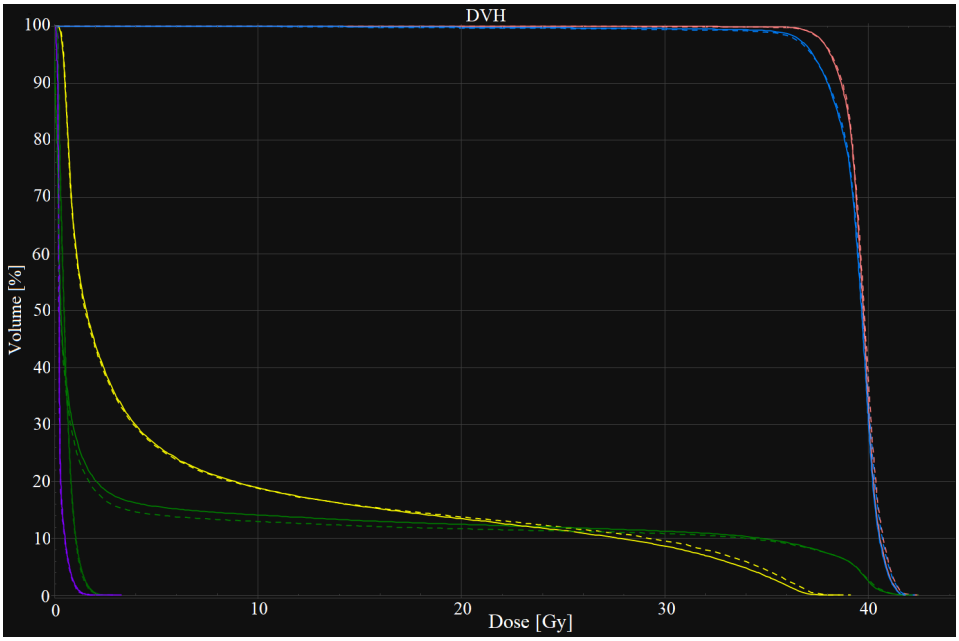

(a) Patient F, photon DVHs of the PAD (dotted line) and ADD (solid line).

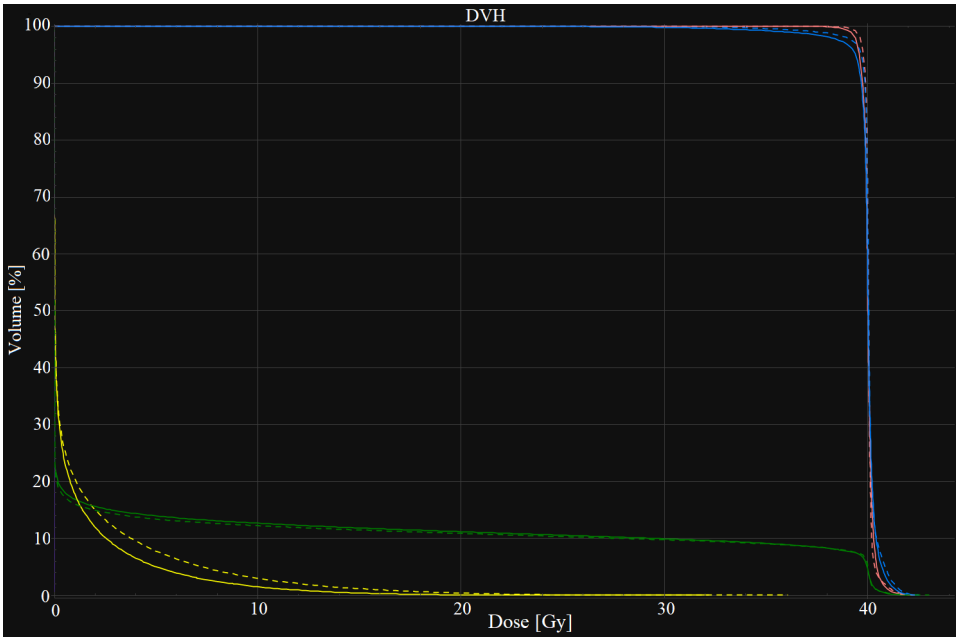

(b) Patient F, proton DVHs of the PAD (dotted line) and ADD (solid line).

Figure 27: DVHs of PAD (dotted line) and ADD (solid line) for photon (27a) and proton (27b) treatment plans. CTV ■, PTV ■, right lung ■, external contour ■, heart ■ (lower green line), and contralateral breast ■. Patient F.

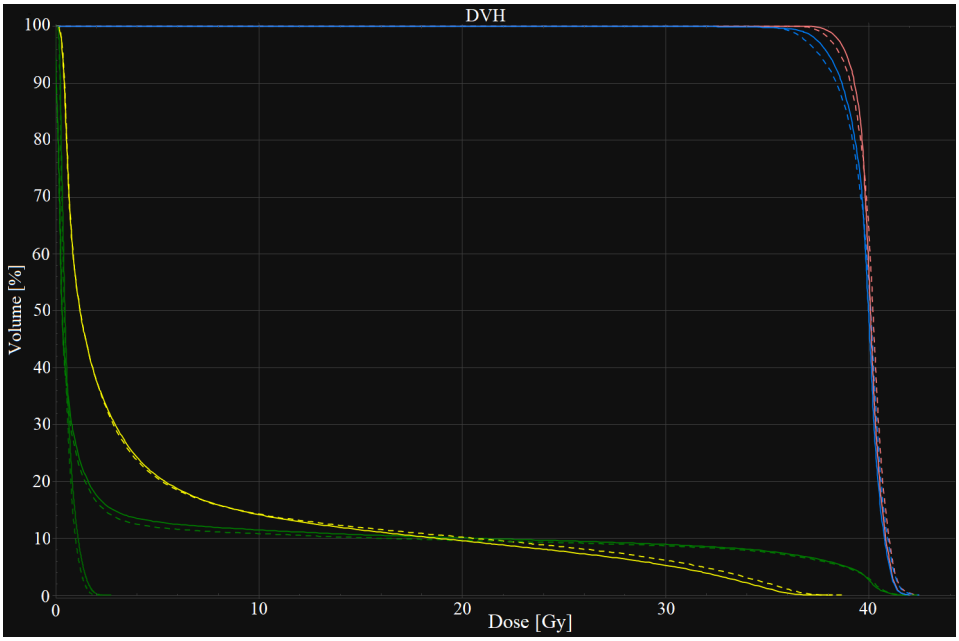

(a) Patient G, photon DVHs of the PAD (dotted line) and ADD (solid line).

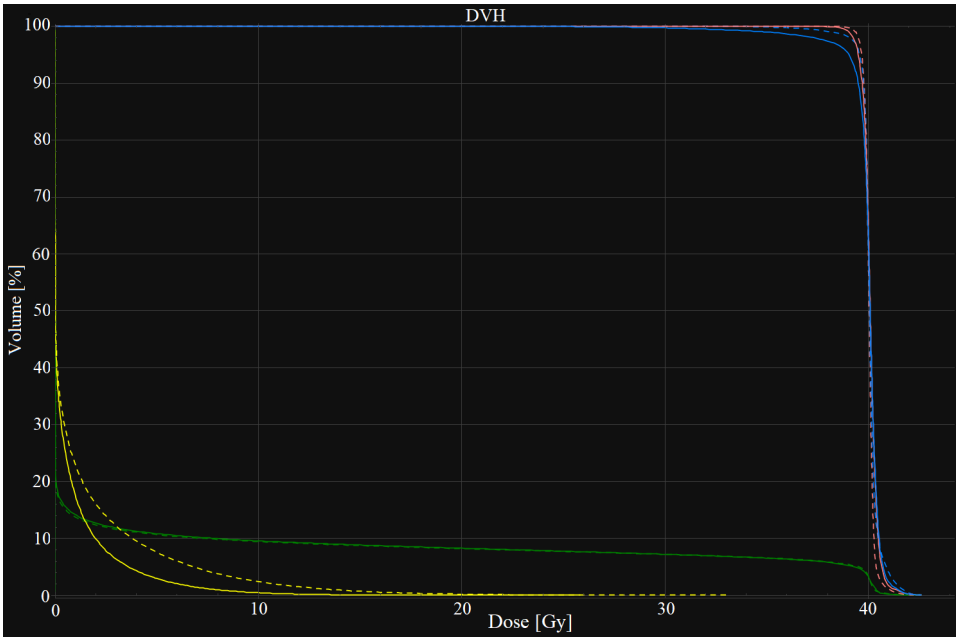

(b) Patient G, proton DVHs of the PAD (dotted line) and ADD (solid line).

Figure 28: DVHs of PAD (dotted line) and ADD (solid line) for photon (28a) and proton (28b) treatment plans. CTV ■, PTV ■, the right lung ■, external contour ■, heart ■ (lower green line). This was the only patient that lacked the contour for the contralateral breast. Patient G.

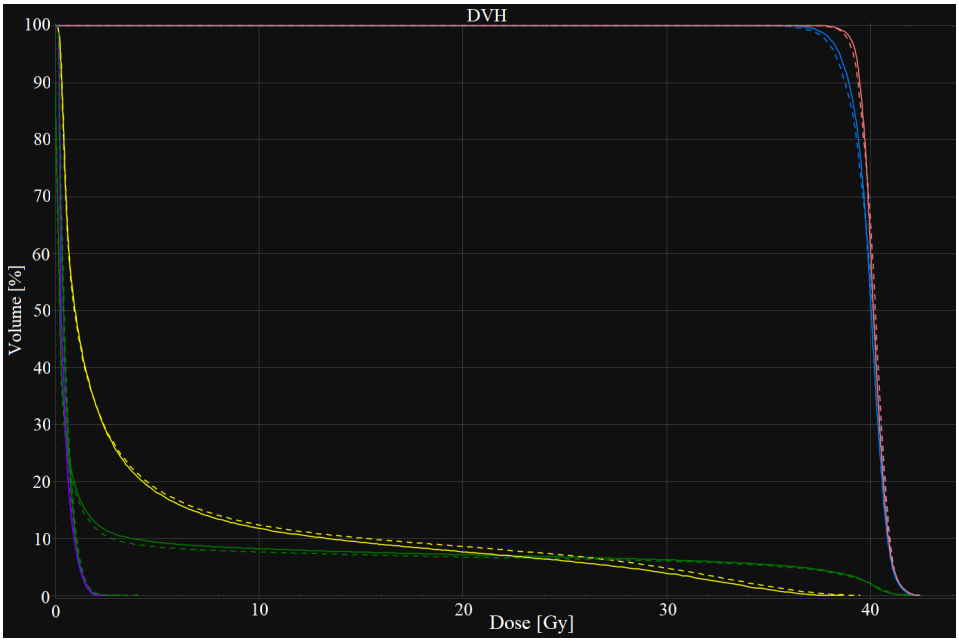

(a) Patient H, photon DVHs of the PAD (dotted line) and ADD (solid line).

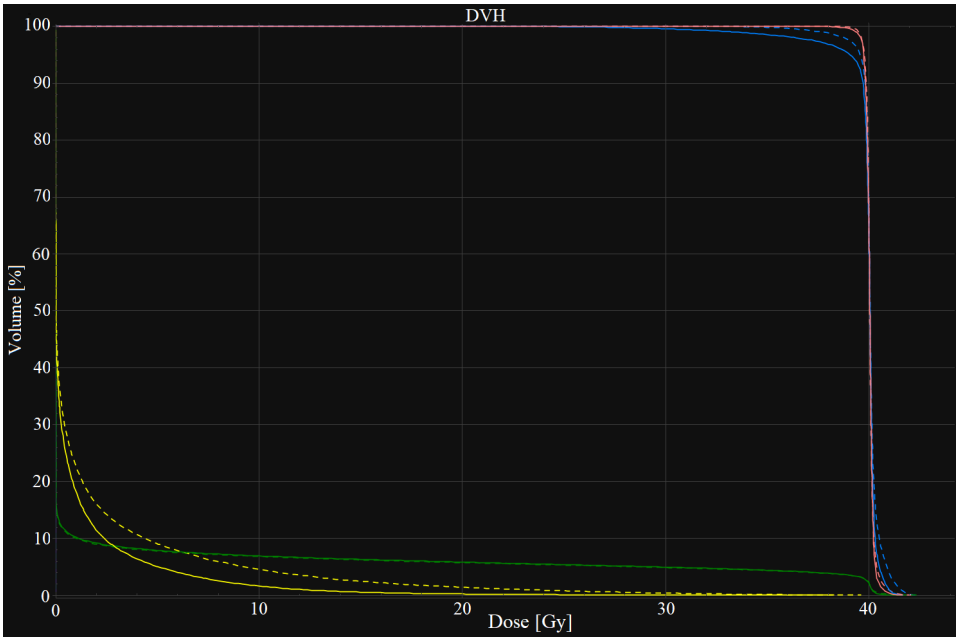

(b) Patient H, proton DVHs of the PAD (dotted line) and ADD (solid line).

Figure 29: DVHs of PAD (dotted line) and ADD (solid line) for photon (29a) and proton (29b) treatment plans. CTV ■, PTV ■, right lung ■, external contour ■, heart ■ (lower green line), and contralateral breast ■. Patient H.

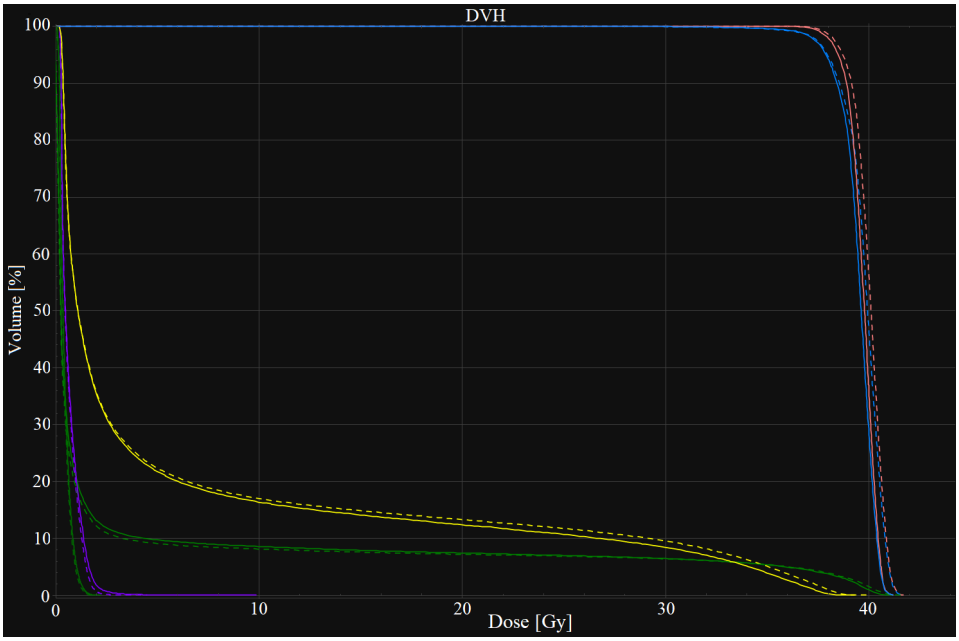

(a) Patient I, photon DVHs of the PAD (dotted line) and ADD (solid line).

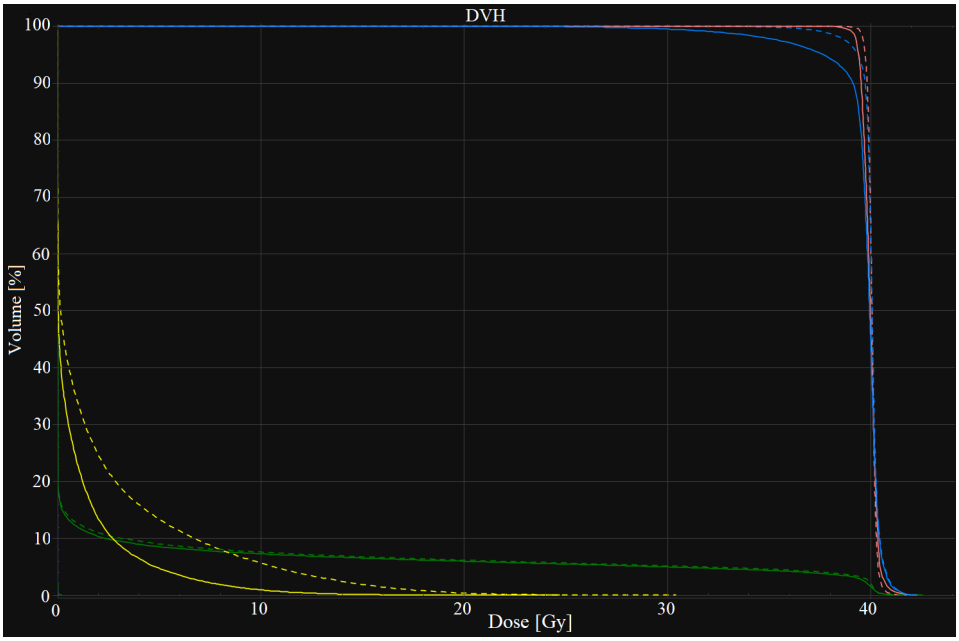

(b) Patient I, proton DVHs of the PAD (dotted line) and ADD (solid line).

Figure 30: DVHs of PAD (dotted line) and ADD (solid line) for photon (30a) and proton (30b) treatment plans. CTV ■, PTV ■, right lung ■, external contour ■, heart ■ (lower green line), and contralateral breast ■. Patient I.

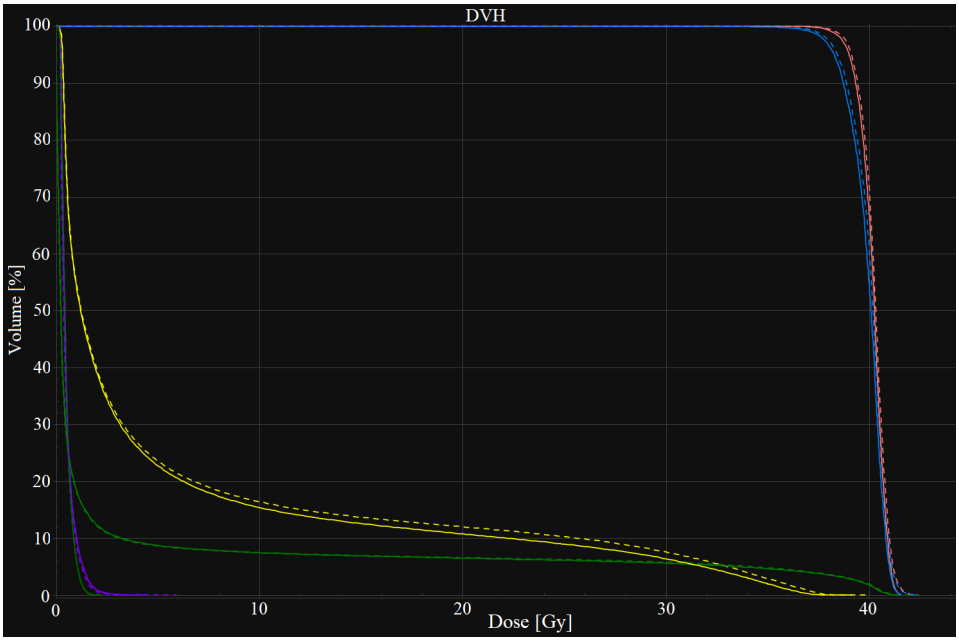

(a) Patient J, photon DVHs of the PAD (dotted line) and ADD (solid line).

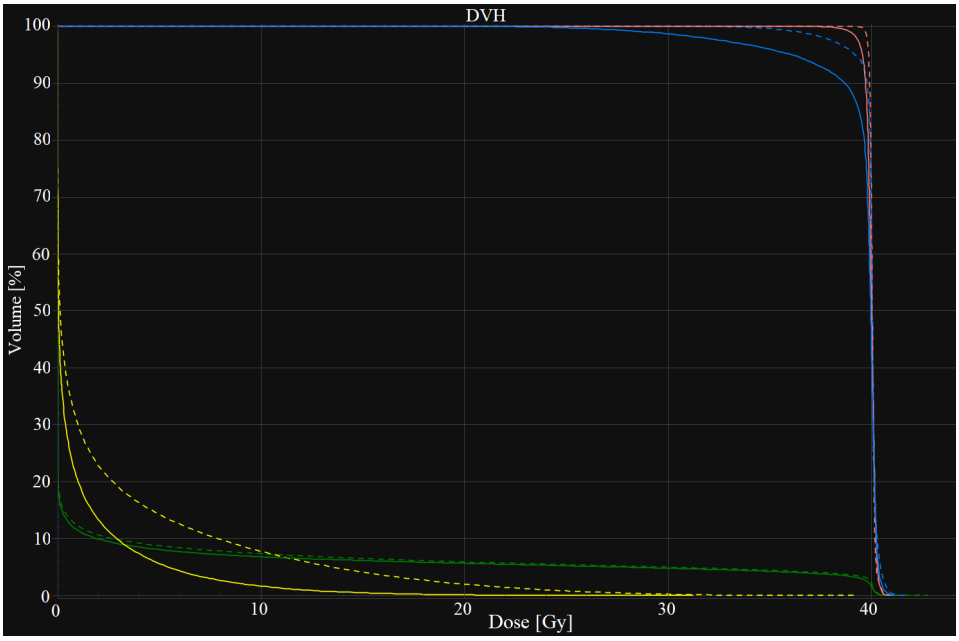

(b) Patient J, proton DVHs of the PAD (dotted line) and ADD (solid line).

Figure 31: DVHs of PAD (dotted line) and ADD (solid line) for photon (31a) and proton (31b) treatment plans. CTV ■, PTV ■, right lung ■, external contour ■, heart ■ (lower green line), and contralateral breast ■. Patient J.